ABSTRACT

MELVIN, ADAM THOMAS. Relating Phosphoinositide 3-kinase (PI3K) Signaling and Cell Motility Dynamics during PDGF-stimulated Chemotaxis. (Under the direction Jason M. Haugh).

Cell migration is essential for wound healing, the immune response, embryogenesis, and cancer metastasis. Chemotaxis, or cell migration directed by an external gradient of chemoattractant, is encountered in various physiological and natural settings and is a means by which cellular processes are coordinated in space and time. This cyclical process of protrusion, adhesion, and retraction is characterized by an asymmetric polarization of 3' phosphoinositides at the leading edge of a migrating cell and is common across multiple cell types. Activated by the phosphoinositide 3-kinase (PI3K) pathway, these 3' PIs act as membrane-bound second messengers which recruit additional signaling proteins, such as the Rho family GTPases, to initiate actin polymerization and membrane protrusion. These protrusions are capable of both cellular translocation as well as gradient sensing.

The characteristics of chemotaxis depend on cell type. Amoeboid cells such as neutrophils and the slime mold, *Dictyostelium discoideum*, respond to shallow gradients of chemoattractants (~1% difference in concentration across cell dimensions) and migrate rapidly (~20 μm/min). Mesenchymal cells such as fibroblasts, on the other hand, require much steeper chemoattractant gradients to evoke similar polarization of PI3K signaling, but the sensitivity of chemotactic movement has yet to be quantitatively characterized. Using a 3' PI-specific, fluorescent biosensor and total internal reflection fluorescence (TIRF) microscopy, the spatial and temporal dynamics of PI3K signaling were monitored during chemotaxis of fibroblasts responding to gradients of the chemoattractant platelet-derived growth factor (PDGF). We show that the asymmetry of PI3K signaling positively correlates with cell directionality during chemotaxis and, consistent with previous work, that highly persistent movement aligned with the external gradient requires a steep gradient (> 10%) in PDGF receptor binding across the cell.

Additionally, we present the development of novel microfluidic devices that generate linear gradients of chemoattractant and their integration with TIRF microscopy. In one particular device, fibroblasts exhibited similar characteristics of PI3K signaling asymmetry

as compared with other methods. Finally, we evaluate the long-term viability of fibroblasts and methods to minimize toxicity in these devices.

Relating Phosphoinositide 3-kinase (PI3K) Signaling and Cell Motility Dynamics during PDGF-stimulated Chemotaxis

by
Adam Thomas Melvin

A dissertation submitted to the Graduate Faculty of
North Carolina State University
in partial fulfillment of the
requirements for the degree of
Doctor of Philosophy

Chemical Engineering

Raleigh, North Carolina

March 2010

APPROVED BY:

_____	_____
Jason Haugh (Chair of Advisory Committee)	Robert Kelly
_____	_____
Balaji Rao	Sam Jones

DEDICATION

To my wife, Liz

BIOGRAPHY

Adam Melvin grew up in Northville, Michigan and always had a fascination with science and mathematics. Upon graduated from Northville High School, he enrolled at the University of Arizona in the fall of 1999, initially majoring in general biology, with aspirations of attending medical school. However, after developing a more passionate interest in mathematics and chemistry courses, he changed majors to chemical engineering at the end of his sophomore year. He spent the next three years engrossed in the CHE curriculum and developed an excitement for the many facets of research stemming from the chemical engineering discipline. This passion was furthered through participation in two summer REU (Research Experience for Undergraduates) programs. During the summer of 2002, he worked for Dr. Gary Rubloff at the University of Maryland on the energy usage of a Cu CVD cluster tool while during the summer of 2003 he was supervised by Dr. Vincent Van Brunt at the University of South Carolina studying the separation of two similar hydrocarbons via silver nitrate as a complexing agent. He graduated *magna cum laude* from U of A in the spring of 2004 with a BS in Chemical Engineering (with honors) and a BA in Chemistry. With a strong desire to learn more about chemical and biomolecular engineering, he enrolled in graduate school North Carolina State University in the fall 2004. Due to his curiosity in biological systems and the mechanics involved in cell migration, Adam joined Dr. Jason Haugh's research group. While working with Dr. Haugh, Adam received the NIH/NCSU Molecular Biotechnology Training Program Fellowship, which provided him with the opportunity to conduct research at Pfizer's Research Technology Center during the summer of 2007.

During his tenure as NC State, Adam has also been very active with teaching and educational development serving a both a teaching assistant (TA) and as an instructor of a core chemical engineering courses. Additionally, he developed a novel TA training workshop entitled "Tips from the Trenches" which provides experience-based advice to new TAs and, in collaboration with Dr. Lisa Bullard, developed a video illustrating the

differences between group work and cheating, which has had a pronounced impact on the reduction of academic integrity violations in the sophomore gateway course.

ACKNOWLEDGEMENTS

Surviving graduate school and earning my PhD has been the most difficult task I have attempted and I would not have made it successfully without the help and support of many people. First, I would like to thank my advisor Dr. Jason Haugh, who has always pushed me to excel in all of my research endeavors and provided insight when I hit road blocks in the lab. I would also like to thank my committee members, Dr. Bala Rao, Dr. Sam Jones, and especially, Dr. Bob Kelly, for providing advice and being understanding with my not-so linear research path. I want to convey my deepest thanks to Dr. Michael Weiger for being a constant source of support and council, as well as a great friend, during all my years at graduate school. I also could not have succeeded in developing a silicon master without the input of Amy McPherson and Dr. Adrian O'Neill of the Walker lab, who provide endless hours of help and guidance with all the equipment necessary to fabricate a microfluidics device. I would like to thank all current and previous members of the Haugh group for their support and assistance, especially Shoeb Ahmed for his work developing the SVA code, Dr. Erik Welf for his help with the angle of orientation analysis, and Murat Cirit for keeping life in the lab interesting. I also had the distinct pleasure to work with two highly qualified undergraduate researchers, David Rhoden and Deidra Dunn, during my time here. I want to extend my warmest thanks to Dr. Lisa Bullard for being an outstanding teaching mentor who is always willing to sit down and talk about anything ranging from research, to teaching, to life in general. I would also like to thank the outstanding support staff in the Chemical Engineering department who have helped take care of any problems that have arisen with ordering, billing, or paying for anything. I'd also like to extend my sincerest thanks to all of my friends who have dragged me out of the lab to play golf or just sit on a patio to unplug from research, even if it was just for a little while. Finally, I would like to thank my loving wife Elizabeth, without whom, I don't think I could have survived graduate school. From her constant encouragement, to bringing me dinner when I'm working at the lab to 2 am, to her willingness to listen to me complain when I have a failed experiment, she has been my rock during this little adventure.

TABLE OF CONTENTS

CHAPTER 2: Asymmetry of PI3K signaling dynamics coincides with directional fidelity of fibroblast chemotaxis

Chapter 3: Development of microfluidic devices to study fibroblast chemotaxis in PDGF gradients

LIST OF TABLES

LIST OF FIGURES

Chapter 1

Signaling pathways controlling chemotaxis and methods used to study them

1.1 INTRODUCTION

Cell migration is a complex process executed by a variety of cell types and organisms to achieve different goals. In mammals, cell migration is essential for development, immune surveillance, and wound healing. Epithelial and neuronal cells migrate during morphogenesis but cease migrating once terminally differentiated, whereas white blood cells and fibroblasts are 'professional' migrating cells that must move to carry out their respective roles in the immune response and wound healing (Friedl & Wolf, 2010). Other eukaryotic cells, such as the slime mold *Dictyostelium discoideum*, migrate as single amoeboid to form a multi-cellular fruiting body that is better equipped to survive periods of nutrient drought. Despite the variety of cell types and purposes for migrating, certain mechanistic similarities (as well as some differences) among these systems have come to light during the past decade or so. Eukaryotic cells adopt an asymmetric morphology with a defined front and rear that is commonly accompanied by the polarization of intracellular signaling molecules at the leading edge. The cell then migrates by an established series of steps referred to as the cell motility cycle (Lauffenburger & Horwitz, 1996), wherein the plasma membrane protrudes in the direction of migration, adhesive contacts are formed with the surface upon which the cell is migrating [in mammals, commonly with proteins associated with the extracellular matrix (ECM)], the cell body is contracted forward, and finally older adhesions are disassembled.

In a homogeneous microenvironment, most migratory cells exhibit *basal motility*; that is, they migrate with some persistence in random directions. Directed migration or *taxis*, on the other hand, is spatially biased by specific, external cues. These cues serve to recruit certain cell types to a particular location, for example the homing of T lymphocytes to lymph nodes in the adaptive immune response and recruitment of neutrophils and macrophages to sites of wounding. A similar process has been strongly implicated in the invasiveness of cancer cells (Condeelis, 2006; Yamaguchi, 2005; Zaman, 2006). Cell migration can be directed by a variety of stimuli, including gradients of adhesive ligands in ECM (haptotaxis),

external forces or gradients of ECM mechanical properties (durotaxis), and gradients of temperature (thermotaxis) and electric field (electrotaxis) (Petrie, Doyle, & Yamada, 2009). Most commonly, however, cell migration is directed by gradients of soluble ligands, a process called chemotaxis. The soluble factors that stimulate chemotaxis, or chemoattractants, bind to specific cell surface receptors that mediate the localized activation of intracellular signaling pathways, which in turn govern the dynamics of the actin cytoskeleton and thus cell movement. Whereas chemotaxis is conceptually simple, it imposes a definite technical challenge: the need to generate and manipulate chemical gradients. Here, we review the field of chemotaxis with some emphasis on methods used to study it.

1.2 PROTOTYPICAL SYSTEMS FOR STUDYING CHEMOTAXIS

1.2.1 Amoeboid chemotaxis: neutrophils and *Dictyostelium discoideum*

Among chemotactic cells, neutrophils and *Dictyostelium discoideum* are by far the best characterized. These cells respond robustly to chemoattractant gradients, even quite shallow ones (~ 1% across the cell), and are capable of fast migration speeds (~20 μm/min) (Merlot, 2003; Schneider & Haugh, 2006; Song, 2006). Further, many of the signal transduction pathways activated in these two, biologically distinct cells share remarkable similarities. Their respective chemoattractants both bind and activate G protein-coupled receptors (GPCRs) that mediate signaling through translocation of phosphoinositide 3-kinase (PI3K) to the plasma membrane, leading to localized accumulation of 3'-phosphorylated phosphoinositide lipids (3' PIs) and activation of Rho-family GTPases and other pathways (Fukata, Nakagawa, & Kaibuchi, 2003).

Neutrophils are involved in the innate immune response in vertebrates and are the most abundant type of white blood cell. They respond to a variety of chemoattractants, including peptides shed by certain bacteria [mimicked by N-formylmethionyl-leucyl-phenylalanine (fMLP), for example], interleukin-8 (IL-8), and the C5a complement fragment (Figure 1.1). Neutrophils are prominently involved in wound healing; they ingest pathogens

and dead cells by a process called phagocytosis, and they are responsible for secreting inflammatory cytokines.

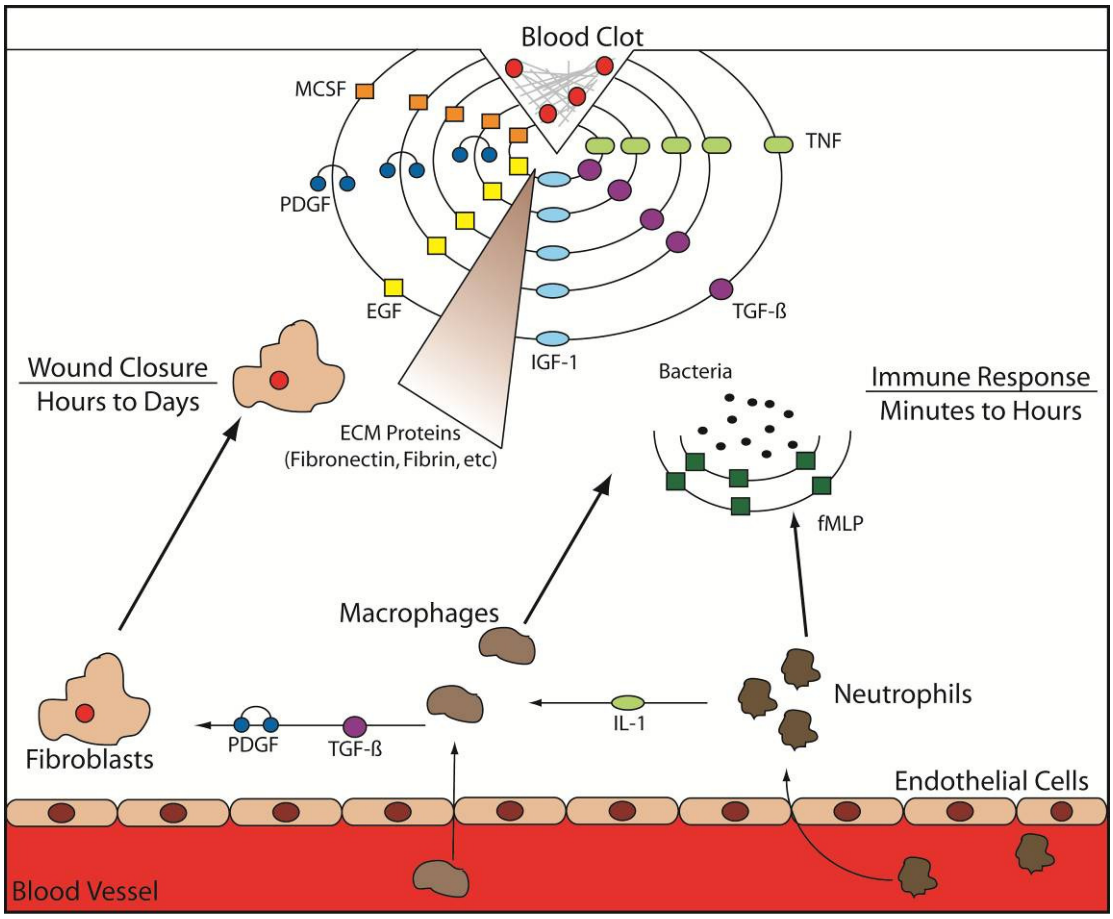

Figure 1.1 Gradients of extracellular cues elicit chemotaxis towards sites of wounding. During wound healing a series of events unfolds to temporally recruit different cell types to the wound site to perform specific duties. Neutrophils and macrophages, members of the acute immune response, a recruited on the order of minutes to hours to remove foreign particles, dead cells and bacteria from the wound site. These cells are recruited out of the blood vessel into surrounding tissue by IL-8, CSF-1, C5a as well as peptides shed by bacteria. Fibroblasts are recruited by gradients of PDGF and adhesive ligands in the ECM. These cells populate the wound over a period of hours to days and ultimately mediate tissue repair and wound closure.

Dictyostelium discoideum is a soil amoeba with a unique life cycle that requires precise chemotaxis to survive periods of starvation. When its bacterial food source is depleted, single cells migrate towards an external gradient of cyclic adenosine monophosphate (cAMP), which they are stimulated to secrete. Thus, these cells perform a

chemotactic relay in which they 'stream' towards a focal point of cAMP production, where they form a multi-cellular slug and, ultimately, a structure called the fruiting body (Vasiev, 2003; Weijer, 2004).

1.2.2 Mesenchymal chemotaxis: fibroblasts

Another chemotactic cell type is the dermal fibroblast, which is responsible for synthesizing and remodeling ECM during wound healing. By comparison with amoeboid cells, fibroblast migration is slower by at least one order of magnitude (speed < 1 μm/min) and is characterized by a more complex cell morphology. They reside in connective tissue and, during the proliferative phase of wound healing, migrate as a population into the provisional matrix; their primary chemotactic cue is a gradient of platelet-derived growth factor (PDGF), which is produced by platelets and macrophages (Figure 1.1). Fibroblasts adhere strongly to immobile ligands in the ECM, balancing the strong contractile forces generated by these cells. This explains their relatively slow migration. Fibroblasts interact with a variety of ECM components, including proteins such as fibronectin and the collagens and glycosaminoglycans such as hyaluronan (Monypenny et al., 2009).

Table 1.1 Key differences between the chemotactic responses of amoeboid cells and tissue fibroblasts.

	Neutrophils / Dictyostelium discoideum	Fibroblasts
Receptor	G protein-coupled receptors	Receptor Tyrosine kinase
Chemoattractant (s)	fMLP, IL-8, C5a (Neutrophils), cAMP (Dicty)	PDGF
Class of PI3K	Class 1B	Class 1A
Migration Speed	~ 20 um/min	~1 um/min
Gradient Response	Shallow gradients (~1-4%)	Steep gradients (>10%)
Observable Gradient Amplification	Yes	No

Quantitative measurements suggest that fibroblasts require far steeper chemotactic gradients (> 10% across the cell) than amoeboid cells (Schneider & Haugh, 2005),

suggesting differences in the intracellular feedback mechanisms that are thought to be responsible for amplification of shallow gradients in neutrophils and *Dictyostelium* (Bosgraaf, Keizer-Gunnink, & van Haastert, 2008; Merlot, 2003).

1.2.3 Dimensionality of cell migration

Cell migration has been traditionally studied on flat, planar surfaces, most typically glass coated with ECM proteins, motivated by the need to observe the cells by light microscopy. In this two-dimensional (2D) model, four basic migration processes are observed: (1) protrusion of the leading edge, (2) adhesion to the ECM, (3) cell body contraction and translocation, and (4) retraction of the cell rear (Figure 1.2).

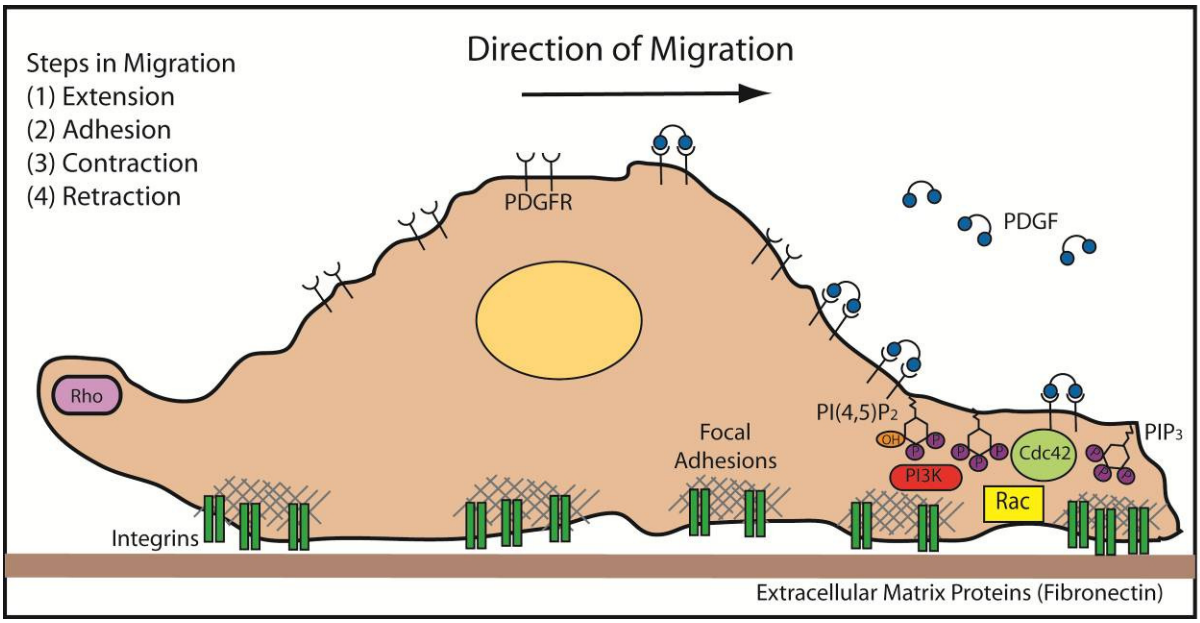

Figure 1.2 Fibroblast migration and chemotaxis in two dimensions. The 2D model for cell migration is the most commonly studied framework for chemotaxis. The asymmetric accumulation of 3' phosphoinositides, PI3K and Rho family GTPases are hallmark events of polarized cell migration. In cells such as fibroblasts (depicted above) integrins also play an important role in the formation of focal adhesions across the contact area, physically linking the actin cytoskeleton and the extracellular matrix.

Coordination of these four steps is essential for efficient cell migration. Disruption of the underlying signaling pathways by genetic or pharmacological means results in impaired migration behavior including reduced speed and/or directional persistence (Petrie et al.,

2009). In the 2D cell migration model, chemotactic gradients can be generated using a variety of methods, including migration chambers, micropipettes, and microfluidic devices (Section 1.4).

Although 2D cell migration remains the gold standard for subcellular imaging and resolution of adhesion, signaling, and cytoskeletal dynamics, it is becoming increasingly apparent that migration in 2D does not closely mimic certain chemical and mechanical properties of the cell's native, three-dimensional (3D) microenvironment, such as the porosity and mechanical compliance of the ECM (Nelson & Bissell, 2006; Yamada & Cukierman, 2007; Zaman, 2007, 2006). Indeed, studies of cell migration in 3D gels have shown marked differences in comparison with 2D migration. For example, 2D migration speed tends to be maximized at intermediate ECM coating density, which offers an optimal balance between traction and adhesion forces (Palecek, 1999); however, in the 3D system, migration is faster and less sensitive to ECM density (Cukierman, 2001). Because of the inherent difficulties associated with microscopic observation of cells in 3D gels, the underlying bases for these differences remain poorly understood. As a compromise, Doyle and colleagues have shown that fibroblast migration on ECM deposited on micro-patterned lines, which is compatible with standard light microscopy, mimics many aspects of migration on ECM fibers *in vivo* (Doyle, Wang, Matsumoto, & Yamada, 2009).

1.3 INTRACELLULAR SIGNALING PATHWAYS DRIVING CELL MIGRATION

As with any biological response, cell migration is governed by intracellular signaling pathways involving interactions among transmembrane receptors, adaptor proteins, kinases, phosphatases, and second messengers that affect the dynamics of actin polymerization. These processes result in the formation of functional structures at the cell's leading edge, such as lamellipodia and filopodia, which adhere to the extracellular matrix at sites called focal adhesions. Here, we review some of the molecular players that have been most prominently implicated in the control of chemotaxis.

1.3.1 Receptor-mediated signaling

Transmembrane, cell-surface receptors are generally responsible for perception of external stimuli. Most often, they possess an extracellular domain or surface, which binds specific ligands and thus confers specificity, and an intracellular region that either associates with heterotrimeric G proteins (in the case of G protein-coupled receptors) or has enzymatic activity (in the case of receptor tyrosine kinases). Almost all of the model cell types used to study chemotaxis use one of these receptor types for gradient sensing.

Receptor tyrosine kinases

The hallmark of a receptor tyrosine kinase (RTK) is the activation of intrinsic kinase activity and the self-phosphorylation of specific tyrosine residues in the cytoplasmic tail of the receptor (Schlessinger, 2000). PDGF binds to two, structurally related receptors of the RTK class and induces their dimerization and phosphorylation (Claesson-Welsh, 1994). The phosphorylated tyrosine residues serve as high-affinity docking sites for specific intracellular enzymes (Figure 1.3). These receptor-proximal enzymes include phospholipase C-γ (Bourette & Rohrschneider, 2000) and PI3K, which dock to the activated receptor via their Src homology 2 (SH2) domains. Other proteins called adaptors mediate formation of multi-protein complexes but do not possess enzymatic activity. These proteins, such as Grb2 and Shc, bind to both receptors and cytosolic enzymes, like the guanine nucleotide exchange factor Sos, to activate signaling. In the case of Sos, its recruitment results in activation of signaling through the small GTPase Ras, leading to cell proliferation and other responses (Han et al., 1998).

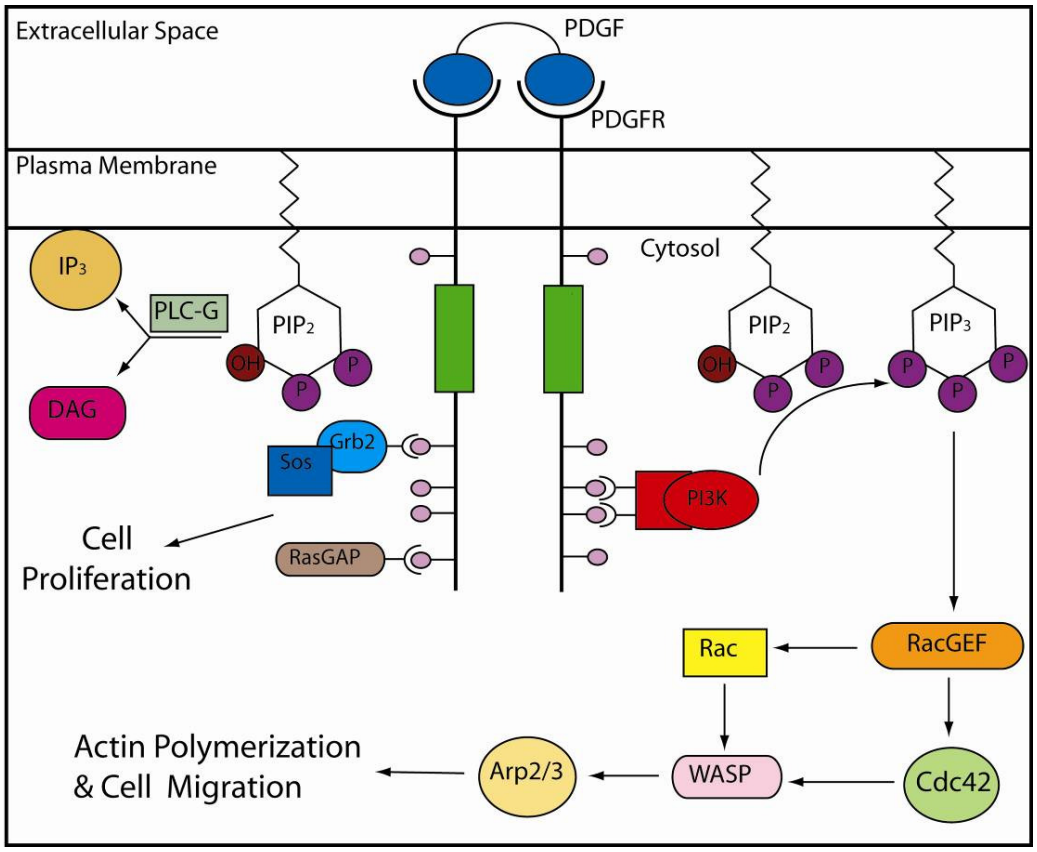

Figure 1.3 Example of a receptor tyrosine kinase: PDGF receptors. A transmembrane receptor composed of an external ligand binding domain and an internal kinase domain. Once the ligand binding domain attracts a PDGF dimer, the intrinsic kinase active of the tyrosine kinase domain activates and autophosphorlyates multiple tyrosine residues across the receptor. The phosphorylated tyrosine residues then recruit an array of signaling molecules, adaptor proteins, and second messengers to elicit cell responses such as proliferation and migration.

G protein-coupled receptors

G-protein coupled receptors (GPCRs) are the largest family of cell-surface receptors and are found in all eukaryotes (Liebmann, 2004). They are seven-transmembrane domain receptors that bind heterotrimeric G proteins, which are complexes of three protein subunits – α, β and γ – with guanine diphosphate (GDP) bound to the α subunit in the inactive state. When an extracellular ligand, such as cAMP, binds to its cognate GPCR, the α subunit releases GDP and binds cytosolic guanine triphosphate (GTP). GTP binding causes a conformational change, which in turn promotes the dissociation of the βγ complex, allowing both α-GTP and βγ to interact with effector proteins (Alberts, 2002). The pathways activated by G proteins involve many of the same processes as those activated by RTKs, such as the

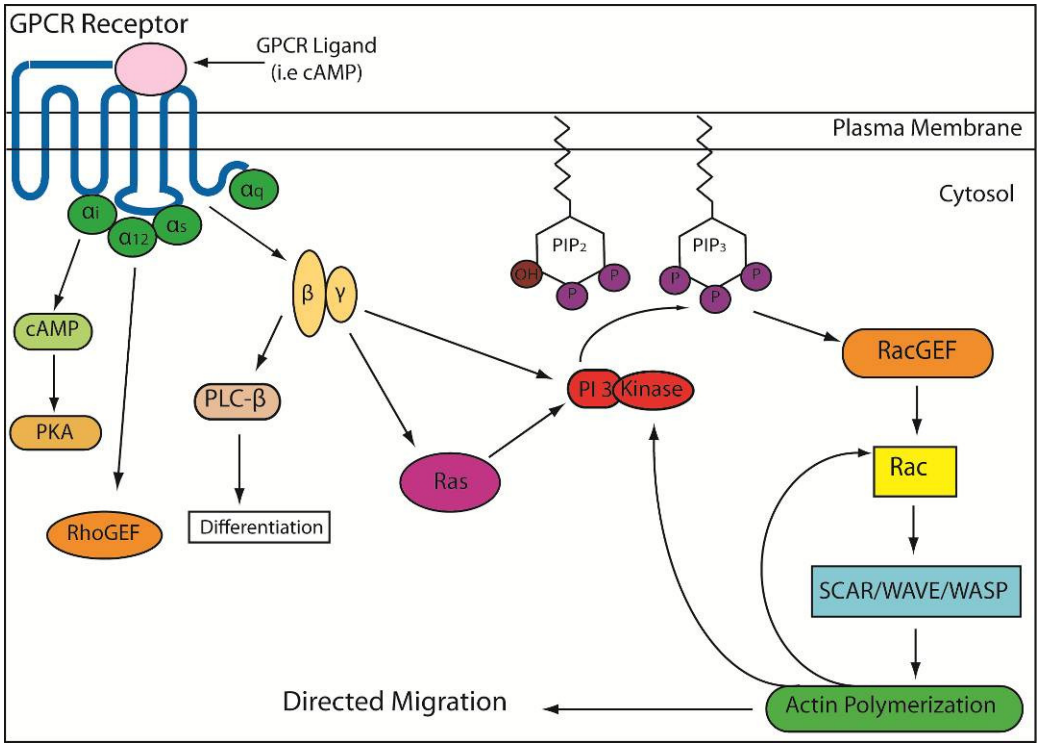

Figure 1.4 G protein-coupled receptor signaling. The seven transmembrane G protein-coupled receptor consists of an external ligand binding domain and internal docking sites for G proteins. In the inactive state these G proteins are bound to GDP, but once a ligand binds to the receptor, GDP is replaced by GTP and the receptor is activated. The G proteins (the α subunit and βγ complex) then initiate a signal cascade recruiting signaling molecules and second messengers capable of eliciting a cellular response such as migration.

activation of PI3K and Ras (Figure 1.4) (Gerard & Gerard, 1994). GPCRs are found in all cell types and play a primary role in gradient sensing by fast-moving, amoeboid cells; the aforementioned chemoattractants cAMP, fMLP, IL-8, and C5a are each recognized by different GPCRs (Naccache et al., 2000; Parent & Devreotes, 1999).

Integrins

Another class of receptors involved in chemotaxis are the integrins, which recognize proteins found in the ECM and, in some cases, on other cells; thus, they generally mediate adhesion (Barczyk, 2010; Schmidt, 2010). These receptors differ from GPCRs and RTKs in that they bind their ligands with a much lower affinity and rely instead on the concentrating effect of surface apposition. Integrins are heterodimeric complexes comprised of two, noncovalently associated glycoproteins subunits, α and β. There are a wide variety of αβ

combinations that confer ligand specificity, such as $\alpha_5\beta_1$ (fibronectin-binding) and $\alpha_6\beta_1$ (laminin-binding) (Durbeej, 2010). Although there have been a few studies to shed light on signaling crosstalk between integrins and other receptor classes like RTKs in the context of migration and cell spreading, the precise mechanisms involved and their prominence in different cell contexts remain poorly understood (Weiger et al., 2009); however, what is certain is that integrin-mediated adhesion affects cell speed and thus impacts basal motility and all forms of directed migration (Friedl & Wolf, 2010; Obara, 2010; Rathinam, 2010).

1.3.2 Phosphoinositide 3-kinases

Phosphoinositide 3-kinases (PI3Ks) are lipid kinases that phosphorylate the 3'-OH position of the inositol ring of phosphoinositides (PIs) using ATP as the phosphate donor. Less than 1% of all inositol-containing lipids are phosphorylated at the 3' position, marking the products of PI3Ks as unique and specific second messengers for cell signaling (Rameh & Cantley, 1999). As an enzyme family, PI3Ks produce four different lipid products: phosphatidylinositol (3)-phosphate [PI(3)P], phosphatidylinositol (3,5)-bisphosphate [$PI(3,4)P_2$], phosphatidylinositol (3,4)-bisphosphate [$PI(3,4)P_2$], and phosphatidylinositol (3,4,5)-trisphosphate (PIP_3). Each of these lipid products have specific downstream targets and are generated by distinct isoforms of PI3K, which are grouped into three distinct classes according to their respective lipid substrates (Vanhaesebroeck & Waterfield, 1999). Class I PI3Ks are heterodimers comprised of catalytic and regulatory subunits that phosphorylate $PI(4,5)P_2$ to produce PIP_3, the lipid second messenger of primary interest for chemotaxis (Ridley, 2001). This class is further classified as class I_A PI3Ks, which engage RTKs and other tyrosine-phosphorylated proteins by virtue of the tandem SH2 domains of the corresponding regulatory subunits (Vanhaesebroeck et al., 1999), and class I_B PI3Ks, which are recruited by $G\beta\gamma$ complexes of heterotrimeric G proteins (Parent & Devreotes, 1999). The action of PI3K at the plasma membrane is responsible for a large array of intracellular signaling processes. The lipid product PIP_3, along with $PI(3,4)P_2$ produced as a result of PIP_3 dephosphorylation of the 5' position, recruits various proteins from the cytosol with pleckstrin homology (PH) domains. One such protein is the serine/threonine kinase Akt,

which functions prominently in glucose metabolism, cell proliferation, cell survival, and regulation of transcription (Brazil & Hemmings, 2001). More pertinent to the remainder of this thesis, fusion proteins comprised of the PH domain of Akt and various fluorescent proteins have proven to be most suitable as biosensors for accumulation of PIP_3/$PI(3,4)P_2$ at the plasma membrane (Gray, Van der Kaay, & Downes, 1999), making it possible to spatially and temporally track the 3' PI products of PI3K using live-cell imaging techniques.

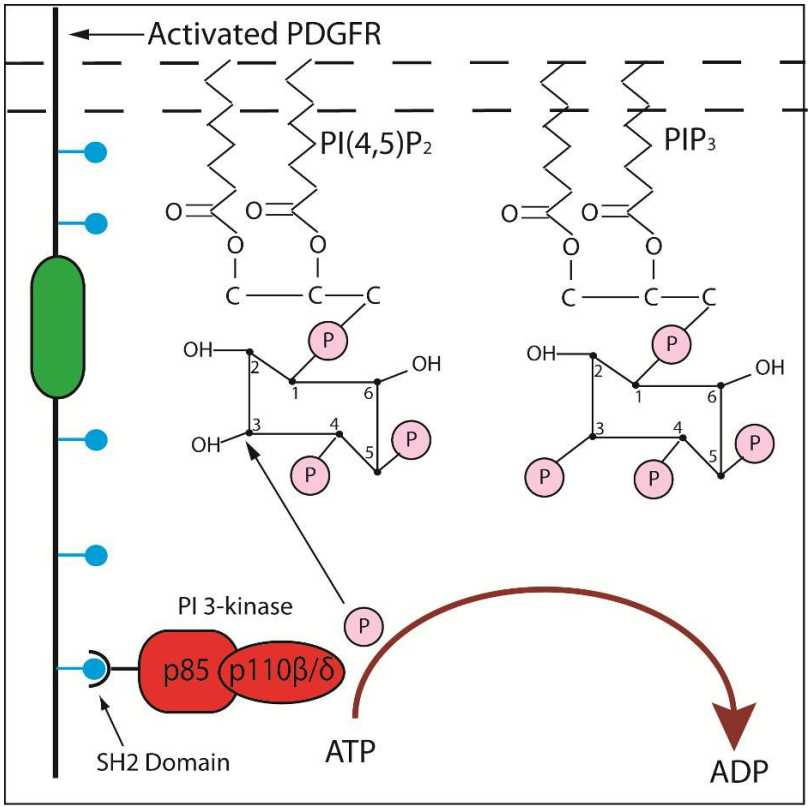

Figure 1.5 Phosphoinositide 3-kinase (PI3K) phosphorylation of the 3' position on membrane bound phosphoinositide lipids. After an RTK or GPCR is activated (in this case an RTK), the SH2 domain of the p85 subunit of PI3K is recruited to and binds to a phosphorylated tyrosine residue on the transmembrane receptor. Once bound, the p110 catalytic subunit facilitates the phosphorylation of the 3' position on the inositol ring of membrane bound phosphoinositides through the exchange of a OH^- group with a PO_4^- group.

Whereas the importance of PI3K signaling in cell motility is well established, its place in chemotactic gradient sensing has been the subject of some controversy. Initially, it was suggested that PI3K acted as the single cellular compass, the sole protein responsible for

directional sensing and migration in response to spatial cues (Weiner, 2002). Although the general importance of PI3K signaling in governing cell motility remains widely accepted, it has been shown recently that other signaling pathways can mediate PI3K-independent chemotaxis, at least in certain cell contexts. Multiple studies of *Dictyostelium discoideum* and neutrophils have demonstrated that PI3K signaling is required for maximal migration speed (Heit, Liu, Colarusso, Puri, & Kubes, 2008) and aids in proper cell orientation in a shallow chemoattractant gradient (Bosgraaf et al., 2008; Gruver, Wikswo, & Chung, 2008). But, at least in *Dictyostelium*, it is established that PI3K signaling is not absolutely required for chemotaxis (Hoeller & Kay, 2007; Kolsch, Charest, & Firtel, 2008). Other gradient sensing pathways that have been implicated in *Dictyostelium* include phospholipase A2, soluble guanylyl cylases and cGMP (Veltman, Keizer-Gunnik, & Van Haastert, 2008; Veltman & van Haastert, 2008), RacG (Somesh, 2006), myosin II heavy chain kinase C (Rubin, 2002), ERK2 (Maeda, 1997), and PIP_3-independent activation of Akt at the leading edge (Kamimura, 2008)

1.3.3 Rho Family GTPases

Rho family GTPases, through their control of actin cytoskeletal dynamics, are central regulators of cell polarity, cell migration, vesicle trafficking, and cytokinesis. Like Ras GTPases, they cycle between inactive, GDP-bound, and active, GTP-bound, states (Figure 1.6). This switch is modulated by three types of proteins. Guanine nucleotide exchange factors (GEFs) catalyze the release of GDP, which is replaced by GTP due to the higher concentration of GTP in the cytosol, whereas GTPase-activating proteins (GAPs) enhance the hydrolysis of GTP to GDP. Guanine nucleotide-dissociation inhibitors (GDIs) regulate the interaction of GTPase proteins with the plasma membrane by sequestering the inactive, GDP-bound form in the cytosol. The dissociation of the GDI and insertion of the GTPase in the plasma membrane allows GEF binding and activation of downstream signaling (Figure 1.6). The most studied and highly conserved Rho GTPases - Rac, RhoA, and Cdc42 - have been shown to play essential roles in cell polarity, directional sensing, and migration. Preliminary studies with these three proteins were conducted via overexpression studies with

dominant negative and constitutively active mutants (Heasman & Ridley, 2008) and then, more recently, with siRNA gene silencing. These preliminary experiments were useful in

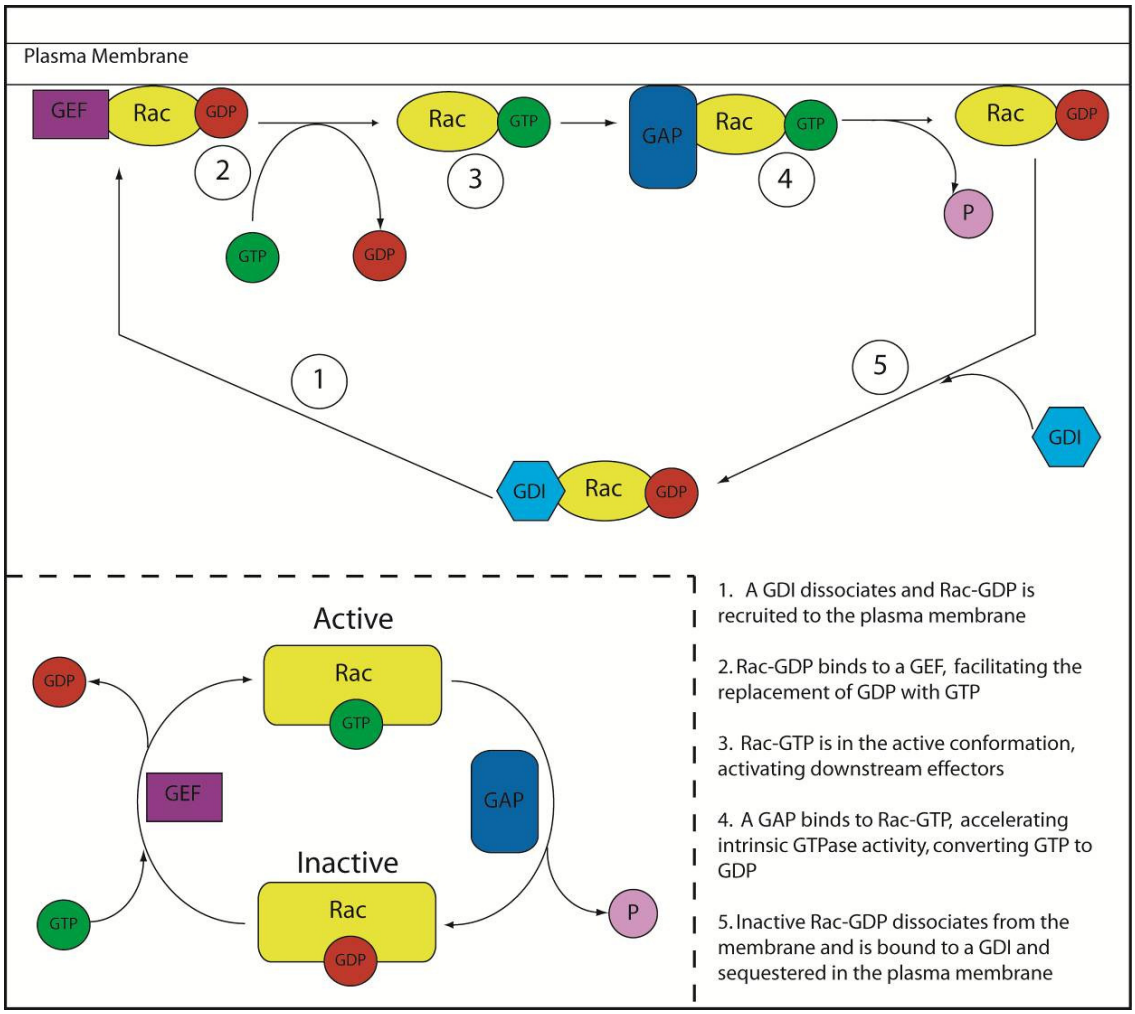

Figure 1.6 Activation cycle of Rho family GTPases. Rho-family GTPases cycle between an active GTP-bound state and an inactive GDP-bound state which is facilitated by GAPs, GEFs and GDIs (inset). A GDP-bound Rac is bound to a GDI in the cytosol. (**1**) The GDI dissociates from the complex causing Rac-GDP recruitment to the plasma membrane where it binds a GEF. (**2**) The GEF facilitates the removal of the GDP which is replaced by the highly abundant GTP, which cause Rac to enter an active conformation (**3**). (**4**) A GAP then accelerates the intrinsic GTPase behavior of Rac, changing GTP to GDP and thus inactivating the complex. (**5**) Rac-GDP is bound by the GDI causing dissociation from the membrane. This process is identical for other members of the family such as Cdc42 and Rho.

determining the more qualitative effects of the Rho family GTPases on cell migration and proliferation; however, with the advent of more quantitative live-cell imaging techniques and

highly selective Rho, Rac and Cdc42 probes, our understanding of their functions has increased dramatically. Herein we highlight some of the recent publications that demonstrate the precise spatial and temporal activation dynamics of these proteins and how their activity is directly related to membrane dynamics, focal adhesion turnover and changes in the actin cytoskeleton - all of which are important for directed cellular migration.

Rac

The Rac subfamily of Rho-family GTPases, including Rac1, Rac2, Rac3, and RhoG, promote lamellipodium formation and membrane ruffling and seem to be essential for chemotaxis. Rac1 is the best characterized of the subfamily and is broadly expressed in many cell types, whereas Rac2 and Rac3 are expressed primarily in hematopoietic and neuronal cells, respectively. RhoG is widely but variably expressed. In preliminary studies, it was found that dominant-negative Rac inhibits lamellipodial protrusion, membrane ruffling, and migration in macrophages, T cells, and fibroblasts and alters their morphology (Ridley, 2001). Lamellipodia are broad, sheet-like membrane protrusions that are produced by an extensive dendritic network of cross-linked actin filaments that defines a migrating cell's leading edge. Rac proteins promote actin polymerization in lamellipodia (Figure 1.7) through multiple pathways, such as through actin nucleating proteins like the Arp2/3 complex (Jaffe & Hall, 2005) and, through the actin-severing protein cofilin, by increasing the density of free F-actin barbed ends (Wang, Eddy, & Condeelis, 2007).

In neutrophils, both Rac1 and Rac2 are required for efficient polarization and chemotaxis (Sun et al., 2004) as well as for proper actin polymerization in lamellipodium (Sun, Magalhaes, & Glogauer, 2007). A slightly different trend is observed in macrophages, where Rac-1 null mutants exhibit defects in cell spreading and membrane ruffling but not in migration (Wells, Walmsley, Ooi, Tybulewicz, & Ridley, 2004). In *Dictyostelium*, the Rac-GEF Dock180, controls actin polymerization and has been shown to affect PI3K and PIP_3 accumulation during cell motility (Para et al., 2009). In PDGF-stimulated chemotaxis of fibroblasts, Rac proteins have been shown to affect migration speed but not directionality (Monypenny et al., 2009). In addition to the control of the lamellipodium, Rac plays an

important in role in integrin-mediated adhesion of macrophages and neutrophils (Allen, Jones, Pollard, & Ridley, 1997; Roberts et al., 1999). Recently, the precise spatial and temporal dynamics of Rac have been studied using novel biosensors capable of tracking active Rac in live cells during membrane extension (Machacek et al., 2009). It was demonstrated that Rac1 (and Cdc42) is activated slightly behind the edge of an advancing membrane, implying that it plays a role in the reinforcement and stabilization of protrusions and not necessarily in their initiation.

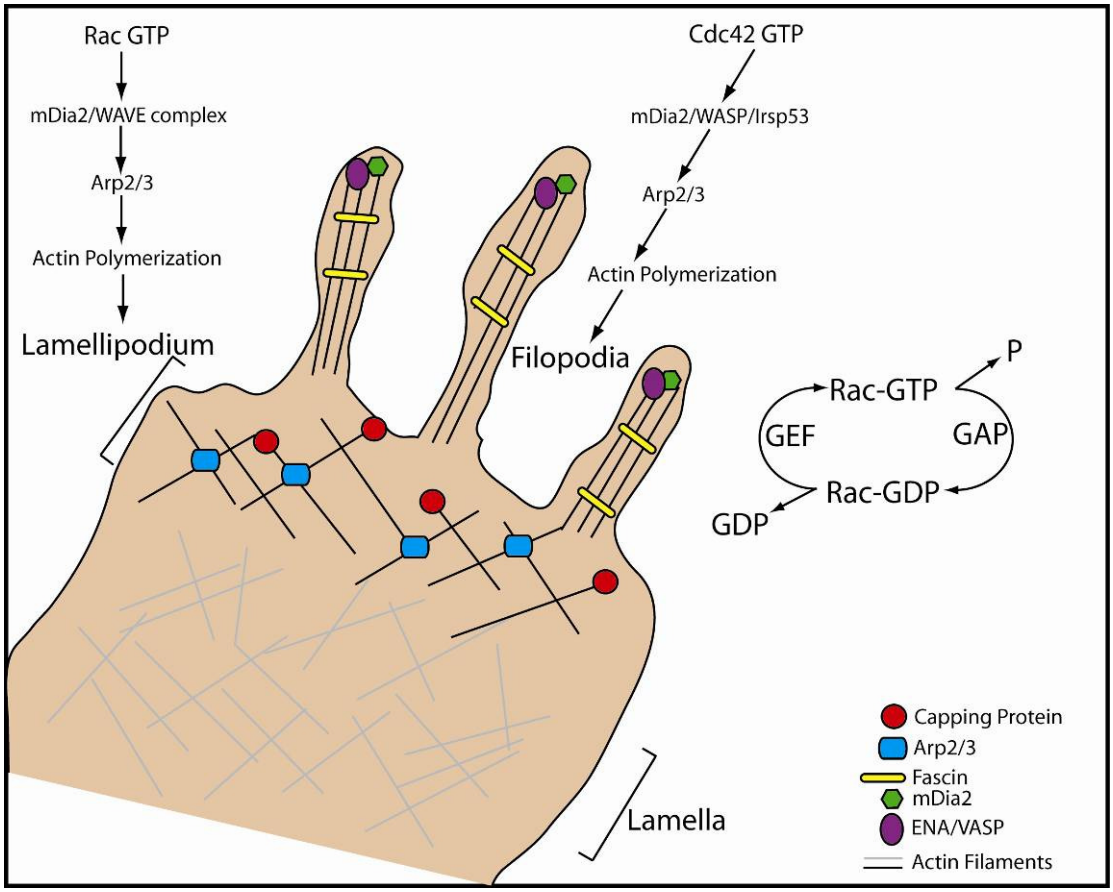

Figure 1.7. Rho family GTPases control actin polymerization during membrane extension. Rac and Cdc42 both play essential roles at the leading edge of a migrating cell. Once activated, Rac-GTP activates a cascade of signals including mDia and Arp2/3 to initiate actin polymerization, which culminates in a type of membrane extension referred to as a lamellipodia, a broad sheet like structure. Cdc42-GTP activates a similar pathway culminating in actin polymerization and membrane protrusions called filopodia, thin protrusion extended from the membrane thought to play a role in gradient sensing. Adapted from Heasman et. al. (Heasman & Ridley, 2008).

Cdc42

Cdc42 plays a conserved role in regulating cell polarity and membrane extensions in migrating cells, albeit in a slightly different manner than Rac proteins. Cdc42 is not present in some of the "professional" migratory cells, such as *Dictyostelium discoideum*; however, it has an essential role in mammalian cells, highlighted by the fact that Cdc42-knockout mice are embryonic lethal at 7.5 days (Chen et al., 2000). The most prominently studied role of Cdc42 is its control of filopodia (Figure 1.7), which are thin, actin-rich plasma membrane protrusions that are thought to function as sensors of the cell's local environment (Mattila & Lappalainen, 2008). Filopodia are also important for establishing nascent adhesions; in fibroblasts, filopodia are seen to extend, adhere to the surface, and then morph into lamellipodia-like protrusions (Guillou et al., 2008). The best characterized pathway for Cdc42 control of filopodia (but not the only one) is through Arp2/3 complex-dependent actin filament nucleation through Wiskott-Aldrich Syndrome Protein (WASP) and N-WASP (Prehoda, Scott, Mullins, & Lim, 2000). Cdc42, along with the abundant lipid $PI(4,5)P_2$, interacts with WASP, which activates Arp2/3 and thus promotes actin polymerization (Stradal & Scita, 2006). In macrophages, Cdc42 controls downstream activation of WASP, and therefore actin polymerization, during CSF-1-mediated chemotaxis (Cammer et al., 2009). In fibroblasts, Cdc42 apparently affect cell speed but not directionality (Monypenny et al., 2009) and plays a role in control actin reorganization through Cortactin (Lai et al., 2009). Further, Cdc42-dependent filopodia serve as a chemoattractant sensing mechanism during neuronal growth cone extension (Gallo & Letourneau, 2004). Beyond its role as a regulatory of actin polymerization, Cdc42 also affects chemotaxis through its regulation of cell polarity, via interactions with the PAR complex (PAR6-PAR3-aPKC) (Pegtel et al., 2007).

Many of the studies evaluating the role of Cdc42 in chemotaxis are often in tandem with experiments involving the role of Rac, most likely due to their similar nature of control of the actin cytoskeleton and membrane extensions. Indeed, certain perturbations such as dominant-negative Rac are known to affect both Rac and Cdc42, clouding the interpretation

of those experiments. With progressive improvements in fluorescent biosensors, it is expected that the specific roles of these proteins in chemotaxis will be better characterized.

Rho

Understanding the role of the Rho subfamily (RhoA, RhoB, and RhoC) in chemotaxis has been the slowest to develop. It was previously thought that Rho proteins only had a small role in chemotaxis, controlling the dissolution of focal adhesions at the cell rear; however, their importance is now better appreciated. This lag in understanding has to do with the relative differences between the three isoforms and how each responds to various inhibitors and knockdowns. Recently, the RhoA GEF, GEF-H1, has been implicated in the control of HeLa chemotaxis by affecting membrane ruffling and protrusion efficiency (Nalbant, Chang, Birkenfeld, Chang, & Bokoch, 2009). Additionally, Rho plays an important role during the endocytic trafficking of receptors, highlighted by recent findings demonstrating that a lack of RhoB impairs PDGF-induced signaling and proliferation (Huang, DuHadaway, Prendergast, & Laury-Kleintop, 2007).

Adding to the complexity of the Rho-family GTPases is the high degree of co-regulatory crosstalk among its members. For example, during membrane protrusion, Rac1 is responsible for the formation of actin-rich structures, while RhoA promotes retrograde actin flow, a transport mechanism by which unsequestered actin monomers are recycled (Kardash et al., 2010). The spatiotemporal coordination between Rho, Rac, and Cdc42 during membrane extensions was highlighted recently in live-cell imaging studies (Machacek et al., 2009), with activation of Rho and membrane protrusion apparently preceding the activation of Rac and Cdc42. Furthermore, the suspected crosstalk between these proteins has been implicated in tandem with PI3K signaling (Cammer et al., 2009), macrophage motility (Ridley, 2001), phagocytosis (Nakaya, Tanaka, Okabe, Hanayama, & Nagata, 2006; Underhill & Ozinsky, 2002), and actin cytoskeletal dynamics (Bristow et al., 2009), either through direct interactions or via binding with the GEFs and GAPs associated with these proteins. Although much is known about the roles of Rac, Cdc42, and Rho proteins, there is

still much to learn about their interactions with effector proteins and their precise roles in chemotaxis.

1.3.4 Dynamics of the actin cytoskeleton

Dynamic actin rearrangements drive membrane protrusion during cell migration. As previously stated, the signaling pathway initiated by chemoattractant receptors and amplified through PI3K and the Rho family GTPases culminates in the polymerization of the actin cytoskeleton. The polymerization of actin monomers into elongated filaments is mediated by nucleating factors, proteins responsible for the formation of a 'nucleus' of actin monomers from which the actin filament is propagated. These factors facilitate polymerization by creating free barbed ends, either by uncapping them or severing actin filaments. The best characterized of the actin nucleating factors are the Arp2/3 complex and formins (Pollard, 2007). The Arp2/3 complex functions by binding to the side of a pre-existing filament, creating a new nucleation core and the beginnings of a second actin filament that branches from the first at a defined angle of 70 degrees. The Arp2/3 complex is activated by members of the aforementioned WASP family (WASP, N-WASP, and WAVE) downstream of Cdc42 and Rac. The other well established group of nucleating factors, the formins, are defined by a formin homology 2 domain that directly promotes actin nucleation by enhancing filament elongation to generate unbranched actin filaments (Wallar, 2003). One such formin, mDia1, has been implicated as an essential part of neutrophil chemotaxis through the RhoA/ROCK pathway (Shi et al., 2009). Other regulators of actin polymerization include Ena/VASP family members (Benz, 2009), actin-binding protein-1 (Cortesio, 2010), cortactin (Lai et al., 2009), cofilin (Sidani et al., 2007). Actin polymerization is halted by capping protein, which bind the barbed end of the actin filament and prevent addition of actin monomers. All of these proteins act in concert to regulate the density of actin filaments and rates of actin polymerization to form leading edge structures such as lamellipodia and filopodia (Figure 1.7).

The actin filaments elongate in such a manner that the plus ends (ATP-bound actin) face the extending portion of the membrane while the minus ends (ADP-bound actin) face

the lamella, the most stable region of the actin cytoskeleton that resides between the lamellipodia and the cell body (Cramer, 1997). Actin polymerizes near the leading edge of the cell, which is accompanied by coherent retrograde motion of the F-actin network away from the leading edge, is referred to as retrograde flow (Gardel et al., 2008). Retrograde flow of actin has implications for the control of leading edge protrusion and maturation of focal adhesions.

1.3.5 Focal adhesion assembly and turnover

Membrane protrusion proceeds in concert with the formation and maturation of integrin-mediated adhesion complexes, which form predominantly at the leading edge of the migrating cell. They are defined as focal complexes, focal adhesions, and fibrillar adhesions depending on their size, location, and dependence on different members of the Rho family GTPases (Deakin & Turner, 2008). Near the leading edge, the actin cytoskeleton dictates where and how these adhesions assemble, mature, and disassemble by serving as a dynamic scaffold network; however, migration-related signaling pathways converge on these integrin-mediated adhesions and regulate actin polymerization in a cycle of feedback control (Vicente-Manzanares, Choi, & Horwitz, 2009). Once the integrins engage the ECM, intracellular proteins such as talin, paxillin, focal adhesion kinase (FAK), and vinculin are recruited to the complex and function to initiate actin polymerization, with talin promoting tighter integrin-ECM interaction, paxillin serving as a scaffold for binding of other signaling proteins, and vinculin acting as an actin-bridging protein (Figure 1.8A).

The maturation of a nascent, or newly formed, focal adhesion to a stable one also requires control of actin polymerization. As the leading edge advances, nascent adhesions assemble at a rate that correlates linearly with that of protrusion (Choi, 2008), while as actin filaments disassemble at the lamellipodia/lamella boundary, most of the nascent adhesions are turned over (Figure 1.8B); however, some adhesions elongate at this boundary and mature centripetally, bound to actin stress fibers through an α-actinin linkage under tension generated by non-muscle myosin (myosin II) motors (Vicente-Manzanares et al., 2009). Elucidating the signaling mechanisms regulating adhesion dynamics is an active thrust of

chemotaxis research, with recent studies implicating Erk1/2 (Smith, Jaffer, Chernoff, & Ridley, 2008), coronin 2A (Marshall, Aloor, & Bear, 2009), PAK1 (Parrini, Camonis, Matsuda, & de Gunzburg, 2009), and PTPD1 (Carlucci et al., 2008) as important components of a scaffold complex that affects both the initiation and maturation of focal adhesions.

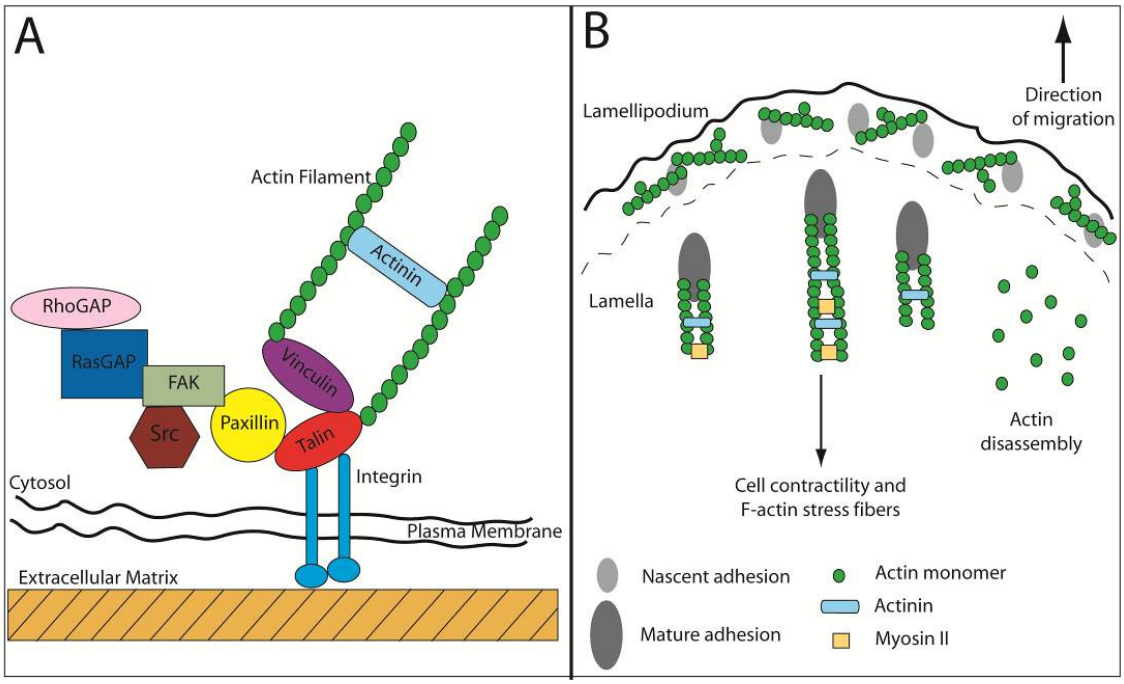

Figure 1.8 Focal adhesion maturation and turnover. (**A**) Integrins bind to the extracellular matrix and recruit signaling molecules such as talin, paxillin, and viniculin which facilitates the polymerization of actin monomers to form actin filaments. (**B**) Nascent focal adhesions form in the lamellipodium at a rate similar to that of membrane protrusions. As actin filaments begin to disassemble near the lamellipodium/lamella boundary most focal adhesions disassemble; however, some of these adhesions elongate forming mature, stable focal adhesions along actin filaments that are crosslinked with α-actinin and stabilized by myosin II.

1.4 METHODS FOR STUDYING CHEMOTAXIS

Over the past forty years, new methods have been developed to study the aforementioned signaling processes and how they govern chemotaxis. These methods range from endpoint studies of cell populations to high-resolution imaging of individual living cells. In this section, we discuss techniques that have been used to study chemotaxis, with emphasis on their relative merits.

1.4.1 Boyden chamber

In 1962, the first method used to quantify chemotaxis was developed by Stephen Boyden (Boyden, 1962). The Boyden chamber, now commonly referred to as the Transwell Assay, is comprised of two reservoirs separated by a porous membrane upon which cells are seeded. The bottom reservoir is charged with the higher concentration of chemoattractant, and thus a gradient forms across the membrane by diffusion. Chemotactic cells are stimulated to migrate through the porous membrane, and their appearance on the other side some time later constitutes the basis of the assay (Figure 1.9A). Because the cells are difficult to see against the porous membrane, they are generally fixed and stained, and the cell numbers in several fields are counted. This assay is easy to perform and does not require specialized equipment. It is arguably the method of choice for high-throughput screening, as the number of chambers assessed in parallel is readily scaled up.

Due to the invasive nature of the Boyden chamber assay, chemotaxis of neutrophils, carcinoma cell lines, and fibroblasts have been the most commonly studied using the Boyden chamber. Recent publications have investigated key regulators of the chemotactic pathway using pharmacological inhibitors, gene knockouts or siRNA silencing. The role of PI3K in chemotaxis has been examined in PDGF-stimulated fibroblasts (Banyard, Anand-Apte, Symons, & Zetter, 2000; Watson, Morris, & Chan, 2009) and smooth muscle cells (Choi et al., 2010) and in G-CSF-stimulated neutrophils (Nakamae-Akahori et al., 2006). Other regulatory proteins such as the 3' phosphatase PTEN (Adachi et al., 2007), the Rho-family GTPases (Lecut et al., 2009), and PDGF receptor endocytosis (Kawada et al., 2009) have been examined in conjunction with chemotaxis. The Boyden chamber has also found great utility in the study of invasive carcinoma cell cells. The signaling of effectors such as adhesive proteins (Oxmann et al., 2008), Rho-family GTPases (Kusama et al., 2006; Niggli, Schlicht, & Affentranger, 2009), the Rho-kinase ROCK (Salhia et al., 2005), and matrix metalloproteases (Fisher et al., 2006) have thus been implicated in cell invasiveness.

The Boyden chamber assay also suffers from several known limitations. Chief among them is that the chemotactic gradient and migration across the membrane are time-dependent, whereas quantification is performed at a particular endpoint. There is no

spatiotemporal control of the chemotactic gradient, which is expected to depend strongly on whether or not the fluids in the reservoirs are agitated, and one cannot directly visualize the cells as they move. Therefore, one can only infer the gross effects of molecular perturbations. Another caveat is that control experiments, in which both reservoirs contain equal chemoattractant concentrations, need to be performed to distinguish chemotaxis from enhanced random migration (chemokinesis).

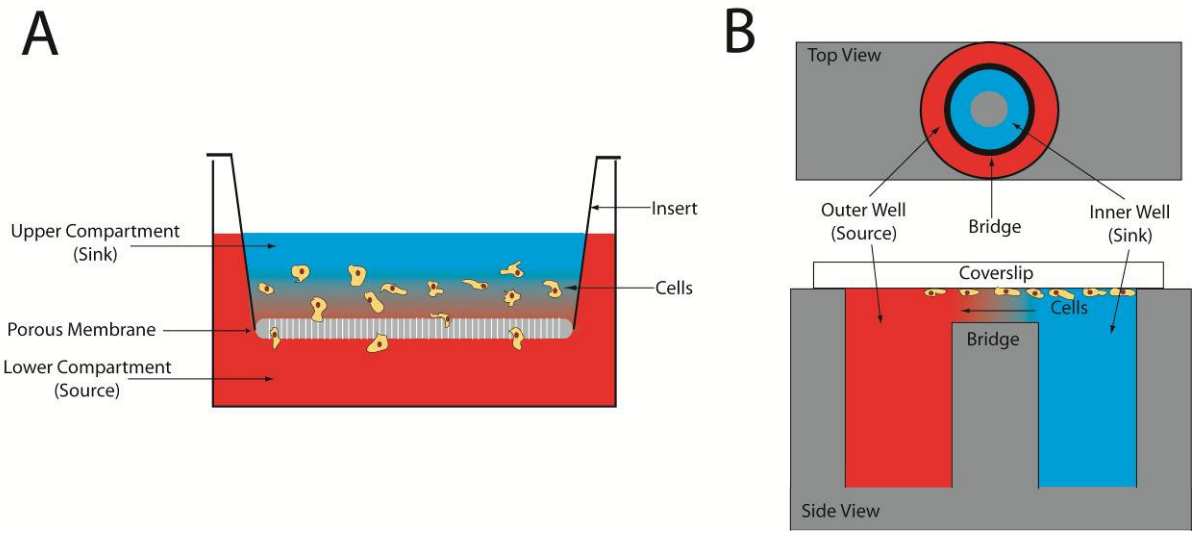

Figure 1.9 Chemotaxis chambers. (**A**) The Boyden chamber (also called the Transwell assay) is a qualitative tool used to study chemotaxis which consists of a lower compartment filled with a chemoattractant (the source) and a top compartment (the sink). The insert (top compartment) has a porous membrane at the bottom which allows chemoattractant to diffuse from the lower to the upper compartments and the cells to migrate in the direction of this gradient. (**B**) The Dunn chamber (a deviation from the Zigmond chamber) is another chemotaxis chamber which develops a gradient from a source of chemoattractant (the outer well) to a sink (the inner well). Cells are plated on a glass coverslip which is fixed to the top of the chamber and a gradient develops across the bridge between the inner and outer wells, which is slightly shorter. In both (**A**) and (**B**) the chemoattractant solution is in red and the buffer solution is in blue.

1.4.2 Dunn and Zigmond chambers

The Zigmond chamber and, later, the Dunn chamber are similar to the Boyden chamber in that the chemotactic gradient forms by diffusion, but they allow for visualization of the migrating cells by light microscopy. The Zigmond chamber, developed in 1977 by Sally Zigmond (Zigmond, 1977, 1988), consists of two parallel channels etched into a glass slide separated by a ridge that lies just below the top surface of the slide. Cells are plated

onto a glass coverslip which is then inverted and placed over the etched channels resulting in a gap between the coverslip and the glass ridge. A small volume of chemoattractant solution is added to one channel (the source) while the same volume of buffer is added to the second channel (the sink), which after some time results in a stable, linear chemoattractant gradient across the cells. The Zigmond chamber has many advantages, with the most prominent being that it produces a reproducible and stable gradient (Postma, 2009). Originally applied to the study of neutrophil chemotaxis, the Zigmond chamber has remained useful in the context of amoeboid chemotaxis. It has been successfully to study the roll of mDia1 (Shi et al., 2009), CD44 (Alstergren et al., 2004), and TNF-α (Vollmer, Alberts, Carper, & Mandell, 1992) during neutrophil polarization and migration as well as studying the role of PI3K in *Dictyostelium* (Bosgraaf et al., 2008).

An improved design was invented by Graham Dunn in 1991 (Zicha, 1997). The Dunn Chamber consists of concentric rings that are filled with sink and source solutions. The two rings are separated by a bridge of a slightly lower height, allowing a linear gradient to be established between the two rings (Figure 1.9B). A coverslip plated with cells is then mounted on top, sealing the device. The Dunn chamber has been used to evaluate the role of Rho-family GTPases on the direction, speed and persistence of PDGF-mediated chemotaxis of fibroblasts (Monypenny et al., 2009). It was also used to study the role of PI3K during *Dictyostelium* chemotaxis and its importance in sensing weaker chemoattractant signals (Takeda, Sasaki, Ha, Seung, & Firtel, 2007). During microglial (macrophages of the brain) migration, this tool was used to study ATP-mediated chemotaxis through the P2Y receptor (Honda et al., 2001; Ohsawa, Irino, Nakamura, Akazawa, & Inoue, 2007). The importance the extracellular matrix protein hyaluronan was also implicated during fibroblast chemotaxis in a Dunn chamber (Tzircotis, Thorne, & Isacke, 2005).

The Zigmond and Dunn chambers share the same disadvantages, namely that they require a fairly long period of time for the gradient to achieve steady state, and they produce gradients of limited steepness; both of these issues directly depend on the distance separating the source and sink reservoirs, and therefore the cells' behavior as a function of time might

depend on where one looks. Perhaps even more critically, although the gradients are very stable at steady state, by the same token they cannot be manipulated during the experiment.

1.4.3 Under agarose assay

The under agarose assay was developed to allow greater control over the positioning, timing and intensity of the chemoattractant gradient delivered to the cells (Nelson, 1975). This method requires the plating of a uniform layer of agarose on either a glass or plastic surface followed by excising voids in the gel at specific locations and distances from one another. The empty portions are then filled with either a cell suspension or a chemoattractant solution. The chemoattractant then diffuses outwards from its well resulting in a gradient, which the cells in the other wells detect and then migrate up. It is called the under-agarose assay because the cells will migrate under the agarose layer from one well to another. As a result, this technique has become popular amongst rapidly migrating cells that can burrow between the agarose and the surface such as neutrophils, monocytes, and, the most common example, *Dictyostelium discoideum*. Studies involving *Dictyostelium* and the under-agarose assay look at a multitude of signaling pathways such as the effect myosin II has on actin filament crosslinking during cell motility (Laevsky & Knecht, 2003), the importance of efficient cytokinesis (Nagasaki & Uyeda, 2008), the cell's elastic properties during chemotaxis (Haupt et al., 2007), the role of cAMP degradation on group migration (Garcia, Rericha, Heger, Goldsmith, & Parent, 2009), and the effect of cGMP on chemotaxis (Veltman & van Haastert, 2008). In neutrophils, there have been studies on the role of the fMLP receptor (Heit et al., 2008; Riesselman et al., 2007), the kinin B1 receptor (Ehrenfeld et al., 2006), and Toll-like receptor agonists (Sabroe, Jones, Whyte, & Dower, 2005) on efficient chemotaxis. The under agarose assay has also been used to evaluate the effect of a gradient of nerve growth factor on neurite outgrowth of the developing axon (Cao & Shoichet, 2001). Furthermore, due to the advantages of this method, it is continually being adapted to better suit the needs of researchers to evaluate efficient chemotaxis (Laevsky & Knecht, 2001) and has even been modified to study 3D chemotaxis (Haessler, Kalinin, Swartz, & Wu, 2009).

The under agarose assay has several desirable features. The gels are relatively easy and cheap to make and provide cells with an environment that is similar to *in vivo* conditions. This assay also allows for significant control over the gradient profile by careful placement of chemoattractant sources that can generate a wide variety of combinatorial gradients. Unfortunately, as with the methods discussed above, there is no control of the gradient after the experiment is initiated.

1.4.4 Micropipette-generated gradients

A drawn glass micropipette is arguably the most versatile of methods for delivering a movable point source of chemoattractant. In this method, a glass capillary is heated and pulled apart, forming a fine glass tip with an internal diameter as small as 1 µm. The glass capillary is then attached to a syringe, backfilled with ~5-25 µL of chemoattractant solution and loaded into a microinjection apparatus. The capillary tip is then carefully positioned under the microscope using a mechanical micromanipulator. The solution is ejected from the pipette into the extracellular environment, either pneumatically or using a volumetric stepper, producing a radial gradient emanating from the tip (Figure 1.10B). The tip is placed just above the focal plane of the cells, which respond to the chemoattractant by migrating towards the tip (Figure 1.10C-E). The flow rate at the tip is determined by the force applied by the pump and the internal diameter of the pipette, and the chemoattractant concentration profile is determined by a combination of convective flow and diffusion. An alternative to this method is to simply allow the chemoattractant to passively diffuse from the pipette. This might seem to make the gradient more predictable; however, this is not the case when one accounts for the time-dependent gradient that develops inside the pipette (Postma, 2009).

The micropipette method offers a number of advantages for the study of chemotaxis (Keenan & Folch, 2008). The tip position is readily controlled both before and during the experiment, and multiple pipettes can be used to generate combinatorial gradients. For these reasons, the method has been applied with great success to the study of fast-moving amoeboid cells. This tool has been used to study how PI3K signaling affects cell speed and chemotactic accuracy in *Dictyostelium* (Gruver et al., 2008) and the role of signal

amplification in neutrophils (Onsum, Wong, Herzmark, Bourne, & Arkin, 2006). Also in *Dictyostelium*, work has been performed studying the importance the 3' PIs and PI3K during cAMP gradient sensing (Takeda et al., 2007) and the controlling effect of adenylyl cyclase (ACA) during chemotaxis (Bagorda et al., 2009).

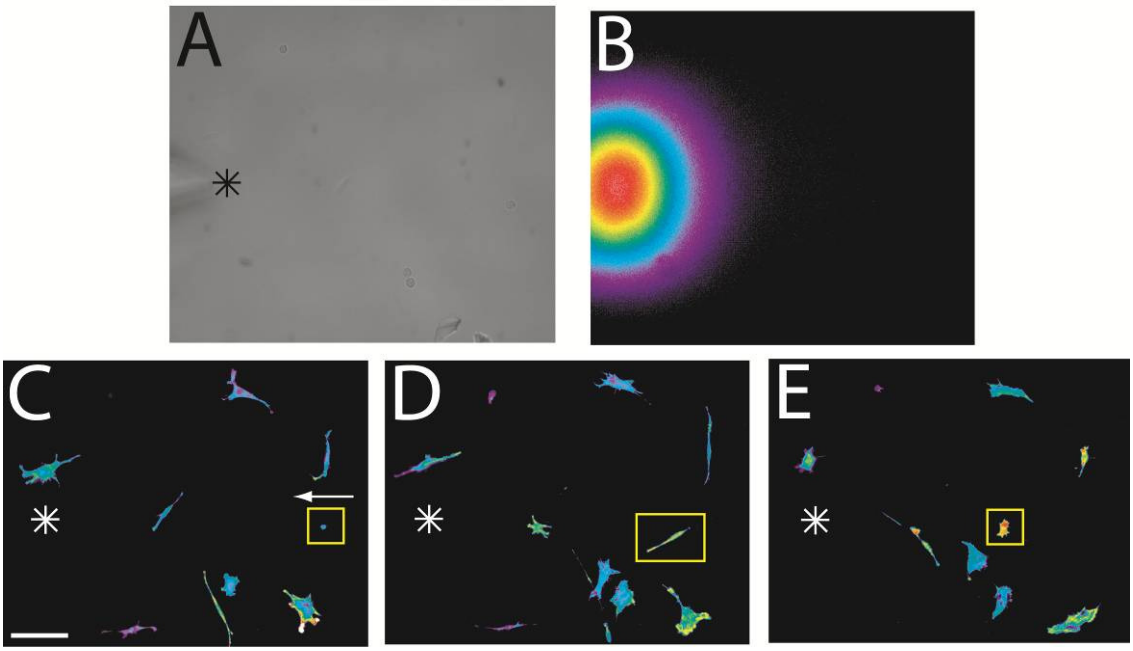

Figure 1.10 Chemotaxis towards a micropipette tip. A micropipette is paired with TIRF microscopy to study PI3K dynamics during PDGF-mediated fibroblast chemotaxis. (**A**) A bright field image shows the pipette location in the same focal plane as the cells while (**B**) TIRF microscopy shows a radial gradient emerging from the pipette tip. (**C-E**) Fibroblasts migrate during a 6 hour time course in response to the PDGF gradient generated by the micropipette. The asterisk represents the tip location and the yellow box highlights a single cell migrating up the gradient. Scale bar is 100 µm.

Other uses of the micropipette method include an investigation into the role of RhoA in establishing a front and back side of a polarized neutrophil during fMLP-mediated chemotaxis (Wong, Pertz, Hahn, & Bourne, 2006), the spatial distribution of C5a receptors from the front to the back during neutrophil chemotaxis (Servant, Weiner, Neptune, Sedat, & Bourne, 1999), and the role of MCSF and MCP-1 during monocyte invasion into endothelial cells as a part of the immune response (Shyy et al., 1993). In slower moving cells, the micropipette approach has been used to study the role of the primary cilium during PDGF-

stimulated chemotaxis of fibroblasts (Schneider et al., 2010) and to investigate chemotaxis of human melanoma cells (Dong, Slattery, Rank, & You, 2002).

Although the micropipette method has proven to be a useful tool, it is not without certain limitations. One is the need for pump-driven flow, which makes the gradient rapid to develop but also somewhat unstable. Additionally, significant variability in tip radius between micropipettes affects the reproducibility of the gradient, and the flow rate and pipette volume dictate the maximum duration of the experiment. Perhaps most critically, since the pipette has to be positioned within the same field as the cells, the gradients tend to be steep, > 10% across the cell unless the cell happens to be oriented at a shallow angle relative to the gradient.

1.4.5 Microfluidic devices

During the past fifteen years, there has been a sharp increase in the development of novel microfluidic devices for a spectrum of applications in the fields of cell biology, surface chemistry, organic chemistry, and chemical engineering. Their utility in the context of chemotaxis arises from their ability to produce controllable gradients. Microfluidic devices are made from master molds generated using soft lithography techniques, with polydimethylsiloxane (PDMS) as the predominant material of choice. PDMS is a soft, flexible, unreactive polymer that is optically clear and inexpensive. It can be bound to glass or another layer of PDMS, resulting in increasingly complex designs. One of the first PDMS gradient generators uses a series of serpentine channels to iteratively split and mix fluids from two inlet streams to produce a series of laminar flow streams of varying chemoattractant concentration (Dertinger, Chiu, Jeon, & Whitesides, 2001; Jeon et al., 2000). These streams are combined in the migration chamber, where the step-like pattern is smoothed by lateral diffusion to produce a more linear gradient of varying steepness in the direction perpendicular to the flow. Additionally, this PDMS microfluidics device is capable of controlling more complex gradients that can be altered mid-experiment or maintaining a constant gradient for extended periods of time (hours to days). In the past ten years, increasingly complex designs have been offered that address many of the technical

limitations of the static migration chambers and the micropipette method. These include nanopore, premixer, and hydrogel-capped gradient generators as well as the use of microfluidic devices to produce micropatterned surfaces (Keenan & Folch, 2008). Here we discuss some of the more recent chemotaxis studies using microfluidics devices.

Many of the initial experiments using microfluidics devices to study chemotaxis involved neutrophils, owing to their fast migration and resistance to flow, with the earliest reports on IL-8 gradients (Jeon et al., 2002; Lin et al., 2004, 2005). Further studies with neutrophils have developed more detailed devices capable of studying receptor desensitization (Keenan, Frevert, Wu, Wong, & Folch, 2010) or chemotaxis in response to gradients of greater complexity (Kim, Lokuta, Huttenlocher, & Beebe, 2009). Other chemotactic cell types studied using microfluidic devices include human endothelial cells (Yin, Noren, Wang, Hang, & Levchenko, 2008), metastatic breast cancer cells (Wang, Saadi, Lin, Nguyen, & Jeon, 2004), and neurons (Millet, Stewart, Sweedler, Nuzzo, & Gillette, 2007).

Recently, we have performed preliminary experiments using a PDMS-based microfluidics device to study fibroblast chemotaxis (Figure 1.11A). This angled ladder design is based on a device developed by Saadi and colleagues to study neutrophil migration (Saadi et al., 2007). The device is capable of generating linear gradients of varying steepness. Another advantage is that most of the flow does not pass over the cells due to a large discrepancy in heights between the center and side channels, which is important because the effects of fluid shear on fibroblasts has not yet been characterized to the same extent as for neutrophils (Walker et al., 2005) and endothelial cells (Wang, Heo, & Hua, 2010; Young & Simmons, 2010). Another utility of this device is that it was designed to be compatible with total internal reflection fluorescence (TIRF) microscopy (Figure 1.11B-C; Chapter 3).

In addition to creating novel devices to study chemotaxis, some groups are developing microfluidics devices in conjunction with older, more established methods. A device has been developed to simulate the under-agarose assay using either dendritic cells (Haessler et al., 2009) or the nematode *Caenorhabditis elegans* (Lockery et al., 2008) while

another device has been developed improving upon the scratch assay commonly used to study random fibroblast migration. This device utilizes capillary pressure to generate a 'virgin surface' without any surface alterations commonly associated with scratch a plate with a pipette tip (Doran, Mills, Parker, Landman, & Cooper-White, 2009). Other devices have been developed with biological applications other than cell migration, such as devices used to direct angiogenesis (Barkefors, Thorslund, Nikolajeff, & Kreuger, 2009) or to separate neutrophils from a blood sample (Agrawal, Toner, & Irimia, 2008).

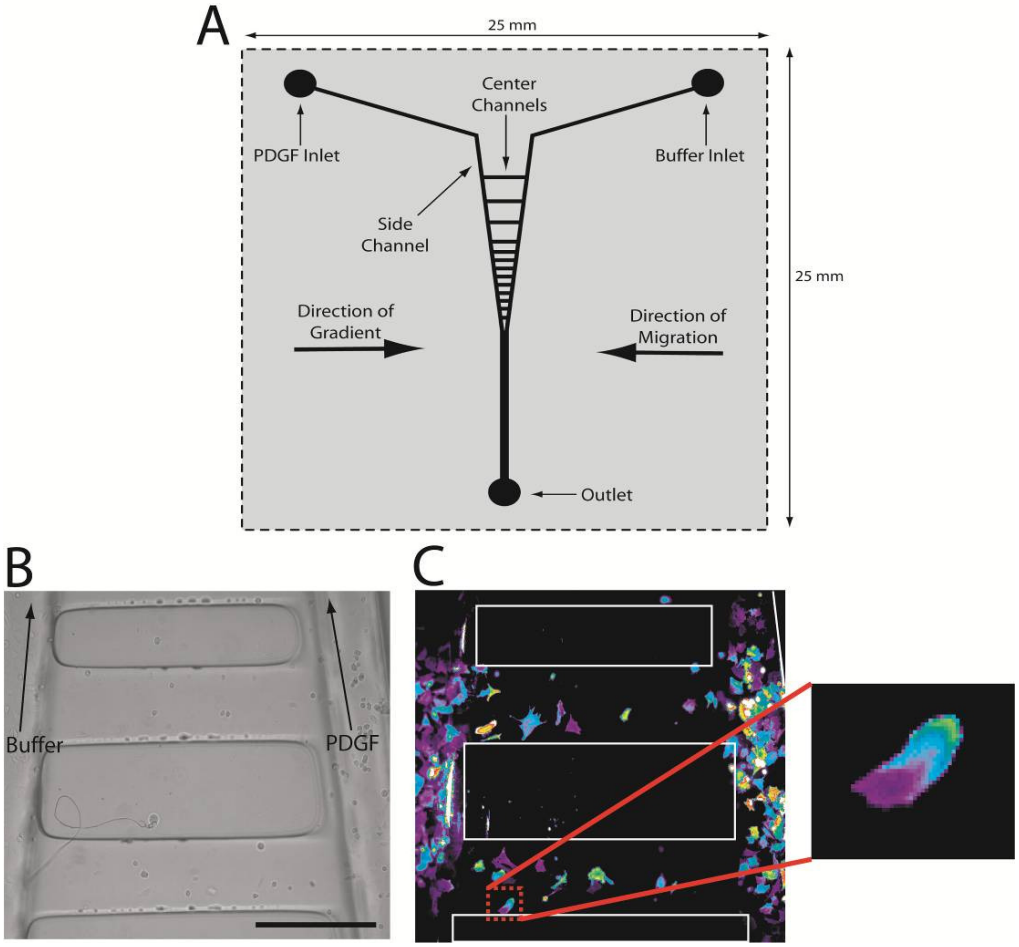

Figure 1.11 PDMS microfluidics device. An example of a flow-driven, PDMS microfluidics device to study fibroblast chemotaxis. (**A**) A solution of chemoattractant (PDGF in this case) is pumped into one inlet and a buffer solution in another, causing a gradient to develop across the center channels by diffusion alone. (**B**) Cells plated in the center channels migrate up the gradient of chemoattractant. (**C**) This particular device is compatible with a fluorescence microscopy technique called total internal reflection fluorescence microscopy, allowing live, single cell spatial and temporal imaging of the contact area of the cell as it migrates.

PDMS-based microfluidics devices have proven their usefulness for studying chemotaxis; however, they should be approached with care. In addition to the potentially detrimental effects of fluid flow, impurities found in PDMS might also be harmful to the cells. It has been observed that some of the oligomers remain un-crosslinked during the PDMS curing reaction, eventually leaching out of the bulk PDMS (Regehr et al., 2009). The exact biological implications of this phenomena are as yet poorly characterized and likely to be cell type-dependent. To minimize this possible hazard, one may treat the PDMS by a series of solvent extractions (Lee, Park, & Whitesides, 2003; Millet et al., 2007).

1.5 CONCLUSIONS

Our molecular-level understanding of chemotaxis has increased dramatically over the past twenty years, due in no small part to the development of novel methods. In a field of study that initially began with simple observations of cells chasing bacteria, we now have a variety methods for generating chemoattractant gradients, to accompany the use of pathway-specific reagents and intracellular biosensors and advanced modalities of fluorescence microscopy. Each of the methods reviewed here has a unique set of advantages and limitations, summarized in Table 1.2. The pattern that emerges is a tradeoff between gradients that develop by diffusion, which can be predictable and stable but slow to develop over appreciable distances, and those aided by convective flow, which generally accelerates the process and allows greater flexibility but tends to make the gradient less stable; flow might also affect the behavior and viability of certain chemotactic cells. Other considerations include limitations on the steepness of the gradient that can be produced and the duration of the experiment. Hence, among the older methods there is some tendency to use micropipettes for fast-moving, amoeboid cells, whereas diffusion chambers tend to be more suitable for slow-moving, mesenchymal cells.

The newest and most versatile tool in the study of chemotaxis is the use of microfluidic devices, which are capable of generating and readily manipulating 2D as well as 3D gradients. Its use, at least among the most technically savvy cell migration researchers, is expected to increase in the coming years. Only by designing and utilizing these new

methods, coupled with the development of novel biosensors for visualizing the wide range of signaling pathways, can research continue to expand on the knowledge of the signals driving chemotaxis and elucidate some of the unknown mechanisms that play vital roles in a cell's ability to sense and respond to external gradients.

Table 1.2 Advantages and limitations of current techniques used in chemotaxis research.

Experimental Technique	Cell types studied	Phenomena studied	Advantages	Limitations
Boyden chamber	Neutrophils, Fibroblasts, Macrophages, Carcinoma cell lines,	Effect of siRNA silencing or soluble inhibitors on signal transduction pathways in the context of migration	Easy to perform and cheap Quick qualitative look at migration Particularly well suited for invasive cell lines	No gradient control Inability to directly visualize cell migration, Incompatible with most microscopy techniques
Zigmond and Dunn chambers	Neutrophils, Dictyostelium discoideum, Fibroblasts, Macrophages	Receptor-mediated chemotaxis and the effect of Rho family GTPases and PI3K on cell speed, directionality, persistence	Reproducable, mathematically predictable gradients, Direct visualization of cells, Quantitative evaluation of cell migration	No utility in gradient control - only one type of gradient can be established, Only viable over short time courses Solution evaporates over time (Zigmond chamber)
Under-agarose assay	Neutrophils, Dictyostelium discoideum, Neuronal cells	GPCR receptor-mediated chemotaxis, actin polymerization dynamics, Effect of steep/shallow gradients on efficient migration	Can produce more versatile gradients depending on agar placement, Direct visualization of cells, Compatible with a many microscopy techniques	Cannot alter the gradient profile once the agar has been placed, Poor gradient reproducibility, Not very compatible with slow moving/non-burrowing cells
Micropipette	Neutrophils, Fibroblasts, Dictyostelium discoideum, monocytes, neuronal cells,	3′ PI signaling during receptor-mediated chemotaxis, Establishing cell polarization, The role of PI3K and ACA during cAMP-mediated chemotaxis	Gradient can be placed in the same focal plane as the cell, Can change gradient location mid-experiment, Direct visualization of cells with many microscopy techniques	Poor gradient control and reproducibility, Day-to-day variability due to capillaries or needle position, Reliance on microinjector impairs tip placement
PDMS-based Microfluidics Device	Neutrophils, T cells, Fibroblasts, Cancer cell lines, Neuronal cells, Dictyostelium discoideum, and many others	2D and 3D receptor-mediated chemotaxis, effects of steep vs. shallow gradients on the chemotactic response, micropatterned surfaces to study the haptotactic response, cell sorting, micro-reactions	Great spatial and temporal control of the gradient, Highly reproducible, Relatively easy fabrication process allowing for rapid production of novel designs	Effects of bulk PDMS on cells and their microenvironment is still relatively unknown, Negative implications associated with shear affects on cell viability, Requires expertise in soft lithography techniques to create new devices

1.6 REFERENCES

Adachi, T., Hanaka, S., Masuda, T., Yoshihara, H., Nagase, H., & Ohta, K. (2007). Transduction of phosphatase and tensin homolog deleted on chromosome 10 into eosinophils attenuates survival, chemotaxis, and airway inflammation. *JOURNAL OF IMMUNOLOGY, 179*(12), 8105-8111.

Agrawal, N., Toner, M., & Irimia, D. (2008). Neutrophil migration assay from a drop of blood. *LAB ON A CHIP, 8*(12), 2054-2061.

Alberts, B., Johnson A, Lewis J, Raff M, Roberts K and Walter P. (2002). Signaling through g-protein-linked cell-surface receptors. In *Molecular biology of the cell 4th edition*.New York, NY: Garland Science.

Allen, W. E., Jones, G. E., Pollard, J. W., & Ridley, A. J. (1997). Rho, rac and cdc42 regulate actin organization and cell adhesion in macrophages. *Journal Of Cell Science, 110*, 707-720.

Alstergren, P., Zhu, B., Glougauer, M., Mak, T., Ellen, R., & Sodek, J. (2004). Polarization and directed migration of murine neutrophils is dependent on cell surface expression of cd44. *CELLULAR IMMUNOLOGY, 231*(1-2), 146-157.

Bagorda, A., Das, S., Rericha, E., Chen, D., Davidson, J., & Parent, C. (2009). Real-time measurements of camp production in live dictyostelium cells. *JOURNAL OF CELL SCIENCE, 122*(21), 3907-3914.

Banyard, J., Anand-Apte, B., Symons, M., & Zetter, B. (2000). Motility and invasion are differentially modulated by rho family gtpases. *ONCOGENE, 19*(4), 580-591.

Barczyk, M., Carracedo, S., Gullberg, D. (2010). Integrins. *Cell and Tissue Research, 339*(1), 269-280.

Barkefors, I., Thorslund, S., Nikolajeff, F., & Kreuger, J. (2009). A fluidic device to study directional angiogenesis in complex tissue and organ culture models. *LAB ON A CHIP, 9*(4), 529-535.

Benz, P. M., Blume, C., Seifert, S., et.al. (2009). Differential vasp phosphorylation controls remodeling of the actin cytoskeleton. *Journal of Cell Science, 122*, 3954-3965.

Bosgraaf, L., Keizer-Gunnink, I., & van Haastert, P. (2008). Pi3-kinase signaling contributes to orientation in shallow gradients and enhances speed in steep chemoattractant gradients. *JOURNAL OF CELL SCIENCE, 121*(21), 3589-3597.

Bourette, R. P., & Rohrschneider, L. R. (2000). Early events in m-csf receptor signaling. *Growth Factors, 17*(3), 155-166.

Boyden, S. (1962). Chemotactic effect of mixtures of antibody and antigen on polymorphonuclear leucocytes. *JOURNAL OF EXPERIMENTAL MEDICINE, 115*(3), 453-466.

Brazil, D. P., & Hemmings, B. A. (2001). Ten years of protein kinase b signalling: A hard akt to follow. *Trends In Biochemical Sciences, 26*(11), 657-664.

Bristow, J., Sellers, M., Majumdar, D., Anderson, B., Hu, L., & Webb, D. (2009). The rho-family gef asef2 activates rac to modulate adhesion and actin dynamics and thereby regulate cell migration. *JOURNAL OF CELL SCIENCE, 122*(24), 4535-4546.

Cammer, M., Gevrey, J., Lorenz, M., Dovas, A., Condeelis, J., & Cox, D. (2009). The mechanism of csf-1-induced wiskott-aldrich syndrome protein activation in vivo a role for phosphatidylinositol 3-kinase and cdc42. *JOURNAL OF BIOLOGICAL CHEMISTRY, 284*(35), 23302-23311.

Cao, X., & Shoichet, M. (2001). Defining the concentration gradient of nerve growth factor for guided neurite outgrowth. *NEUROSCIENCE, 103*(3), 831-840.

Carlucci, A., Gedressi, C., Lignitto, L., Nezi, L., Villa-Moruzzi, E., Avvedimento, E., et al. (2008). Protein-tyrosine phosphatase ptpd1 regulates focal adhesion kinase autophosphorylation and cell migration. *JOURNAL OF BIOLOGICAL CHEMISTRY, 283*(16), 10919-10929.

Chen, F., Ma, L., Parrini, M., Mao, X., Lopez, M., Wu, C., et al. (2000). Cdc42 is required for pip2-induced actin polymerization and early development but not for cell viability. *CURRENT BIOLOGY, 10*(13), 758-765.

Choi, C. K., Vicente-Manzanares, M., Zareno, J., et. al. (2008). Actin and alpha-actinin orchestrate the assembly and maturation of nascent adhesions in a myosin ii motor-independent manner. *Nature Cell biology, 10*, 1039-1050.

Choi, K., Kim, J., Song, N., Son, J., Hwang, M., Byun, S., et al. (2010). Phosphoinositide 3-kinase is a novel target of piceatannol for inhibiting pdgf-bb-induced proliferation and migration in human aortic smooth muscle cells. *CARDIOVASCULAR RESEARCH, 85*(4), 836-844.

Claesson-Welsh, L. (1994). Platelet-derived growth factor receptor signals. *Journal of Biological Chemistry, 269*, 32023-32026.

Condeelis, J., Pollard, J.W. (2006). Macrophages: Obligate partners for tumor cell migration, invasion, and metastasis. *Cell, 124*(2), 263-266.

Cortesio, C. L., Perrin, B.J., Bennin, D.A., Huttenlocher, A. (2010). Actin-binding protein-1 interacts with wasp-interacting protein to regulate growth factor-induced dorsal ruffle formation. *MOLECULAR BIOLOGY OF THE CELL, 21*, 186-197.

Cramer, L. P. (1997). Molecular mechanism of actin-dependent retrograde flow in the lamellipodia of motile cells. *Frontiers in Bioscience, 2*, d260-270.

Cukierman, E., Pankov, R., Stevens, D.R., Yamada, K.M. (2001). Taking cell-matrix adhesions to the third dimension. *Science, 294*, 1708-1712.

Deakin, N., & Turner, C. (2008). Paxillin comes of age. *JOURNAL OF CELL SCIENCE, 121*(15), 2435-2444.

Dertinger, S., Chiu, D., Jeon, N., & Whitesides, G. (2001). Generation of gradients having complex shapes using microfluidic networks. *ANALYTICAL CHEMISTRY, 73*(6), 1240-1246.

Dong, C., Slattery, M., Rank, B., & You, J. (2002). In vitro characterization and micromechanics of tumor cell chemotactic protrusion, locomotion, and extravasation. *ANNALS OF BIOMEDICAL ENGINEERING, 30*(3), 344-355.

Doran, M., Mills, R., Parker, A., Landman, K., & Cooper-White, J. (2009). A cell migration device that maintains a defined surface with no cellular damage during wound edge generation. *LAB ON A CHIP, 9*(16), 2364-2369.

Doyle, A., Wang, F., Matsumoto, K., & Yamada, K. (2009). One-dimensional topography underlies three-dimensional fibrillar cell migration. *JOURNAL OF CELL BIOLOGY, 184*(4), 481-490.

Durbeej, M. (2010). Laminins. *Cell and Tissue Research, 339*(1), 259-268.

Ehrenfeld, P., Millan, C., Matus, C., Figueroa, J., Burgos, R., Nualart, F., et al. (2006). Activation of kinin b-1 receptors induces chemotaxis of human neutrophils. *JOURNAL OF LEUKOCYTE BIOLOGY, 80*(1), 117-124.

Fisher, K., Pop, A., Koh, W., Anthis, N., Saunders, W., & Davis, G. (2006). Tumor cell invasion of collagen matrices requires coordinate lipid agonist-induced g-protein and membrane-type matrix metalloproteinase-i-dependent signaling. *MOLECULAR CANCER, 5*, -.

Friedl, P., & Wolf, K. (2010). Plasticity of cell migration: A multiscale tuning model. *JOURNAL OF CELL BIOLOGY, 188*(1), 11-19.

Fukata, M., Nakagawa, M., & Kaibuchi, K. (2003). Roles of rho-family gtpases in cell polarisation and directional migration. *Current Opinion In Cell Biology, 15*(5), 590-597.

Gallo, G., & Letourneau, P. (2004). Regulation of growth cone actin filaments by guidance cues. *JOURNAL OF NEUROBIOLOGY, 58*(1), 92-102.

Garcia, G., Rericha, E., Heger, C., Goldsmith, P., & Parent, C. (2009). The group migration of dictyostelium cells is regulated by extracellular chemoattractant degradation. *MOLECULAR BIOLOGY OF THE CELL, 20*(14), 3295-3304.

Gardel, M., Sabass, B., Ji, L., Danuser, G., Schwarz, U., & Waterman, C. (2008). Traction stress in focal adhesions correlates biphasically with actin retrograde flow speed. *JOURNAL OF CELL BIOLOGY, 183*(6), 999-1005.

Gerard, C., & Gerard, N. P. (1994). C5a anaphylatoxin and its 7 transmembrane-segment receptor. *Annual Review Of Immunology, 12*, 775-808.

Gray, A., Van der Kaay, J., & Downes, C. P. (1999). The pleckstrin homology domains of protein kinase b and grp1 (general receptor for phosphoinositides-1) are sensitive and selective probes for the cellular detection of phosphatidylinositol 3,4-bisphosphate and/or phosphatidylinositol 3,4,5-trisphosphate in vivo. *Biochemical Journal, 344*, 929-936.

Gruver, J., Wikswo, J., & Chung, C. (2008). 3 '-phosphoinositides regulate the coordination of speed and accuracy during chemotaxis. *BIOPHYSICAL JOURNAL, 95*(8), 4057-4067.

Guillou, H., Depraz-Depland, A., Planus, E., Vianaya, B., Chaussy, J., Grichine, A., et al. (2008). Lamellipodia nucleation by filopodia depends on integrin occupancy and downstream rac1 signaling. *EXPERIMENTAL CELL RESEARCH, 314*(3), 478-488.

Haessler, U., Kalinin, Y., Swartz, M., & Wu, M. (2009). An agarose-based microfluidic platform with a gradient buffer for 3d chemotaxis studies. *BIOMEDICAL MICRODEVICES, 11*(4), 827-835.

Han, J. W., Luby-Phelps, K., Das, B., Shu, X. D., Xia, Y., Mosteller, R. D., et al. (1998). Role of substrates and products of pi3-kinase in regulating activation of rac-related guanosine triphosphatases by vav. *Science, 279*(5350), 558-560.

Haupt, B., Osbourn, M., Spanhoff, R., de Keijzer, S., Muller-Taubenberger, A., Snaar-Jagalska, E., et al. (2007). Asymmetric elastic properties of dictyostelium discoideum in relation to chemotaxis. *LANGMUIR, 23*(18), 9352-9357.

Heasman, S., & Ridley, A. (2008). Mammalian rho gtpases: New insights into their functions from in vivo studies. *NATURE REVIEWS MOLECULAR CELL BIOLOGY, 9*(9), 690-701.

Heit, B., Liu, L., Colarusso, P., Puri, K., & Kubes, P. (2008). Pi3k accelerates, but is not required for, neutrophil chemotaxis to fmlp. *JOURNAL OF CELL SCIENCE, 121*(2), 205-214.

Hoeller, O., & Kay, R. (2007). Chemotaxis in the absence of pip3 gradients. *CURRENT BIOLOGY, 17*(9), 813-817.

Honda, S., Sasaki, Y., Ohsawa, K., Imai, Y., Nakamura, Y., Inoue, K., et al. (2001). Extracellular atp or adp induce chemotaxis of cultured microglia through g(i/o)-coupled p2y receptors. *JOURNAL OF NEUROSCIENCE, 21*(6), 1975-1982.

Huang, M., DuHadaway, J., Prendergast, G., & Laury-Kleintop, L. (2007). Rhob regulates pdgfr-beta trafficking and signaling in vascular smooth muscle cells. *ARTERIOSCLEROSIS THROMBOSIS AND VASCULAR BIOLOGY, 27*(12), 2597-2605.

Jaffe, A., & Hall, A. (2005). Rho gtpases: Biochemistry and biology. *ANNUAL REVIEW OF CELL AND DEVELOPMENTAL BIOLOGY, 21*, 247-269.

Jeon, N., Baskaran, H., Dertinger, S., Whitesides, G., Van de Water, L., & Toner, M. (2002). Neutrophil chemotaxis in linear and complex gradients of interleukin-8 formed in a microfabricated device. *NATURE BIOTECHNOLOGY, 20*(8), 826-830.

Jeon, N., Dertinger, S., Chiu, D., Choi, I., Stroock, A., & Whitesides, G. (2000). Generation of solution and surface gradients using microfluidic systems. *LANGMUIR, 16*(22), 8311-8316.

Kamimura, Y., Xiong, Y., et. al. (2008). Pip3-independent activation of torc2 and pkb at the cell's leading edge mediates chemotaxis. *Current Biology, 18*(14), 1034-1043.

Kardash, E., Reichman-Fried, M., Maitre, J., Boldajipour, B., Papusheva, E., Messerschmidt, E., et al. (2010). A role for rho gtpases and cell-cell adhesion in single-cell motility in vivo. *NATURE CELL BIOLOGY, 12*(1), 47-U112.

Kawada, K., Upadhyay, G., Ferandon, S., Janarthanan, S., Hall, M., Vilardaga, J., et al. (2009). Cell migration is regulated by platelet-derived growth factor receptor endocytosis. *MOLECULAR AND CELLULAR BIOLOGY, 29*(16), 4508-4518.

Keenan, T., & Folch, A. (2008). Biomolecular gradients in cell culture systems. *LAB ON A CHIP, 8*(1), 34-57.

Keenan, T., Frevert, C., Wu, A., Wong, V., & Folch, A. (2010). A new method for studying gradient-induced neutrophil desensitization based on an open microfluidic chamber. *LAB ON A CHIP, 10*(1), 116-122.

Kim, D., Lokuta, M., Huttenlocher, A., & Beebe, D. (2009). Selective and tunable gradient device for cell culture and chemotaxis study. *LAB ON A CHIP, 9*(12), 1797-1800.

Kolsch, V., Charest, P., & Firtel, R. (2008). The regulation of cell motility and chemotaxis by phospholipid signaling. *JOURNAL OF CELL SCIENCE, 121*(5), 551-559.

Kusama, T., Mukai, M., Endo, H., Ishikawa, O., Tatsuta, M., Nakamura, H., et al. (2006). Inactivation of rho gtpases by p190 rhogap reduces human pancreatic cancer cell invasion and metastasis. *CANCER SCIENCE, 97*(9), 848-853.

Laevsky, G., & Knecht, D. (2001). Under-agarose folate chemotaxis of dictyostelium discoideum amoebae in permissive and mechanically inhibited conditions. *BIOTECHNIQUES, 31*(5), 1140-+.

Laevsky, G., & Knecht, D. (2003). Cross-linking of actin filaments by myosin ii is a major contributor to cortical integrity and cell motility in restrictive environments. *JOURNAL OF CELL SCIENCE, 116*(18), 3761-3770.

Lai, F., Szczodrak, M., Oelkers, J., Ladwein, M., Acconcia, F., Benesch, S., et al. (2009). Cortactin promotes migration and platelet-derived growth factor-induced actin reorganization by signaling to rho-gtpases. *MOLECULAR BIOLOGY OF THE CELL, 20*(14), 3209-3223.

Lauffenburger, D., & Horwitz, A. (1996). Cell migration: A physically integrated molecular process. *CELL, 84*(3), 359-369.

Lecut, C., Frederix, K., Johnson, D., Deroanne, C., Thiry, M., Faccinetto, C., et al. (2009). P2x(1) ion channels promote neutrophil chemotaxis through rho kinase activation. *JOURNAL OF IMMUNOLOGY, 183*(4), 2801-2809.

Lee, J., Park, C., & Whitesides, G. (2003). Solvent compatibility of poly(dimethylsiloxane)-based microfluidic devices. *ANALYTICAL CHEMISTRY, 75*(23), 6544-6554.

Liebmann, C. (2004). G protein-coupled receptors and their signaling pathways: Classical therapeutical targets susceptible to novel therapeutic concepts. *Current Pharmaceutical Design, 10*(16), 1937-1958.

Lin, F., Nguyen, C., Wang, S., Saadi, W., Gross, S., & Jeon, N. (2004). Effective neutrophil chemotaxis is strongly influenced by mean il-8 concentration. *BIOCHEMICAL AND BIOPHYSICAL RESEARCH COMMUNICATIONS, 319*(2), 576-581.

Lin, F., Nguyen, C., Wang, S., Saadi, W., Gross, S., & Jeon, N. (2005). Neutrophil migration in opposing chemoattractant gradients using microfluidic chemotaxis devices. *ANNALS OF BIOMEDICAL ENGINEERING, 33*(4), 475-482.

Lockery, S., Lawton, K., Doll, J., Faumont, S., Coulthard, S., Thiele, T., et al. (2008). Artificial dirt: Microfluidic substrates for nematode neurobiology and behavior. *JOURNAL OF NEUROPHYSIOLOGY, 99*(6), 3136-3143.

Machacek, M., Hodgson, L., Welch, C., Elliott, H., Pertz, O., Nalbant, P., et al. (2009). Coordination of rho gtpase activities during cell protrusion. *NATURE, 461*(7260), 99-103.

Maeda, M., Firtel, R.A. (1997). Activation of the mitrogen-activated protein kinase erk2 by the chemoattractant folic acid in dictyostelium. *Journal of Biological Chemistry, 272*(38), 23690-23695.

Marshall, T., Aloor, H., & Bear, J. (2009). Coronin 2a regulates a subset of focal-adhesion-turnover events through the cofilin pathway. *JOURNAL OF CELL SCIENCE, 122*(17), 3061-3069.

Mattila, P., & Lappalainen, P. (2008). Filopodia: Molecular architecture and cellular functions. *NATURE REVIEWS MOLECULAR CELL BIOLOGY, 9*(6), 446-454.

Merlot, S., Firtel, R.A. (2003). Leading the way: Directional sensing through phosphatidylinositol 3-kinase and other signaling pathways. *Journal of Cell Science, 116*(17), 3471-3478.

Millet, L., Stewart, M., Sweedler, J., Nuzzo, R., & Gillette, M. (2007). Microfluidic devices for culturing primary mammalian neurons at low densities. *LAB ON A CHIP, 7*(8), 987-994.

Monypenny, J., Zicha, D., Higashida, C., Oceguera-Yanez, F., Narumiya, S., & Watanabe, N. (2009). Cdc42 and rac family gtpases regulate mode and speed but not direction of primary fibroblast migration

during platelet-derived growth factor-dependent chemotaxis. *MOLECULAR AND CELLULAR BIOLOGY, 29*(10), 2730-2747.

Naccache, P. H., Levasseur, S., Lachance, G., Chakravarti, S., Bourgoin, S. G., & McColl, S. R. (2000). Stimulation of human neutrophils by chemotactic factors is associated with the activation of phosphatidylinositol 3-kinase gamma. *Journal Of Biological Chemistry, 275*(31), 23636-23641.

Nagasaki, A., & Uyeda, T. (2008). Chemotaxis-mediated scission contributes to efficient cytokinesis in dictyostelium. *CELL MOTILITY AND THE CYTOSKELETON, 65*(11), 896-903.

Nakamae-Akahori, M., Kato, T., Masuda, S., Sakamoto, E., Kutsuna, H., Hato, F., et al. (2006). Enhanced neutrophil motility by granulocyte colony-stimulating factor: The role of extracellular signal-regulated kinase and phosphatidylinositol 3-kinase. *IMMUNOLOGY, 119*(3), 393-403.

Nakaya, M., Tanaka, M., Okabe, Y., Hanayama, R., & Nagata, S. (2006). Opposite effects of rho family gtpases on engulfment of apoptotic cells by macrophages. *Journal Of Biological Chemistry, 281*(13), 8836-8842.

Nalbant, P., Chang, Y., Birkenfeld, J., Chang, Z., & Bokoch, G. (2009). Guanine nucleotide exchange factor-h1 regulates cell migration via localized activation of rhoa at the leading edge. *MOLECULAR BIOLOGY OF THE CELL, 20*(18), 4070-4082.

Nelson, C., & Bissell, M. (2006). Of extracellular matrix, scaffolds, and signaling: Tissue architecture regulates development, homeostasis, and cancer. *ANNUAL REVIEW OF CELL AND DEVELOPMENTAL BIOLOGY, 22*, 287-309.

Nelson, R. D., Quie, P.G., Simmons, R.L. (1975). Chemotaxis under agarose: A new and simple method for measuring chemotaxis and spontaneous migration of human polymorphonuclear leukocytes and monocytes. *J. Immunology, 115*, 1650-1656.

Niggli, V., Schlicht, D., & Affentranger, S. (2009). Specific roles of rac1 and rac2 in motile functions of ht1080 fibrosarcoma cells. *BIOCHEMICAL AND BIOPHYSICAL RESEARCH COMMUNICATIONS, 386*(4), 688-692.

Obara, M., Sakuma, T., Fujikawa, K. (2010). The third type iii module of human fibronectin mediates cell adhesion and migration. *Journal of Biochemistry, 147*(3), 327-335.

Ohsawa, K., Irino, Y., Nakamura, Y., Akazawa, C., & Inoue, K. (2007). Involvement of p2x(4) and p2y(12) receptors in atp-induced microglial chemotaxis. *GLIA, 55*(6), 604-616.

Onsum, M., Wong, K., Herzmark, P., Bourne, H., & Arkin, A. (2006). Morphology matters in immune cell chemotaxis: Membrane asymmetry affects amplification. *PHYSICAL BIOLOGY, 3*(3), 190-199.

Oxmann, D., Held-Feindt, J., Stark, A., Hattermann, K., Yoneda, T., & Mentlein, R. (2008). Endoglin expression in metastatic breast cancer cells enhances their invasive phenotype. *ONCOGENE, 27*(25), 3567-3575.

Palecek, S. P., Horwitz, A.F., Lauffenburger, D.A. (1999). Kinetic model for integrin-mediated adhesion release during cell migration. *ANNALS OF BIOMEDICAL ENGINEERING, 27*(2), 219-235.

Para, A., Krischke, M., Merlot, S., Shen, Z., Oberholzer, M., Lee, S., et al. (2009). Dictyostelium dock180-related racgefs regulate the actin cytoskeleton during cell motility. *MOLECULAR BIOLOGY OF THE CELL, 20*(2), 699-707.

Parent, C. A., & Devreotes, P. N. (1999). A cell's sense of direction. *Science, 284*(5415), 765-770.

Parrini, M., Camonis, J., Matsuda, M., & de Gunzburg, J. (2009). Dissecting activation of the pak1 kinase at protrusions in living cells. *JOURNAL OF BIOLOGICAL CHEMISTRY, 284*(36), 24133-24143.

Pegtel, D., Ellenbroek, S., Mertens, A., van der Kammen, R., de Rooij, J., & Collard, J. (2007). The par-tiam1 complex controls persistent migration by stabilizing microtubule-dependent front-rear polarity. *CURRENT BIOLOGY, 17*(19), 1623-1634.

Petrie, R., Doyle, A., & Yamada, K. (2009). Random versus directionally persistent cell migration. *NATURE REVIEWS MOLECULAR CELL BIOLOGY, 10*(8), 538-549.

Pollard, T. D. (2007). Regulation of actin filament assembly by arp2/3 complex and formins. *Annual Review of Biophysics and Biomolecular Structure, 36*, 451-477.

Postma, M., van Haastert J.M. (2009). Mathematics of experimentally generated chemoattractant gradients. *Methods in Molecular Biology, 571*, 473-488.

Prehoda, K., Scott, J., Mullins, R., & Lim, W. (2000). Integration of multiple signals through cooperative regulation of the n-wasp-arp2/3 complex. *SCIENCE, 290*(5492), 801-806.

Rameh, L. E., & Cantley, L. C. (1999). The role of phosphoinositide 3-kinase lipid products in cell function. *Journal Of Biological Chemistry, 274*(13), 8347-8350.

Rathinam, R., Alahari, S.K. (2010). Important role of integrins in the cancer biology. *Cancer and Metastasis Reviews, 29*(1), 223-237.

Regehr, K., Domenech, M., Koepsel, J., Carver, K., Ellison-Zelski, S., Murphy, W., et al. (2009). Biological implications of polydimethylsiloxane-based microfluidic cell culture. *LAB ON A CHIP, 9*(15), 2132-2139.

Ridley, A. (2001). Rho gtpases and cell migration. *JOURNAL OF CELL SCIENCE, 114*(15), 2713-2722.

Ridley, A. J. (2001). Rho proteins, pi 3-kinases, and monocyte/macrophage motility. *Febs Letters, 498*(2-3), 168-171.

Riesselman, M., Miettinen, H., Gripentrog, J., Lord, C., Mumey, B., Dratz, E., et al. (2007). C-terminal tail phosphorylation of n-formyl peptide receptor: Differential recognition of two neutrophil chemoattractant receptors by monoclonal antibodies nfpr1 and nfpr2. *JOURNAL OF IMMUNOLOGY, 179*(4), 2520-2531.

Roberts, A., Kim, C., Zhen, L., Lowe, J., Kapur, R., Petryniak, B., et al. (1999). Deficiency of the hematopoietic cell-specific rho family gtpase rac2 is characterized by abnormalities in neutrophil function and host defense. *IMMUNITY, 10*(2), 183-196.

Rubin, H., Ravid, S. (2002). Polarization of myosin ii heavy chain-protein kinase c in chemotaxing dictyostelium cells. *Journal of Biological Chemistry, 277*(39), 36005-36008.

Saadi, W., Rhee, S., Lin, F., Vahidi, B., Chung, B., & Jeon, N. (2007). Generation of stable concentration gradients in 2d and 3d environments using a microfluidic ladder chamber. *BIOMEDICAL MICRODEVICES, 9*(5), 627-635.

Sabroe, I., Jones, E., Whyte, M., & Dower, S. (2005). Regulation of human neutrophil chemokine receptor expression and function by activation of toll-like receptors 2 and 4. *IMMUNOLOGY, 115*(1), 90-98.

Salhia, B., Rutten, F., Nakada, M., Beaudry, C., Berens, M., Kwan, A., et al. (2005). Inhibition of rho-kinase affects astrocytoma morphology, motility, and invasion through activation of rac1. *CANCER RESEARCH, 65*(19), 8792-8800.

Schlessinger, J. (2000). Cell signaling by receptor tyrosine kinases. *Cell, 103*, 211-225.

Schmidt, S., Friedl, P. (2010). Interstitial cell migration: Integrin-dependent and alternative adhesion mechanisms. *Cell and Tissue Research, 339*(1), 83-92.

Schneider, I., & Haugh, J. (2005). Quantitative elucidation of a distinct spatial gradient-sensing mechanism in fibroblasts. *JOURNAL OF CELL BIOLOGY, 171*(5), 883-892.

Schneider, I., & Haugh, J. (2006). Mechanisms of gradient sensing and chemotaxis - conserved pathways, diverse regulation. *CELL CYCLE, 5*(11), 1130-1134.

Schneider, L., Cammer, M., Lehman, J., Nielsen, S., Guerra, C., Veland, I., et al. (2010). Directional cell migration and chemotaxis in wound healing response to pdgf-aa are coordinated by the primary cilium in fibroblasts. *CELLULAR PHYSIOLOGY AND BIOCHEMISTRY, 25*(2-3), 279-292.

Servant, G., Weiner, O., Neptune, E., Sedat, J., & Bourne, H. (1999). Dynamics of a chemoattractant receptor in living neutrophils during chemotaxis. *MOLECULAR BIOLOGY OF THE CELL, 10*(4), 1163-1178.

Shi, Y., Zhang, J., Mullin, M., Doug, B., Alberts, A., & Siminovitch, K. (2009). The mdial formin is required for neutrophil polarization, migration, and activation of the larg/rhoa/rock signaling axis during chemotaxis. *JOURNAL OF IMMUNOLOGY, 182*(6), 3837-3845.

Shyy, Y., Wickham, L., Hagan, J., Hsieh, H., Hu, Y., Telian, S., et al. (1993). Human monocyte colony-stimulating factor stimulates the gene-expression of monocyte chemotactic protein-1 and increases the adhesion of monocytes to endothelial monolayers. *JOURNAL OF CLINICAL INVESTIGATION, 92*(4), 1745-1751.

Sidani, M., Wessels, D., Mouneimne, G., Ghosh, M., Goswami, S., Sarmiento, C., et al. (2007). Cofilin determines the migration behavior and turning frequency of metastatic cancer cells. *JOURNAL OF CELL BIOLOGY, 179*(4), 777-791.

Smith, S., Jaffer, Z., Chernoff, J., & Ridley, A. (2008). Pak1-mediated activation of erk1/2 regulates lamellipodial dynamics. *JOURNAL OF CELL SCIENCE, 121*(22), 3729-3736.

Somesh, B. P., Vlahou, G., et. al. (2006). Racg regulates morpohology, phagocytosis, and chemotaxis. *Eukaryotic Cell, 5*(10), 1648-1663.

Song, L. L., Nadkarni, S.M., Bodeker, H.U., et al. (2006). Dictyostelium discoideum chemotaxis: Threshold for directed motion. *European Journal of Cell Biology, 85*, 981-989.

Stradal, T., & Scita, G. (2006). Protein complexes regulating arp2/3-mediated actin assembly. *CURRENT OPINION IN CELL BIOLOGY, 18*(1), 4-10.

Sun, C., Downey, G., Zhu, F., Koh, A., Thang, H., & Glogauer, M. (2004). Rac1 is the small gtpase responsible for regulating the neutrophil chemotaxis compass. *BLOOD, 104*(12), 3758-3765.

Sun, C., Magalhaes, M., & Glogauer, M. (2007). Rac1 and rac2 differentially regulate actin free barbed end formation downstream of the fmlp receptor. *JOURNAL OF CELL BIOLOGY, 179*(2), 239-245.

Takeda, K., Sasaki, A., Ha, H., Seung, H., & Firtel, R. (2007). Role of phosphatidylinositol 3-kinases in chemotaxis in dictyostelium. *JOURNAL OF BIOLOGICAL CHEMISTRY, 282*(16), 11874-11884.

Tzircotis, G., Thorne, R., & Isacke, C. (2005). Chemotaxis towards hyaluronan is dependent on cd44 expression and modulated by cell type variation in cd44-hyaluronan binding. *JOURNAL OF CELL SCIENCE, 118*(21), 5119-5128.

Underhill, D. M., & Ozinsky, A. (2002). Phagocytosis of microbes: Complexity in action. *Annual Review Of Immunology, 20*, 825-852.

Vanhaesebroeck, B., Jones, G. E., Allen, W. E., Zicha, D., Hooshmand-Rad, R., Sawyer, C., et al. (1999). Distinct pi(3)ks mediate mitogenic signalling and cell migration in macrophages. *Nature Cell Biology, 1*(1), 69-71.

Vanhaesebroeck, B., & Waterfield, M. D. (1999). Signaling by distinct classes of phosphoinositide 3-kinases. *Experimental Cell Research, 253*(1), 239-254.

Vasiev, B., Weijer, C.J. (2003). Modeling of dictystelium discoideum slug migration. *Journal of Theoretical Biology, 223*(3), 347-359.

Veltman, D., Keizer-Gunnik, I., & Van Haastert, P. (2008). Four key signaling pathways mediating chemotaxis in dictyostelium discoideum. *JOURNAL OF CELL BIOLOGY, 180*(4), 747-753.

Veltman, D., & van Haastert, P. (2008). The role of cgmp and the rear of the cell in dictyostelium chemotaxis and cell streaming. *JOURNAL OF CELL SCIENCE, 121*(1), 120-127.

Vicente-Manzanares, M., Choi, C., & Horwitz, A. (2009). Integrins in cell migration - the actin connection. *JOURNAL OF CELL SCIENCE, 122*(2), 199-206.

Vollmer, K., Alberts, J., Carper, H., & Mandell, G. (1992). Tumor-necrosis-factor-alpha decreasees neutrophil chemotaxis to n-formyl-1-methionyl-1-leucyl-1-phenylalanine - analysis of single cell-movement. *JOURNAL OF LEUKOCYTE BIOLOGY, 52*(6), 630-636.

Walker, G., Sai, J., Richmond, A., Stremler, M., Chung, C., & Wikswo, J. (2005). Effects of flow and diffusion on chemotaxis studies in a microfabricated gradient generator. *LAB ON A CHIP, 5*(6), 611-618.

Wallar, B. J., Alberts, A.S. (2003). The formins: Active scaffolds that remodel the cytoskeleton. *Trends in Cell Biology, 13*, 1335-1340.

Wang, J., Heo, J., & Hua, S. (2010). Spatially resolved shear distribution in microfluidic chip for studying force transduction mechanisms in cells. *LAB ON A CHIP, 10*(2), 235-239.

Wang, S., Saadi, W., Lin, F., Nguyen, C., & Jeon, N. (2004). Differential effects of egf gradient profiles on mda-mb-231 breast cancer cell chemotaxis. *EXPERIMENTAL CELL RESEARCH, 300*(1), 180-189.

Wang, W., Eddy, R., & Condeelis, J. (2007). The cofilin pathway in breast cancer invasion and metastasis. *NATURE REVIEWS CANCER, 7*(6), 429-440.

Watson, A., Morris, V., & Chan, B. (2009). Coordinated integrin and growth factor regulation of primary keratinocyte migration mediated through extracellular signal regulated kinase and phosphoinositide 3-kinase. *ARCHIVES OF DERMATOLOGICAL RESEARCH, 301*(4), 307-317.

Weiger, M., Wang, C., Krajcovic, M., Melvin, A., Rhoden, J., & Haugh, J. (2009). Spontaneous phosphoinositide 3-kinase signaling dynamics drive spreading and random migration of fibroblasts. *JOURNAL OF CELL SCIENCE, 122*(3), 313-323.

Weijer, C. J. (2004). Dictyostelium morphogenesis. *Current Opinion in Genetics and Development, 14*(4), 392-398.

Weiner, O. D. (2002). Regulation of cell polarity during eukaryotic chemotaxis: The chemotactic compass. *Current Opinion In Cell Biology, 14*(2), 196-202.

Wells, C. M., Walmsley, M., Ooi, S., Tybulewicz, V., & Ridley, A. J. (2004). Rac1-deficient macrophages exhibit defects in cell spreading and membrane ruffling but not migration. *Journal Of Cell Science, 117*(7), 1259-1268.

Wong, K., Pertz, O., Hahn, K., & Bourne, H. (2006). Neutrophil polarization: Spatiotemporal dynamics of rhoa activity support a self-organizing mechanism. *PROCEEDINGS OF THE NATIONAL ACADEMY OF SCIENCES OF THE UNITED STATES OF AMERICA, 103*(10), 3639-3644.

Yamada, K., & Cukierman, E. (2007). Modeling tissue morphogenesis and cancer in 3d. *CELL, 130*(4), 601-610.

Yamaguchi, H., Wyckoff, J., Condeelis, J. (2005). Cell migration in tumors. *Current Opinion in Cell Biology, 17*(5), 559-564.

Yin, Z., Noren, D., Wang, C., Hang, R., & Levchenko, A. (2008). Analysis of pairwise cell interactions using an integrated dielectrophoretic-microfluidic system. *MOLECULAR SYSTEMS BIOLOGY, 4*, -.

Young, E., & Simmons, C. (2010). Macro- and microscale fluid flow systems for endothelial cell biology. *LAB ON A CHIP, 10*(2), 143-160.

Zaman, M. H., Matsudaira, P. Lauffenburger, D.A. (2007). Understanding effects of matrix protease and matrix organization on directional persistence and translational speed in three-dimensional cell migration. *Annals of Biomedical Engineering, 35*(1), 91-100.

Zaman, M. H., Trapani, L.M., Siemeski, A., et. al. (2006). Migration of tumor cells in 3d matrices is governed by matrix stiffness along with cell-matrix adhesion and proteolysis. *PROCEEDINGS OF THE NATIONAL ACADEMY OF SCIENCES OF THE UNITED STATES OF AMERICA, 103*(29), 10889-10894.

Zicha, D., Dunn, G., and Jones, G. (1997). Analyzing chemotaxis using the dunn direct-viewing chamber. *Method in Molecular Biology, 75*, 449-457.

Zigmond, S. H. (1977). Ability of polymorphonuclear leukocytes to orient in gradients of chemotactic factors. *Journal of Cell Biology, 75*(2), 606-616.

Zigmond, S. H. (1988). Orientation chamber in chemotaxis. *Methods in Enzymology, 162*, 65-72.

Chapter 2
Asymmetry of PI3K signaling dynamics coincides with directional fidelity of fibroblast chemotaxis

2.1 INTRODUCTION

Directed cell migration is an essential process in many physiological and pathological processes, such as wound healing, embryogenesis, the immune response, and cancer metastasis. Cell migration biased by chemical gradients, or chemotaxis, is the most commonly encountered and best understood mechanism for instructing cells to move from place to place. Cell crawling is characterized by cyclic protrusion, adhesion and retraction processes that are governed by intracellular signaling pathways that work in concert to control the speed and directional persistence of movement (Lauffenburger & Horwitz, 1996). Cells sense chemotactic gradients in a spatial manner, through a contrast in the occupancy of cell surface receptors and thus the levels of activated signaling molecules at the cell's front and rear. Much of what is currently known about the intracellular pathways governing chemotaxis has been gleaned from two model cell types: neutrophils and the slime mold *Dictyostelium discoideum* (Devreotes, 1988). These professional migrating cells have been extensively studied due to their rapid migration (~20 μm/min) and their responses to relatively shallow gradients of chemoattractants (Schneider & Haugh, 2006). Although the two eukaryotic cell types lie at opposite ends of the evolutionary spectrum and respond to distinct stimuli, their chemotactic mechanisms exhibit remarkably similar features, including sensing mediated by G protein-coupled receptors leading to the production of 3' phosphoinositides (PI) at the plasma membrane by phosphoinositide 3-kinase (PI3K), a pathway that modulates Rho-family GTPases and other pathways to affect actin-based cell motility (Gruver, Wikswo, & Chung, 2008; Ridley, 2001; Takeda, Sasaki, Ha, Seung, & Firtel, 2007).

The asymmetric accumulation of 3' PI lipids at the leading edge of a migrating cell is one of the hallmarks of spatial gradient sensing. Early experiments with neutrophils and *Dictyostelium* demonstrated that these cells show biased polarization and migration in

response to very shallow gradients of chemoattractants (~1% difference in concentration across cell dimensions). In the face of steeper gradients, the cells' responses are more robust, with seemingly 'all-or-none' polarization of 3' PI signaling and actin polymerization (Parent & Devreotes, 1999; Servant et al., 2000). In recent years, additional studies have implicated other signaling molecules like the 3' phosphatase PTEN (Iijima, 2002; Wessels, Lusche, Kuhl, Heid, & Soll, 2007) and small GTPases of the Rho family (Heasman & Ridley, 2008) as key regulators of the PI3K-dependent chemotaxis pathway. The role of PI3K signaling in amoeboid chemotaxis is not without controversy, however, since it has been shown that PI3K activity is not absolutely required for chemotaxis of *Dictyostelium* (Andrew & Insall, 2007; Kay, Langridge, Traynor, & Hoeller, 2008) or neutrophils (Nishio, 2007). Recent studies in *Dictyostelium*, have established that whereas PI3K is not required for the chemotactic responses to steep gradients, it is essential for sensing shallow gradients (Bosgraaf, Keizer-Gunnink, & van Haastert, 2008) in addition to affecting overall migration speed (Heit, Liu, Colarusso, Puri, & Kubes, 2008).

Another prominent example of chemotaxis is the collective migration of dermal fibroblasts, which respond to gradients of platelet-derived growth factor (PDGF) during wound healing (Singer & Clark, 1999). Fibroblasts differ from amoeboid cells in chemoattractant receptor type – PDGF receptors are receptor tyrosine kinases – and migration speed (< 1 μm/min). Nonetheless, fibroblast motility and PDGF-stimulated chemotaxis rely on the localized activation of PI3K, which elicits an asymmetric polarization of 3' PI lipids at the leading edge (Haugh, Codazzi, Teruel, & Meyer, 2000); a major difference, however, is that the PDGF gradient sensing mechanism does not significantly amplify the external gradient at the level of the intracellular 3' PI pattern, such that far steeper PDGF gradients (> 10%) are needed to elicit robust polarization of PI3K signaling in fibroblasts (Schneider & Haugh, 2005). What remains unclear, however, is whether or not this trend holds at the level of the cellular response; one cannot discount the possibilities that signaling is amplified downstream of PI3K or in a parallel signaling pathway. The slow migration of fibroblasts presents a definite challenge for long-term imaging of gradient sensing and chemotaxis.

In this study, we analyze, for the first time, the fidelity of the PDGF gradient sensing mechanism, i.e. the ability of fibroblasts to migrate persistently in the direction of the gradient, in relation to stochastic PI3K signaling dynamics during chemotaxis. We employ a novel technique to establish a stable PDGF gradient, namely the slow release of PDGF from small (~ 40-50 μm diameter) alginate microspheres. Using total internal reflection fluorescence (TIRF) microscopy, we show that PI3K signaling and cell directionality are tightly correlated during fibroblast chemotaxis, consistent with previous analyses of random fibroblast migration (Weiger, Ahmed, Welf, & Haugh, 2010). Additionally, we demonstrate that high-fidelity fibroblast chemotaxis is observed only when there is a steep gradient in PDGF receptor occupancy, which is tempered when the local PDGF concentration is sufficient to saturate receptor binding. Finally, we show that motility is impaired in the presence of the PI3K inhibitor LY294002. These results verify that PI3K signaling and fibroblast migration is not significantly biased by shallow PDGF gradients; even when migrating randomly, however, the directionality of migration follows that of PI3K signaling polarity.

2.2 MATERIALS AND METHODS

2.2.1 Cell culture and reagents

Stable expression of the 3' phosphoinositide-specific biosensor construct EGFP-AktPH (Haugh et al., 2000) in NIH 3T3 mouse fibroblasts (American Type Culture Collection) was achieved by retroviral infection after cloning into the NotI/BamH1 sites of the pBm-IRES-puro vector (a gift from Dr. Steven Wiley, Pacific Northwest National Laboratory). The ecotropic ΦNX packaging cell line was transiently transfected, and virus-containing supernatants were used for serial infection of NIH 3T3 cells resulting in >80% transfection efficiency, as previously described (Kaur, Park, Lewis, & Haugh, 2006). Cells were maintained in regular growth medium (Dulbecco's modified Eagle's medium supplemented with 10% v/v fetal bovine serum and 1% v/v penicillin/streptomycin/ glutamate) in a 37^{o}C incubator with 5% carbon dioxide. All tissue culture reagents were

purchased from Invitrogen (Carlsbad, CA) and cells were used between passages 10-40. Human plasma fibronectin was obtained from BD Biosciences (San Jose, CA), and human recombinant PDGF-BB was from Peprotech (Rocky Hill, NJ). Imaging buffer was prepared according to the following recipe: 20 mM HEPES pH 7.4, 125 mM NaCl, 5 mM KCl, 1.5 mM $MgCl_2$, 1.5 mM $CaCl_2$, 10 mM glucose, and 2 mg/mL fatty acid-free bovine serum albumin, supplemented with 1% v/v fetal bovine serum. Alginate microspheres (a generous gift from Darrell Irvine, MIT) were stored in suspension at 4°C until use.

2.2.2 Chemotaxis experiments

The day before each experiment, EGFP-AktPH-expressing NIH 3T3 cells were seeded on 60 mm tissue culture plates to yield an appropriate density of cells (~30% confluency). The day of the experiment, adhesive surfaces were prepared as clean, sterile glass coverslips coated with fibronectin (10 µg/mL) for 60 minutes at 37°C, washed with deionized, sterile water, and dried. The cells were detached by a brief trypsin-EDTA treatment and suspended in imaging buffer. Following centrifugation at 100 rcf for 3 min, the cells were resuspended in imaging buffer to a final density of 10^4 cells/mL, and a volume of 1 mL was added to the cover slip, contained by a teflon ring adhered to the cover slip with vacuum grease. The suspension was incubated on the cover slip for 2 hours at 37°C to allow cells to adhere and spread.

Meanwhile, PDGF-loaded microspheres were prepared as follows. The day before the experiment, a 15-µL aliquot of the stock suspension of alginate beads is pelleted at 12,000g for 3 min. Most of the supernatant is discarded, and the beads are resuspended in 25 µL of 1 µM PDGF-BB and placed on a shaker at 4°C for 24 hours to facilitate PDGF loading in the beads. The next day, the beads are removed from the shaker, resuspended in 1 mL imaging buffer and spun down at 12000 rcf for 3 min. The supernatant is discarded, and the wash step is repeated two more times, with the beads finally being suspended in 600 µL of imaging buffer.

A 50-µL volume of the bead suspension was added to the solution covering the cells with 20 minutes remaining in the 2-hour adhesion/spreading period (to allow the beads to

settle on the surface of the cover slip). The objective of the microscope was lowered into the buffer, and finally 200 µL of mineral was layered on top of the imaging buffer (to prevent evaporation). The cells were allowed to migrate for 6-7 hours at 37°C. In some experiments, 100 µM LY294002 was added after 4 hours.

2.2.3 TIRF microscopy

TIRF microscopy was used to selectively excite fluorophores within ~100 nm of the cell contact area, effectively illuminating the plasma membrane of fibroblasts and ~5-10% of the cytoplasm directly above it (Schneider & Haugh, 2004). The details and theory behind TIRF microscopy are included in APPENDIX A. Our prism-based TIRF microscope has been described previously (Schneider & Haugh, 2005; Weiger et al., 2009). Briefly, the glass coverslip is optically coupled to the prism with 518F immersion oil (Zeiss). A laser beam is then aimed through the prism at an angle greater than the critical angle, imparting an evanescent wave that selectively excites the intracellular biosensor (EGFP) close to the glass-water interface. A 60 mW, 488 nm line from a tunable wavelength argon ion laser head (Melles Griot, Irvine, CA) was used, together with a 515/30 nm bandpass emission filter (Chroma, Brattleboro, VT). 20X and 10X water immersion objectives (Zeiss Achroplan) and 0.63X camera mount were used. Digital images were acquired at 2-minute intervals using a Hamamatsu ORCA ER cooled CCD (Hamamatsu, Bridgewater, NJ) with a fixed exposure time X gain of 1000-1600 ms. Image acquisition was controlled using Metamorph imaging software (Universal Imaging, West Chester, PA).

2.2.4 Image and data analysis

Signal Vector Analysis

During the chemotaxis experiments, the CCD camera, controlled via Metamorph imaging software, captures a digital 'stack', a series of sequential images that were segmented and analyzed further, as previously described (Weiger et al., 2010; Weiger et al., 2009). After an initial background subtraction, the pixels in each image are binned according to intensity into four groups using the *k*-means segmentation algorithm. The pixels in the

acellular background are thus assigned to bin 1, whereas the pixels associated with intense fluorescence (hot spots of PI3K signaling) reside in bin 4.

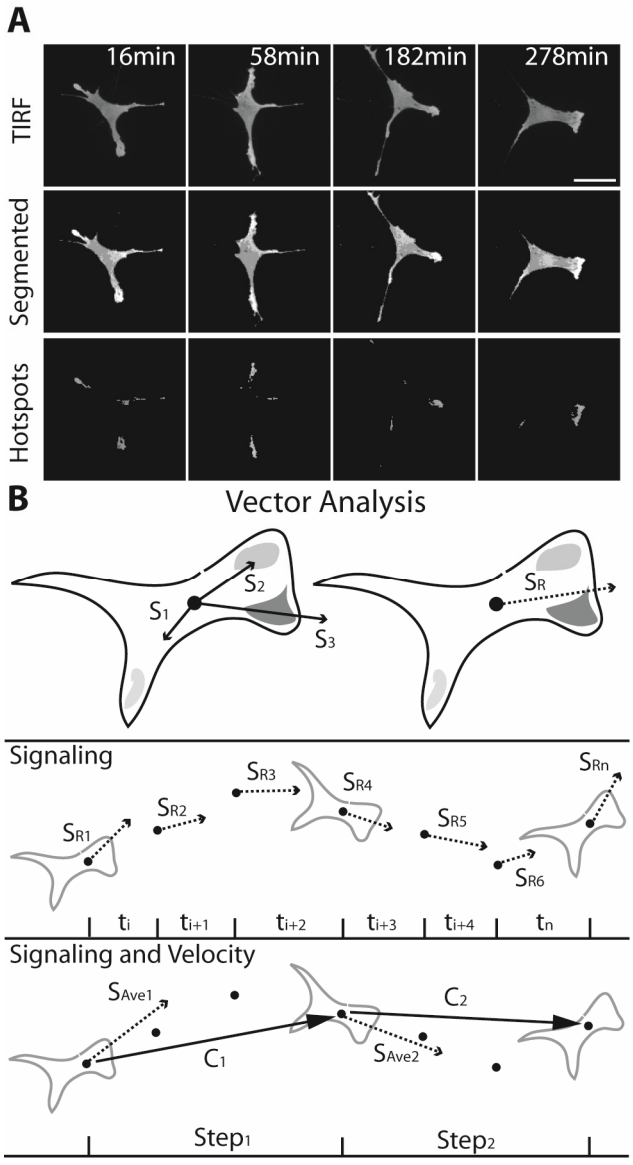

Figure 2.1 Signal vector analysis. (A) The *k*-means segmentation algorithm is applied to TIRF images from a migrating cell, effectively binning them into background, cell and hot spot regions. (B) The hot spots are then assigned vector values relative to the cell centroid ($\mathbf{s_i}$) and summed to generate the signaling vector ($\mathbf{S_R}$) which is compared to the directionality vector ($\mathbf{C}$) over a defined time step of 12 minutes. Courtesy of Michael Weiger (Weiger, 2008).

For each image, masks were generated that define regions of interest corresponding to the entire cell contact area (bins 2-4) and hot spot regions (bin 4 only) (Figure 2.1A). Additional MATLAB code was designed to calculate the area (A), average intensity (F), and centroid coordinates of each labeled region with a minimum hot spot area cutoff of 20 pixels to ensure contiguous regions and not imaging artifacts. For each image, the signaling vector is calculated according to equation 2.1.

$$\mathbf{S}_i = A_i F_i \frac{\mathbf{x}_i}{\sqrt{x_i^2 + y_i^2}}; \quad \mathbf{S}_R = \sum_{i=1}^{N} \mathbf{S}_i . \tag{2.1}$$

The coordinates of the cell's centroid are subtracted from those of each of its hot spots, i, defining the position of the hot spot relative to the cell centroid, $\mathbf{x_i} = (x_i, y_i)$, and its vector, $\mathbf{s}_i$, is defined with the magnitude equal to the fluorescence volume (A_iF_i). The overall, resultant signaling vector, $\mathbf{S}_R$, is the sum of these individual, signaling vectors. The temporal resolution of image acquisition, Δt (2 min), was found to be too fine for tracking the cell centroid movement vector ($\mathbf{C}$), so a time step of $6\Delta t$ was used. For the purpose of relating vectors, the signaling vector assigned to a particular cell movement step, from t_i to $t_i + 6\Delta t$, was taken as the average of six $\mathbf{S}_R$ calculated for t_i, $t_i + \Delta t$, . . . , $t_i + 5\Delta t$ ($\mathbf{S}_{Ave}$) (Figure 2.1B).

Cells analyzed for chemotactic behavior had to have met the follow criteria: (1) the cell had to remain in the field of view for the duration of the experiments, (2) the cell had to have a minimum contact area of 300 pixels, (3) the cell could not come in to contact with another cell during the 6 hours of migration, and (4) the cell had to exhibit significant displacement between its starting and finishing positions. Any cells not meeting these criteria were omitted from the analysis.

PDGF gradient calculations

The following analysis was devised to relate the orientation of cell movement and signaling vectors to that of the chemoattractant gradient. The concentration of PDGF is defined as L, following the common notation used to model chemotaxis and, more generally receptor-ligand binding. During the period of observation, we expect first-order release kinetics from the bead:

$$\frac{d\langle [L]_b \rangle}{dt} = -k_{release}\langle [L]_b \rangle; \qquad \langle [L]_b \rangle = [L]_{b,0} e^{-k_{release} t}. \tag{2.2}$$

The quantity in elbow brackets is the average volumetric concentration of ligand adsorbed to the bead material. Assuming a quasi-steady flux J_S at the bead surface,

$$J_S = -D\frac{d[L]}{dr}\bigg|_{r=R_b} = \frac{V_b}{S_b} k_{release}\langle [L]_b \rangle = \frac{R_b}{3} k_{release}\langle [L]_b \rangle. \tag{2.3}$$

$[L](r)$ is the concentration of the ligand in solution as a function of distance r from the center of the bead, and D is its diffusivity. V_b, S_b, and R_b are the volume, external surface area, and radius of the bead respectively, assuming an approximately spherical shape. Quasi-steady conservation of the released ligand in solution, assuming spherical coordinates and a semi-infinite medium, gives

$$\frac{D}{r^2}\frac{d}{dr}\left(r^2 \frac{d[L]}{dr}\right) \approx 0;$$

$$\frac{d[L]}{dr} = -\frac{J_S}{D}\left(\frac{R_b}{r}\right)^2 = -\frac{k_{release} R_b^{\,3}}{3Dr^2}\langle [L]_b \rangle; \tag{2.4}$$

$$[L](r) = \frac{k_{release} R_b^{\,3}}{3Dr}\langle [L]_b \rangle.$$

Converting the above to Cartesian coordinates,

$$[L](x,y,z) = \frac{k_{release} R_b^{\,3}}{3Dd_b}\langle [L]_b \rangle;$$

$$\frac{\partial [L]}{\partial x} = -(x - x_b)\left(\frac{R_b}{d_b}\right)^3 \frac{k_{release}}{3D}\langle [L]_b \rangle; \tag{2.5}$$

$$\frac{\partial [L]}{\partial y} = -(y - y_b)\left(\frac{R_b}{d_b}\right)^3 \frac{k_{release}}{3D}\langle [L]_b \rangle;$$

$$d_b(x,y,z) = \left[(x - x_b)^2 + (y - y_b)^2 + (z - z_b)^2\right]^{1/2}.$$

To account for the impermeable cover slip at $z = 0$, we invoke the method of images as follows.

$$[L](x,y,z) = \frac{k_{release} {R_b}^3}{3Dd_b} \langle [L]_b \rangle \left\{ 1 + \frac{\left[(x-x_b)^2 + (y-y_b)^2 + (z-z_b)^2 \right]^{-1/2}}{\left[(x-x_b)^2 + (y-y_b)^2 + (z+z_b)^2 \right]^{-1/2}} \right\} \tag{2.6}$$

Considering that the cells are at the $z = 0$ plane, and taking $z_b = R_b$, we determine the relative distance, d_b, between any distance (x,y) and the center of the bead (x_b,y_b) and calculate the ligand concentration field produced by each bead and the components of its gradient vector as follows.

$$\begin{aligned}
[L](x,y,0) &= \frac{2k_{release} {R_b}^3}{3Dd_b} \langle [L]_b \rangle; \\
\left. \frac{\partial [L]}{\partial x} \right|_{z=0} &= -(x-x_b) \left(\frac{R_b}{d_b} \right)^3 \frac{2k_{release}}{3D} \langle [L]_b \rangle; \\
\left. \frac{\partial [L]}{\partial y} \right|_{z=0} &= -(y-y_b) \left(\frac{R_b}{d_b} \right)^3 \frac{2k_{release}}{3D} \langle [L]_b \rangle; \\
d_b(x,y,0) &= \left[(x-x_b)^2 + (y-y_b)^2 + {R_b}^2 \right]^{-1/2}.
\end{aligned} \tag{2.7}$$

Next, assuming independent contributions from multiple beads and summing over them, and defining the PDGF gradient vector as **G**,

$$\begin{aligned}
[L](x,y,0) &= \frac{2k_{release}}{3D} \langle [L]_b \rangle \sum_{i=1}^{n} \frac{{R_{b,i}}^3}{d_{b,i}}; \\
G_x = \left. \frac{\partial [L]}{\partial x} \right|_{z=0} &= -\frac{2k_{release}}{3D} \langle [L]_b \rangle \sum_{i=1}^{n} (x - x_{b,i}) \left(\frac{R_{b,i}}{d_{b,i}} \right)^3; \\
G_y = \left. \frac{\partial [L]}{\partial y} \right|_{z=0} &= -\frac{2k_{release}}{3D} \langle [L]_b \rangle \sum_{i=1}^{n} (y - y_{b,i}) \left(\frac{R_{b,i}}{d_{b,i}} \right)^3.
\end{aligned} \tag{2.8}$$

It is noted that the common prefactor in front of these sums (assumed to be the same for all beads) may be ignored, insofar as only the direction of the gradient is relevant. We define the vector $\mathbf{G}_c$ as the gradient vector evaluated at the cell centroid coordinates (x_c,y_c).

Hence, the properties of the gradient were calculated as follows. The normalized concentration of ligand, $[L]_{norm}$, is calculated according to Equation 2.8 except without the presumably constant prefactor:

$$[L]_{norm}(x,y) = \sum_{i=1}^{n} \frac{{R_{b,i}}^3}{d_{b,i}}. \tag{2.9}$$

The relative gradient, *RG*, of PDGF is determined from the magnitude of $\mathbf{G}_c$ as follows.

$$RG = \frac{\|\mathbf{G}_c\|}{[L]}. \tag{2.10}$$

Angle of Orientation calculations

The angle of any vector (denoted in equation 2.11 as **V**) relative to the positive x-axis in the counterclockwise direction (by convention), set on a (0,2π) scale, is calculated as follows. In the equation below, sgn is the sign function (returns 1 for a positive argument, -1 for a negative argument):

$$\theta_{V,2\pi} = \operatorname{sgn} V_x \operatorname{sgn} V_y \tan^{-1}\left|\frac{V_y}{V_x}\right| + \left[1 - \operatorname{sgn} V_y \frac{(1+\operatorname{sgn} V_x)}{2}\right]\pi. \tag{2.11}$$

Thus, subtracting the angle of the gradient vector $\mathbf{G_c}$ from the cell movement vector **C** will be on a (-2π,2π) scale. This angle, θ_{MB}, is set on a (-π,π) scale as follows.

$$\begin{aligned} \theta_{MB,2\pi} &= \theta_{M,2\pi} - \theta_{B,2\pi}; \\ \theta_{MB} &= \theta_{MB,2\pi} + \left[\operatorname{sgn}(\pi - \theta_{MB,2\pi}) - \operatorname{sgn}(\pi + \theta_{MB,2\pi})\right]\pi. \end{aligned} \tag{2.12}$$

The same formula is used to compute the angle, θ_{SB}, between the signaling vector **S** and the gradient vector **G**.

$$\begin{aligned} \theta_{SB,2\pi} &= \theta_{S,2\pi} - \theta_{B,2\pi}; \\ \theta_{SB} &= \theta_{SB,2\pi} + \left[\operatorname{sgn}(\pi - \theta_{SB,2\pi}) - \operatorname{sgn}(\pi + \theta_{SB,2\pi})\right]\pi. \end{aligned} \tag{2.13}$$

According to the equations above, the angles of the signaling (θ_{SB}) and direction of movement (θ_{MB}) vectors relative to the PDGF gradient were calculated for each time step, 6Δ*t* (Figure 2.2A). Values of θ_{MB} and θ_{SB} equal to zero correspond to perfectly aligned chemotaxis (Figure 2.2B).

Because the alginate beads were not adhered to the surface, they were seen to move during some of the experiments. In those instances, a best-fit location was determined from the coordinates of the bead center at hourly intervals. When a bead appeared during the

middle of the time course, an additional criterion was applied. We determined that a bead must be in roughly the same location for at least four hours; i.e., any bead that would appear for two hours or less was not considered in the analysis.

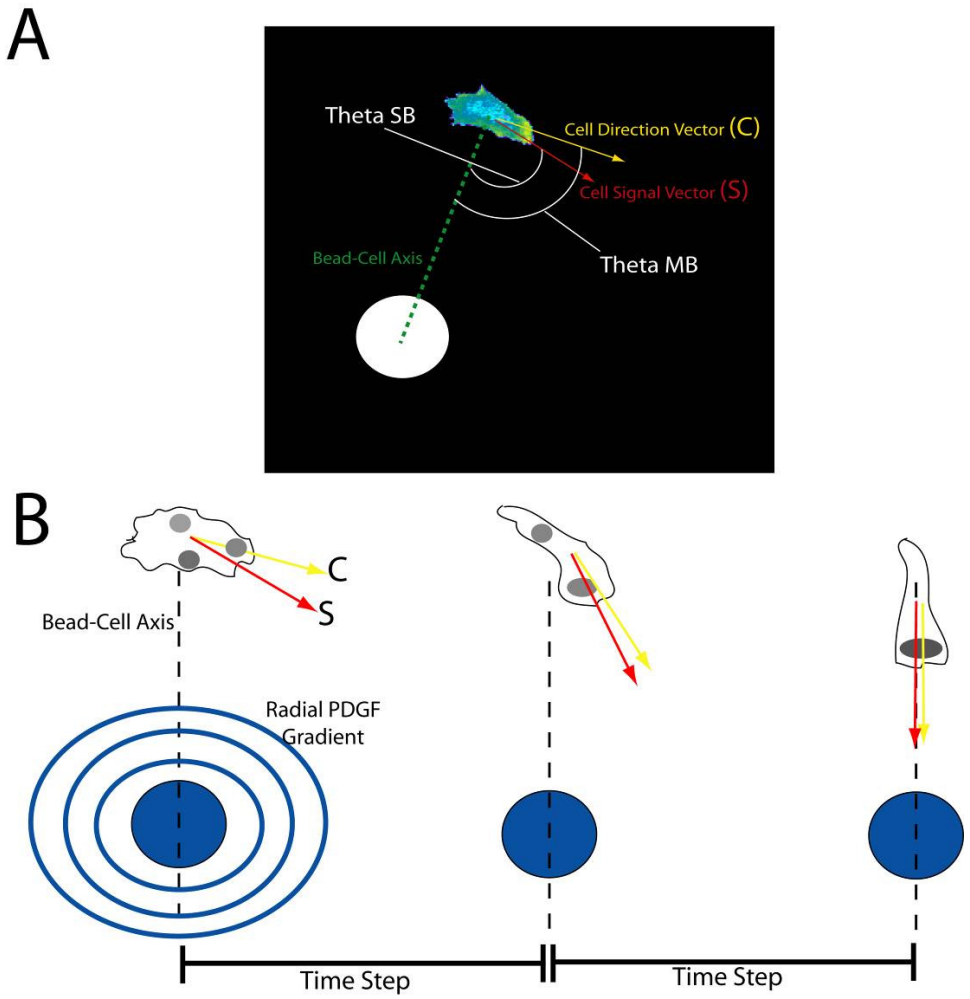

Figure 2.2 Angle of orientation. (A) The persistence between PI3K signaling and directionality is compared using the angle of orientation calculation, where the cell signaling (**S**) and direction (**C**) vectors are compared to the gradient vector (**G**), a metric representing the gradient of chemoattractant being released from an alginate bead. The direction and signal vectors are compared by θ_{MB} and θ_{SB}, the angles between the direction and signaling vectors relative to the gradient vector, respectively. (B) As migration proceeds, the signaling and direction vectors will be parallel with the PDGF gradient ($\theta_{MB} = \theta_{SB} = 0$) in the limit of perfectly aligned chemotaxis.

2.3 RESULTS

2.3.1 Observation of PI3K signaling dynamics during fibroblast chemotaxis to PDGF

Stable expression of the 3'-phosphoinositide-specific Akt pleckstrin homology domain, fused with enhanced green fluorescent protein (EGFP-AktPH), was established in NIH 3T3 fibroblasts, which were monitored by TIRF microscopy as they migrated across fibronectin-coated cover slips. PDGF gradients were formed by diffusion from alginate microspheres, which had been soaked in a high concentration of PDGF. The negatively charged alginate acts as an 'electrostatic sponge', binding the basic protein PDGF and, after washing the beads to remove unbound PDGF, releasing it at a slow rate. With the reasonable assumptions that PDGF is distributed in the surrounding medium by diffusion only and that rebinding to the alginate is negligible, the relative magnitude of the PDGF concentration and the components of its gradient vector at any position are readily calculated (Materials and Methods).

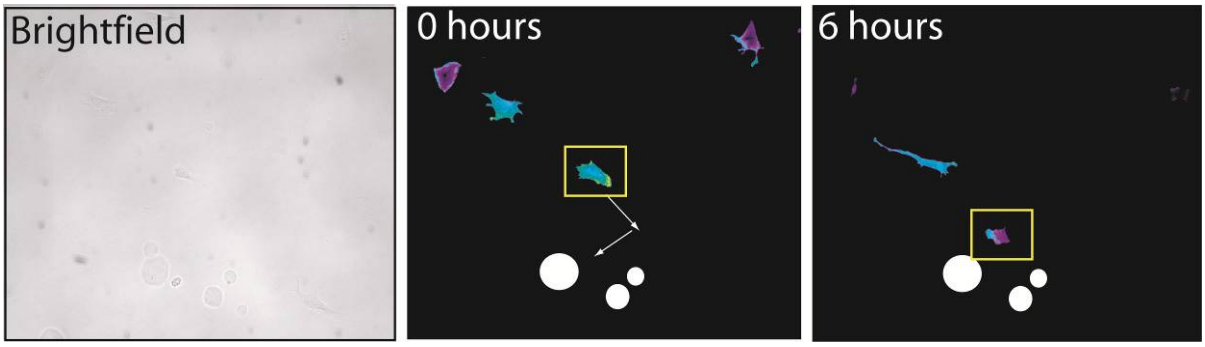

Figure 2.3 Fibroblasts migrate towards PDGF-loaded alginate beads. Alginate beads were added to the 1 mL imaging buffer solution on top of NIH 3T3 fibroblasts stably expressing the 3' phosphoinositide probe EGFP-AktPH. A 6 hour time course was performed, capturing an image every 2 minutes to monitor fibroblast chemotaxis to the alginate beads, which diffuse a radial gradient of PDGF. As shown above highlighted by the yellow box, the cells would persistently migrate towards the alginate beads (white dots). Hourly bright field images were taken to monitor bead position/movement during the time course.

As previously characterized in randomly migrating fibroblasts (Weiger et al., 2010; Weiger et al., 2009), PI3K signaling was asymmetrically polarized, with higher TIRF intensity in the protrusive regions of migrating cells and lower intensity elsewhere (Figure 2.3). The 'hot

spots' mostly correlated with the direction of migration and were quite often oriented towards the sources of PDGF. Control experiments performed using beads mock-soaked without PDGF confirmed the specificity of the response (results not shown).

2.3.2 Directionality of cell movement is correlated with asymmetric PI3K signaling during fibroblast chemotaxis

To elucidate the relationship between PI3K signaling and cell directionality during fibroblast chemotaxis, we calculated the signaling and cell movement vectors of a migrating fibroblasts using signal vector analysis (SVA); the fidelity of chemotaxis was quantified in terms of the alignment of those vectors with that of the PDGF gradient, calculated from the sizes and locations of the alginate beads (Materials and Methods).

Under certain conditions, our cells exhibited high-fidelity chemotaxis, with the directionality of cell movement converging to align with the PDGF gradient; apparently even more so, cell movement was closely and persistently aligned with the orientation of the PI3K signaling pattern in these cells (Figure 2.4). In other instances, our cells displayed more erratic movements, but again, fibroblast motility most typically correlated with the pattern of PI3K signaling (Figure 2.5). Qualitative analysis suggests that such behavior might arise for a variety of reasons, including: competition among multiple protrusions, resulting in 'zig-zag' movement; migration of the cell to a position that is close enough to a bead to saturate receptor occupancy (Figure 2.5B&D); and distant separation between the cell and the nearest bead, which results in a relatively shallow gradient (Figure 2.5C). Nonetheless, the migration of these cells were biased by the PDGF gradients they perceived, as seen from the increase in local PDGF concentration with time (Figure 2.5ii).

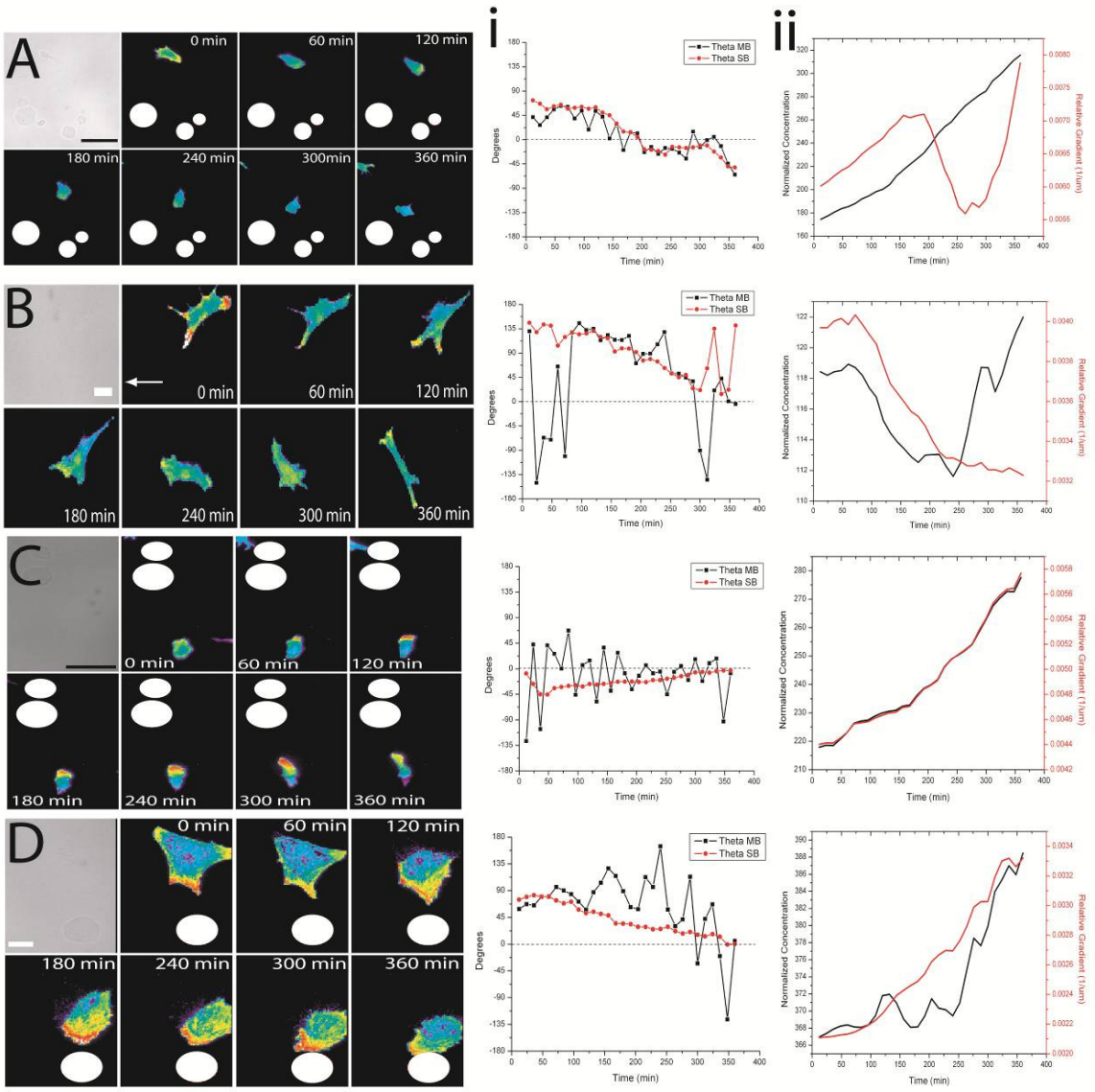

Figure 2.4 Correspondence of asymmetric PI3K signaling with directionality of fibroblast chemotaxis. Persistent migration of fibroblasts in response to a gradient of PDGF is monitored in multiple cells during a 6 hour time course. At the beginning of the time course the cells will slowly sense the gradient and, over time, orient themselves with the source of PDGF and migrate towards it (**A-D**). (**i**) The fidelity between the cell directionality and PI3K signaling is compared by studying the angle created between the directional and signaling vectors with the bead-cell axis (θ_{MB} and θ_{SB} respectively). (**ii**) The relative gradient a cell experiences as well as the normalized concentration of chemoattractant are also calculated. White dots represent the alginate beads while the white arrow (**B**) indicates the location of the alginate bead.

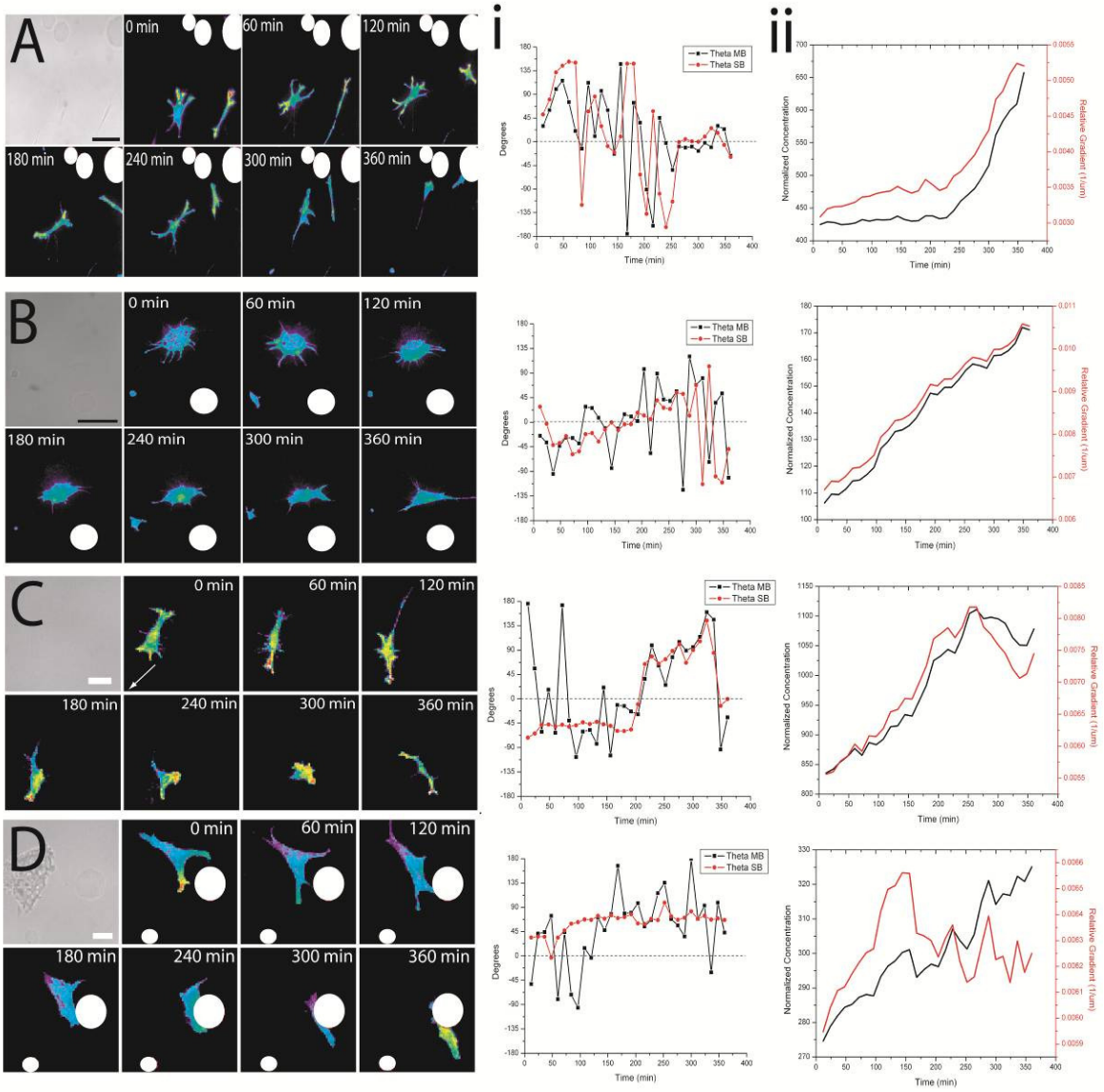

Figure 2.5 Extreme proximity or distance strongly impacts persistent migration. When a cell is very close (**B and D**) or very far (**C**) from a bead, the persistence of migration as well as the correlation between PI3K signaling and directionality is lost. As follows, being in the midst of a high bead density also impacts persistence (**A**) (**i**) The fidelity between the cell directionality and PI3K signaling are compared via θ_{MB} and θ_{SB}, similar to Figure 2.4 as well as (**ii**) determining the relative gradient and normalized concentration of chemoattractant. White dots represent the alginate beads, and the white arrow in (**C**) indicates the location of the alginate bead in that case.

2.3.3 The spatial arrangement of PDGF sources affects the PDGF gradient and, therefore, fibroblast chemotaxis

At best, cells perceive chemoattractant gradients in their local vicinity, not the location(s) where chemoattractant molecules are released.

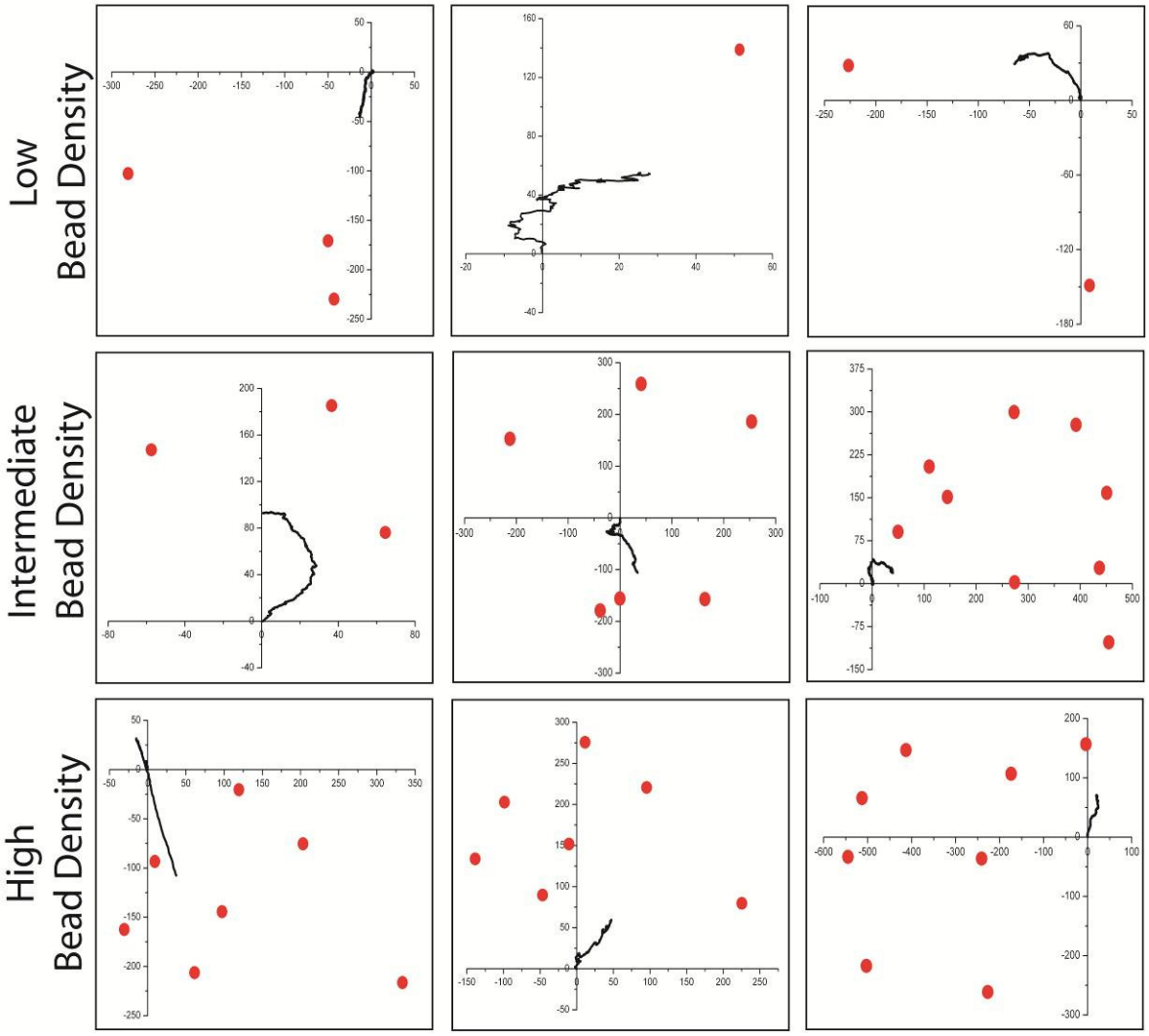

Figure 2.6 The spatial arrangement of PDGF sources affects chemotaxis. Cell tracking plots were generated by zeroing the starting position of the cell centroid during fibroblast chemotaxis. The coordinates of the beads were then adjusted to correspond with the (0,0) starting position of the cell and then the position of the cell was tracked throughout the time course. The plots were grouped into low bead density (~1-3 beads/frame), intermediate bead density (~3-7 beads/frame) and high bead density (>7 beads/frame). The black lines represents the movement of the cell centroid during a six hours time hour while the red dots represent the location of the alginate beads.

To illustrate the ability of our cells to perceive cues emitted from multiple sources, we tracked cells from nine independent experiments and related their movements to the positions of the alginate microspheres (Figure 2.6). As expected, when there was a relatively low density of beads (~1-3 beads/frame), the cell was more likely to migrate towards the closest one. In contrast, in the less common cases when higher densities of beads were observed, it was less obvious that the cells were faithfully tracking the overall gradient. This is why a quantitative analysis is important; estimation of the overall gradient, which depends on the relative sizes and locations of the beads (Materials and Methods), confirmed that these cells tended to follow the local PDGF gradient vector, with potentially significant contributions from multiple beads.

2.3.4 Chemotactic fidelity is sensitive to PDGF gradient steepness

We have previously shown that the asymmetry of PDGF-stimulated PI3K signaling in fibroblasts requires steep gradients with intermediate midpoint concentrations (Schneider & Haugh, 2005). Here, chemotactic movements of fibroblasts were found to follow a similar trend. A total of 52 cells, observed in 21 independent experiments, were analyzed with regard to their local PDGF gradient properties, cell movement trajectories, and PI3K signaling patterns. For each migration interval, the angles between the cell movement and PDGF gradient vectors (Figure 2.7A&B), between the PI3K signaling and PDGF gradient vectors (Figure 2.7C&D), and between the cell movement and PI3K signaling vectors (Figure 2.7E) were related to the normalized PDGF concentration and gradient steepness at the cell centroid.

The results show that the cells were best aligned with the gradient, both in signaling pattern and migration response, when the PDGF gradient was steep and its midpoint concentration was lower. For the purpose of comparison, a relative gradient of 10^{-3}/μm corresponds to a gradient of 5% across a typical cell length of 50 μm. This suggests that fibroblasts are not capable of gradient amplification as manifested in their chemotactic migration behaviors. The low chemotactic fidelity at higher PDGF concentrations is

consistent with the saturation of receptors, but might also reflect physical interactions of the cells in very close proximity with alginate beads.

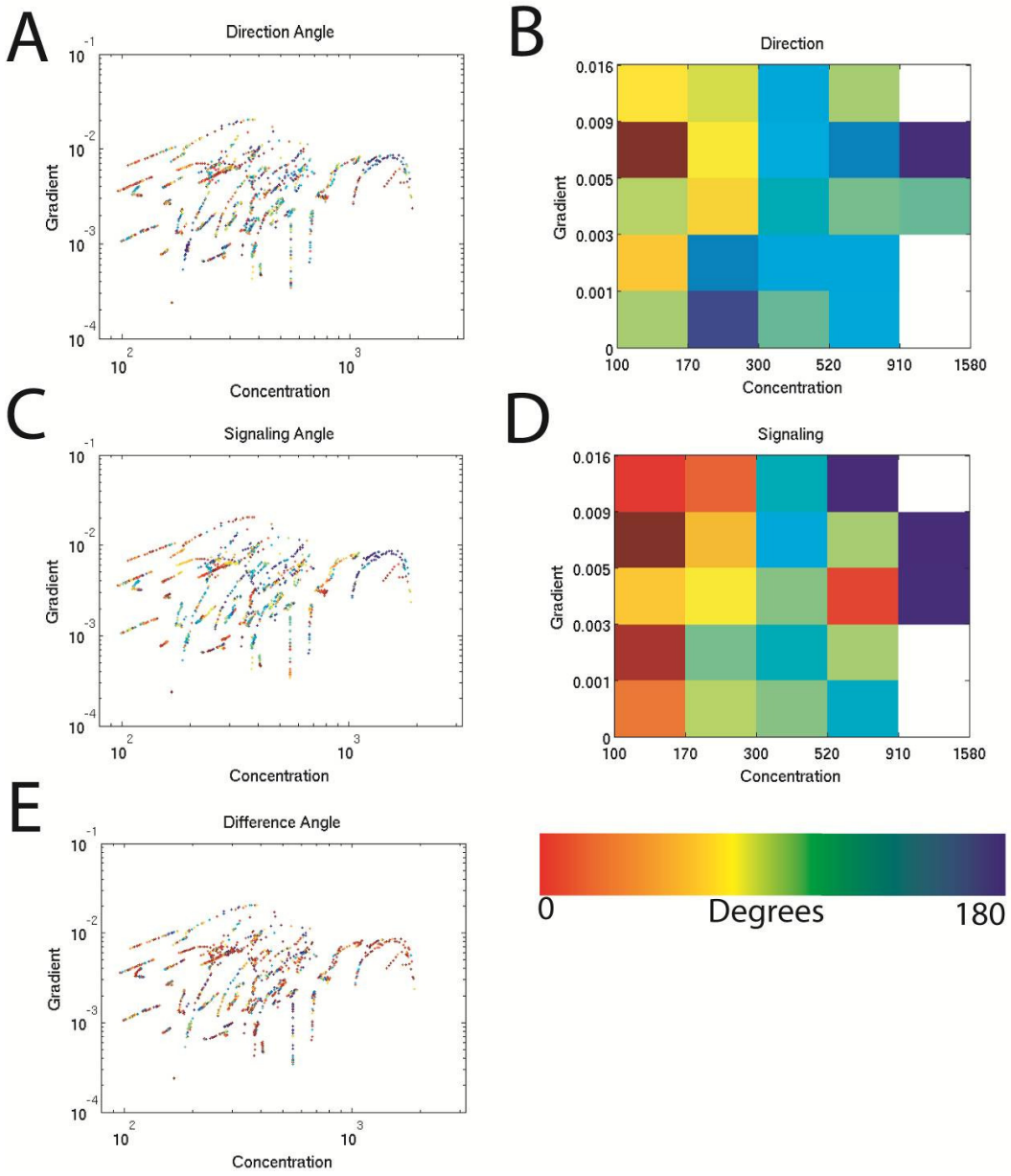

Figure 2.7 Impact of chemoattractant concentration and gradient steepness on persistent migration. Effects of normalized concentration and gradient steepness, determined for each time interval, on (**A**) the cell directionality angle θ_{MB}, (**C**) the signaling angle θ_{SB}, and (**E**) the difference between the two. Warmer colors indicate angles closer to zero. The scatter plots were binned in (**B**) θ_{MB} and (**D**) θ_{SB}, illustrating further that chemotactic fidelity is highest for steeper gradient and lower concentrations. The white regions of the heat map denote bins that do not contain data.

The properties of the PDGF gradient notwithstanding, the orientation of cell migration generally followed the pattern of PI3K signaling (Figure 2.7E). This indicates that, when the cell does not accurately sense the gradient, it moves in concert with stochastic dynamics of PI3K signaling, consistent with the random migration behavior of these cells (Weiger et al., 2010; Weiger et al., 2009).

2.3.5 PI3K inhibition impairs fibroblast chemotaxis

To further characterize the role of PI3K signaling in PDGF-directed fibroblast migration, the EGFP-AktPH-expressing cells were treated with the PI3K inhibitor LY294002 after four hours of chemotaxis. It was previously established that high concentrations of LY294002 are needed to block PI3K activation in NIH 3T3 cells (Haugh et al., 2000); accordingly, even at a concentration of 100 μM, cell-to-cell variations in the degree of PI3K inhibition and the inhibition of cell motility were observed. Most often, however, PI3K inhibition prompted a dramatic decrease in TIRF intensity and cell motility, with the cell contact area temporarily adopting a rounded-up morphology, followed by recovery of adhesion but not resumption of directed migration (Figure 2.8).

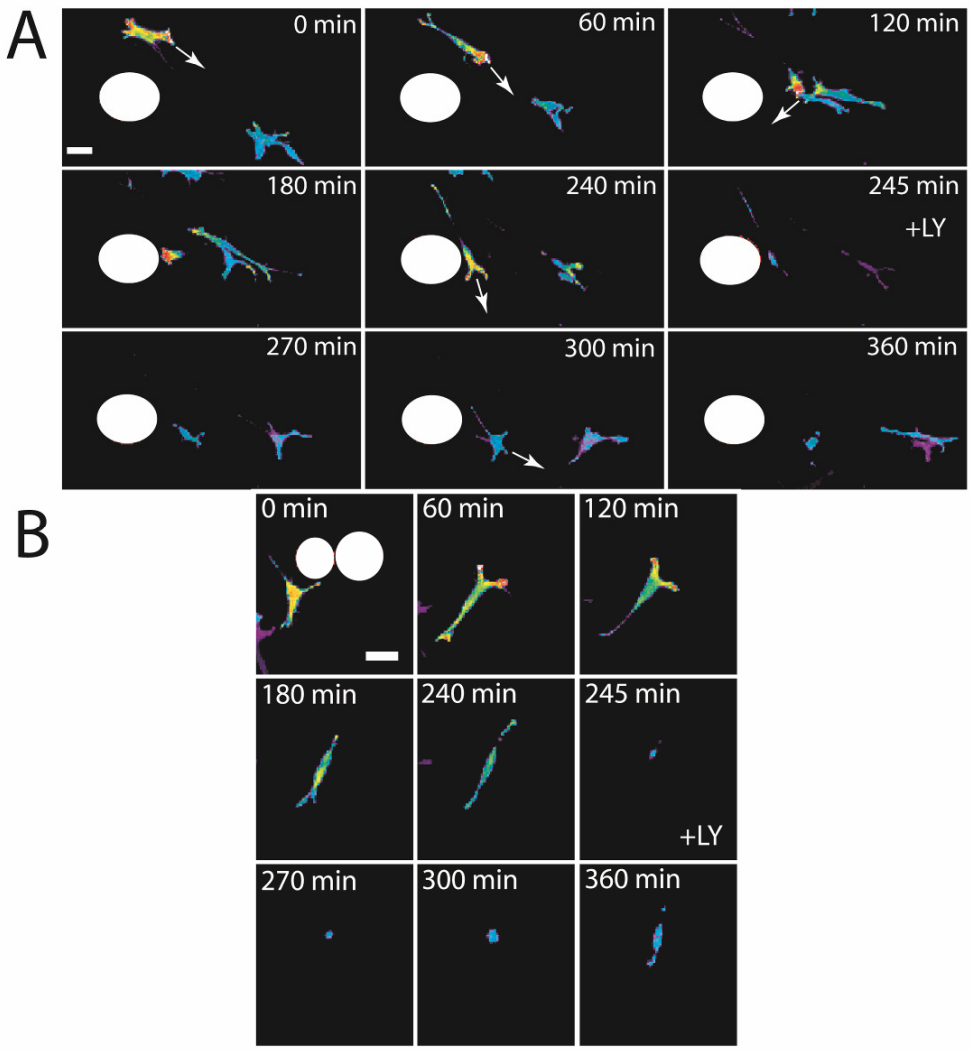

Figure 2.8 Pharmacological inhibition of PI3K impairs persistent fibroblast chemotaxis. (**A-B**) Two example cells demonstrate persistent migration towards the PDGF point source (beads are represented by white dots) for the first 240 minutes of the time course. 100 µM LY294002 treatment causes a dramatic decrease in the contact area of the cell as well as the rate of migration. The cell eventually recovers anywhere between 30-100 minutes post-LY treatment, but exhibits greatly reduced PI3K signaling and non-aligned migration towards empty space.. The white arrows (**A**) indicate the direction of the migration cell pre- and post-LY treatment. Scale bar is 30 µm.

2.4 DISCUSSION

Localization of PI3K-dependent signaling pathways is apparently important for cell motility in most if not all chemotactic cells. Here, using TIRF microscopy and alginate beads to deliver gradients of PDGF, we showed that fibroblasts respond to PDGF gradients with correlated PI3K signaling and biased migration responses, exhibiting robust chemotactic

fidelity only for certain gradient conditions. Cells located too close to a large alginate bead are likely to see a saturating concentration of PDGF, whereas very distant cells have difficulty sensing what would be a shallow PDGF gradient. In contrast, those cells that were moderately close to a smaller bead were apparently exposed to more favorable chemotactic stimuli, consistent with our previous analysis (Schneider & Haugh, 2005) (Figure 2.9).

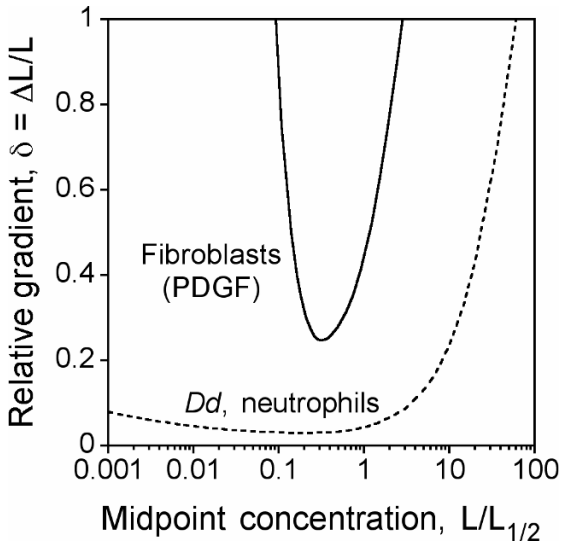

Figure 2.9 Sensitivity of spatial gradient sensing mechanisms. The degree to which PI3K signaling and cytoskeletal dynamics are polarized for chemotaxis depends on the steepness of the chemoattractant gradient, typically expressed in relative terms as the fractional or percent difference across the cell, and on its midpoint concentration. *Dictyostelium* and neutrophils are sensitive to shallow gradients over a broad range of midpoint concentrations (dashed curve), whereas fibroblasts require significantly steeper gradients within a narrow range of midpoint concentrations, reproduced from (Schneider & Haugh, 2006)

Our findings are parsimonious with recent findings that lower PDGF concentrations promote cell migration, whereas higher concentrations promote cell proliferation (De Donatis et al., 2008). Saturation of receptor occupancy is expected to maximize, not diminish, cell proliferation, survival, and responses that are not spatially specified.

We demonstrated that chemotaxis of fibroblasts, but not their random changes in contact area morphology, is abrogated by a pharmacological inhibitor of PI3K. These results solidify previous reports that PI3K plays a role in the spatial sensing of extracellular gradients in certain contexts, yet it is not absolutely required for migration (Kay et al., 2008; Kolsch, Charest, & Firtel, 2008). In fibroblasts, more research is pointing towards the

importance of the Rho-family GTPases Rac and Cdc42 in governing cell speed (Kardash et al., 2010; Monypenny et al., 2009) while suggesting a role for PI3K in directional sensing. The interplay between PI3K and Rac is a developing story, especially in the context of chemotaxis. Inhibiting PI3K signaling during fibroblast motility partially reduces Rac activity, which is important because localized Rac activity plays a central role in making the choice between random and directed migration (Pankov, 2005).

Although we have further verified the importance of PI3K signaling in fibroblast chemotaxis, it is important to connect these results to the activation of other pathways, most notably the Rho-family GTPases. Moreover, correlating chemoattractant receptor-mediated signaling with adhesion and cytoskeletal dynamics remains an exciting frontier that we hope will also shed additional light on the differences between mesenchymal and amoeboid migration.

2.5 REFERENCES

Andrew, N., & Insall, R. (2007). Chemotaxis in shallow gradients is mediated independently of ptdins 3-kinase by biased choices between random protrusions. *NATURE CELL BIOLOGY, 9*(2), 193-U191.

Bosgraaf, L., Keizer-Gunnink, I., & van Haastert, P. (2008). Pi3-kinase signaling contributes to orientation in shallow gradients and enhances speed in steep chemoattractant gradients. *JOURNAL OF CELL SCIENCE, 121*(21), 3589-3597.

De Donatis, A., Comito, G., Buricchi, F., Vinci, M., Parenti, A., Caselli, A., et al. (2008). Proliferation versus migration in platelet-derived growth factor signaling - the key role of endocytosis. *JOURNAL OF BIOLOGICAL CHEMISTRY, 283*(29), 19948-19956.

Devreotes, P. N., Zigmond, S.H. (1988). Chemotaxis in eukaryotic cells: A focus on leukocytes and dictyostelium. *Annual Review of Cell and Developmental Biology, 4*, 649-686.

Gruver, J., Wikswo, J., & Chung, C. (2008). 3 '-phosphoinositides regulate the coordination of speed and accuracy during chemotaxis. *BIOPHYSICAL JOURNAL, 95*(8), 4057-4067.

Haugh, J., Codazzi, F., Teruel, M., & Meyer, T. (2000). Spatial sensing in fibroblasts mediated by 3 ' phosphoinositides. *JOURNAL OF CELL BIOLOGY, 151*(6), 1269-1279.

Heasman, S., & Ridley, A. (2008). Mammalian rho gtpases: New insights into their functions from in vivo studies. *NATURE REVIEWS MOLECULAR CELL BIOLOGY, 9*(9), 690-701.

Heit, B., Liu, L., Colarusso, P., Puri, K., & Kubes, P. (2008). Pi3k accelerates, but is not required for, neutrophil chemotaxis to fmlp. *JOURNAL OF CELL SCIENCE, 121*(2), 205-214.

Iijima, M., Devreotes, P. (2002). Tumor suppressor pten mediates sensing of chemoattractant gradients. *Cell, 109*(5), 599-610.

Kardash, E., Reichman-Fried, M., Maitre, J., Boldajipour, B., Papusheva, E., Messerschmidt, E., et al. (2010). A role for rho gtpases and cell-cell adhesion in single-cell motility in vivo. *NATURE CELL BIOLOGY, 12*(1), 47-U112.

Kaur, H., Park, C., Lewis, J., & Haugh, J. (2006). Quantitative model of ras-phosphoinositide 3-kinase signalling cross-talk based on co-operative molecular assembly. *BIOCHEMICAL JOURNAL, 393*, 235-243.

Kay, R., Langridge, P., Traynor, D., & Hoeller, O. (2008). Changing directions in the study of chemotaxis. *NATURE REVIEWS MOLECULAR CELL BIOLOGY, 9*(6), 455-463.

Kolsch, V., Charest, P., & Firtel, R. (2008). The regulation of cell motility and chemotaxis by phospholipid signaling. *JOURNAL OF CELL SCIENCE, 121*(5), 551-559.

Lauffenburger, D., & Horwitz, A. (1996). Cell migration: A physically integrated molecular process. *CELL, 84*(3), 359-369.

Monypenny, J., Zicha, D., Higashida, C., Oceguera-Yanez, F., Narumiya, S., & Watanabe, N. (2009). Cdc42 and rac family gtpases regulate mode and speed but not direction of primary fibroblast migration during platelet-derived growth factor-dependent chemotaxis. *MOLECULAR AND CELLULAR BIOLOGY, 29*(10), 2730-2747.

Nishio, M., Watanabe, K., Sasaki, J., Taya, C., et. al. (2007). Control of cell polarity and motility by the ptdins(3,4,5)p3 phosphatase ship1. *Nature Cell Biology, 9*(1), 36-44.

Pankov, R., et. al. (2005). A rac switch regulates random versus directionally persistent cell migration. *Journal of Cell Biology, 170*, 793-802.

Parent, C. A., & Devreotes, P. N. (1999). A cell's sense of direction. *Science, 284*(5415), 765-770.

Ridley, A. (2001). Rho gtpases and cell migration. *JOURNAL OF CELL SCIENCE, 114*(15), 2713-2722.

Schneider, I., & Haugh, J. (2004). Spatial analysis of 3 ' phosphoinositide signaling in living fibroblasts: Ii. Parameter estimates for individual cells from experiments. *BIOPHYSICAL JOURNAL, 86*(1), 599-608.

Schneider, I., & Haugh, J. (2005). Quantitative elucidation of a distinct spatial gradient-sensing mechanism in fibroblasts. *JOURNAL OF CELL BIOLOGY, 171*(5), 883-892.

Schneider, I., & Haugh, J. (2006). Mechanisms of gradient sensing and chemotaxis - conserved pathways, diverse regulation. *CELL CYCLE, 5*(11), 1130-1134.

Servant, G., Weiner, O., Herzmark, P., Balla, T., Sedat, J., & Bourne, H. (2000). Polarization of chemoattractant receptor signaling during neutrophil chemotaxis. *SCIENCE, 287*(5455), 1037-1040.

Singer, A., & Clark, R. (1999). Mechanisms of disease - cutaneous wound healing. *NEW ENGLAND JOURNAL OF MEDICINE, 341*(10), 738-746.

Takeda, K., Sasaki, A., Ha, H., Seung, H., & Firtel, R. (2007). Role of phosphatidylinositol 3-kinases in chemotaxis in dictyostelium. *JOURNAL OF BIOLOGICAL CHEMISTRY, 282*(16), 11874-11884.

Weiger, M. (2008). *Integration of soluble and adhesive signals during fibroblast migration.* North Carolina State University, Raleigh, NC.

Weiger, M., Ahmed, S., Welf, E., & Haugh, J. (2010). Directional persistence of cell migration coincides with stability of asymmetric intracellular signaling. *BIOPHYSICAL JOURNAL, 98*(1), 67-75.

Weiger, M., Wang, C., Krajcovic, M., Melvin, A., Rhoden, J., & Haugh, J. (2009). Spontaneous phosphoinositide 3-kinase signaling dynamics drive spreading and random migration of fibroblasts. *JOURNAL OF CELL SCIENCE, 122*(3), 313-323.

Wessels, D., Lusche, D., Kuhl, S., Heid, P., & Soll, D. (2007). Pten plays a role in the suppression of lateral pseudopod formation during dictyostelium motility and chemotaxis. *JOURNAL OF CELL SCIENCE, 120*(15), 2517-2531.

CHAPTER 3

Development of microfluidic devices to study fibroblast chemotaxis in PDGF gradients

3.1 INTRODUCTION

Chemotaxis, or the directed migration of cells to external, chemical cues, is an essential process in a variety of cell types and organisms. In mammalian cells, it plays an essential role during wound healing, embryogenesis, and the immune response (Petrie, Doyle, & Yamada, 2009), as well as the metastasis of cancer cells. In other cells, such as the slime mold *Dictyostelium discoideum*, chemotaxis plays a pivotal role in the discovery of a new nutrient source or in the generation of a multicellular fruiting body to survive during periods of nutrient drought (Veltman, Keizer-Gunnik, & Van Haastert, 2008; Veltman & van Haastert, 2008). Chemotaxis of these cells involves the local production and degradation of a membrane-bound phosopholipid, phosphatidylinositol (3,4,5)-trisphosphate (PIP_3), at the plasma membrane resulting in a net accumulation at the leading edge of a migrating cell (Kolsch, Charest, & Firtel, 2008). This leads to actin polymerization, membrane extensions and, ultimately, cell displacement. There is a large body of work in the literature studying the effect of the intracellular machinery involved with the accumulation of PIP_3 at the leading edge of a migrating cell, focusing on the enzymes responsible for the generation of PIP_3, phosphoinositide 3-kinase (PI3K), and the degradation of PIP_3, the phosphatase PTEN (Andrew & Insall, 2007; Hoeller & Kay, 2007; Wessels, Lusche, Kuhl, Heid, & Soll, 2007). The interplay of these opposing enzymatic activities are thought to be responsible for amplifying shallow external gradients to promote robust chemotactic responses, yet it is not clear if a common amplification mechanism is conserved across all chemotactic cells to mediate polarized accumulation of PIP_3.

The bulk of the fundamental studies on chemotaxis have been carried using two model cell systems, *Dictyostelium* and human leukocytes, due to their rapid migration speeds and ability to sense shallow gradients of chemoattractants (Schneider & Haugh, 2006); these cells exhibit amoeboid motility, by which they protrusion at the front of the cell is balanced by contractile, “squeezing” forces at the cell rear. Other cells, such as fibroblasts and other

mesenchymal cells, move much more slowly and exhibit a different motility mechanism, whereby traction forces are generated through adhesion sites at the front of the cell (Lauffenburger & Horwitz, 1996); hence, it remains unclear to what extent the molecular mechanisms of chemotaxis may be generalized.

Contributing to the uncertainty in the field is the inadequacy of the methods used to study chemotaxis (reviewed in Chapter 1). Traditional methods, such as the Boyden chamber assay, are limited to qualitative studies of cell migration and are not compatible with fluorescence microscopy techniques. Other methods, such as flow from a micropipette, suffer from limited control of the gradient and small volume of solution only allowing for a few hours of migration (Soon, Mouneimne, Segall, Wyckoff, & Condeelis, 2005; Zheng, Felder, Connor, & Poo, 1994). To properly study fibroblast chemotaxis, new techniques that allow for the generation of stable, controllable chemoattractant gradients for long periods of time (hours to days) and which are compatible with fluorescence microscopy need to be developed and adopted.

Over the past decade there has been a rapid development of microfluidics-based methods for generating stable concentration gradients with controllable profiles (Keenan & Folch, 2008). Most commonly, poly-dimethylsiloxane (PDMS) replicas of a silicon master, generated by soft lithography techniques, have been used to create devices with micron-scale channels capable of creating a wide variety of gradients (Weibel, Garstecki, & Whitesides, 2005). PDMS offers several advantages, including suitable (and tunable) mechanical properties, optical transparency, moderate water permeability, and low cost (Weibel & Whitesides, 2006). Microfluidic devices have already proven useful in the study of neutrophil chemotaxis to IL-8 (Jeon et al., 2002; Lin et al., 2004, 2005) and breast cancer cell chemotaxis to gradients of EGF (Wang, Saadi, Lin, Nguyen, & Jeon, 2004). Furthermore, the complexity and utility of these PDMS microfluidics devices have increased dramatically over the past few years. Devices capable of evaluating neutrophil receptor desensitization (Keenan, Frevert, Wu, Wong, & Folch, 2010), of separating neutrophils from a whole blood sample (Agrawal, Toner, & Irimia, 2008), and replicating three-dimensional environments to study blood vessel growth (Barkefors, Thorslund, Nikolajeff, & Kreuger, 2009) have been

reported. A PMDS-based microfluidics device has been successfully used to study random migration of mouse fibroblasts, replicating the common "scratch-wound" assay without having to scratch the surface (Doran, Mills, Parker, Landman, & Cooper-White, 2009); however, there remains a limited body of work on the use of microfluidic devices to study fibroblast chemotaxis over the long time periods needed to observe significant cell movement.

This paper presents a study of two simple microfluidic devices used to generate stable gradients of soluble factors for experiment durations of 6-8 hours and which are compatible with total internal reflection fluorescence (TIRF) microscopy. The first design utilizes serpentine based micro-channels flowing into a main experimental chamber (Dertinger, Chiu, Jeon, & Whitesides, 2001). The device allows for precise control of the gradient and has almost no upper time limit for experimentation; however, designs of this type are difficult to maintain clear of air bubbles, and they directly expose the cells to fluid shear, both of which tend to compromise cell viability during long experiments. The second device is a ladder design adapted from Saadi and colleagues (Saadi et al., 2007) that establishes a controllable gradient without exposing the cells to direct flow. Here we describe the polarization of PI3K signaling in NIH 3T3 mouse fibroblasts as they responded to PDGF gradients within the ladder device. The cells generally failed to migrate, however, as their viability was not maintained beyond ~ 2 hours in the device. While the cause of the cell death remains undetermined, we ruled out leaching of unreacted siloxane monomers (Regehr et al., 2009) and other potentially toxic chemicals as a potential cause.

3. 2 MATERIALS AND METHODS

3.2.1 Microfluidics device design

Serpentine Device Design

Our first choice for a device design was developed based on previous work carried out by the Whitesides group for generating stable gradients of small molecules (Dertinger et al., 2001; Jeon et al., 2000), adapted to fit on a 25 mm X 25 mm footprint so as to be

compatible with our TIRF microscopy setup. Preliminary work with this device, including design and fabrication, was carried out by Dr. Michael Weiger (Weiger, 2008).

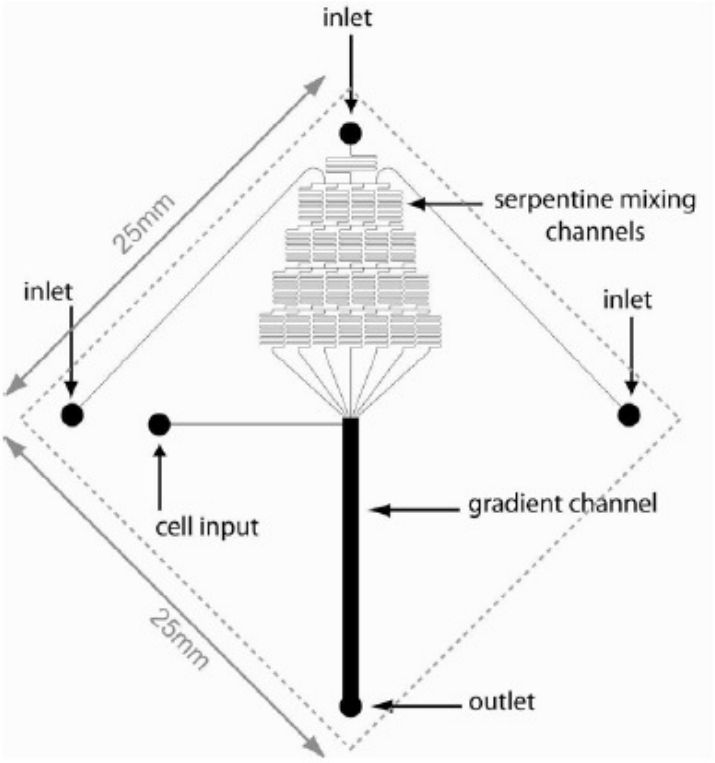

FIGURE 3.1 Serpentine microfluidics device design. A 25 X 25 mm device designed to fit on top of a glass coverslip that consists of 3 inlet ports, a cell inlet port, an outlet port, a series of serpentine mixing channels that splits and mixes 2 experimental solutions into 7 individual streams of varied concentrations that recombine in the main gradient channel to study directed fibroblast migration. (*Figure courtesy of Dr. Michael Weiger)*

The device consists of three inlet ports, one outlet port, a cell inlet port, a series of branching, serpentine channels for mixing, and a main channel into which all of the serpentine channels converge (Figure 3.1). The network of serpentine channels is designed to repeatedly split, combine and mix the two inlet streams in order to increase the number streams carrying different concentrations, with a total of 7 channels emerging and combing into the main channel. The result is a set of distinct streams of increasing concentration perpendicular to the direction of flow. Laminar flow is achieved in the channels of this device due the relatively small dimensions (~70 µm X 75 µm) and flow rates used during

experimentation (0.5-10 µL/min). Due to laminar flow conditions, the mixing of the chemoattractant with the buffer solutions occurs only by diffusion, and so the length of the serpentine mixing channels were designed to be long enough to accommodate proper diffusive mixing. As flow continues down the main channel, the chemoattractant continues to diffuse from high concentration to low concentration, producing a smooth, linear gradient. To study fibroblast chemotaxis and prevent issues that would arise from forcing cells to travel through the serpentine meshwork, a separate cell inlet port was designed to allow insertion of cells directly to the main channel where the migration could be studied. Additional schematics for this particular design, including channel dimensions and estimated flow rates, have been reported elsewhere (Weiger, 2008).

Ladder Device Design

Due to technical limitations and experimental difficulties with the serpentine device, a second device was designed, in which the flow across the migrating cells is minimized. This 'ladder' design has two inlet ports, two large side channels for fluid flow, and a series of center channels of varying lengths (or 'rungs') spanning the two side channels, wherein chemotaxis would be observed (Figure 3.2). The two side channels ultimately combine into a larger exit channel.

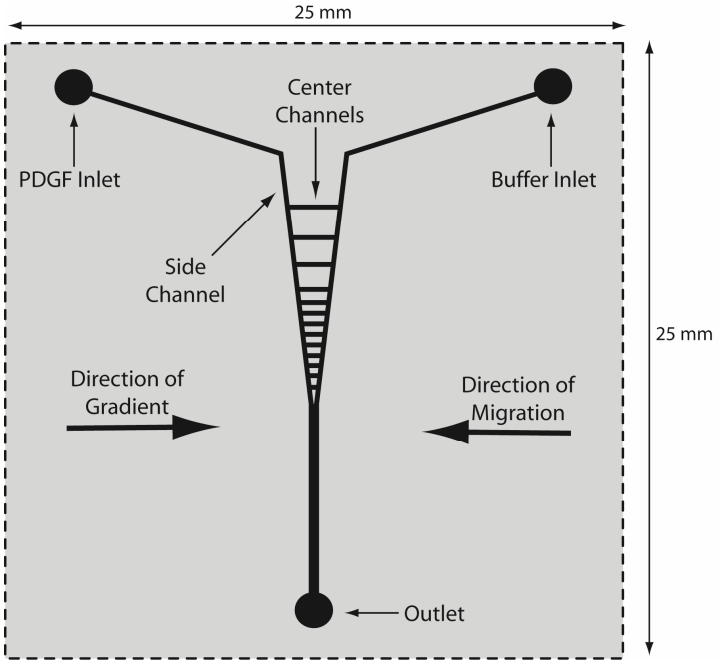

Figure 3.2 Ladder microfluidics device design. A 25 X 25 mm device consisting of two inlet ports and a single outlet port. Flow of chemoattractant and buffer through the device occurs in the two side channels while a gradient develops across the center channels spanning the two side channels. The cells are seeded inside the center channels, and the cells respond to the gradients that develop in the center channels.

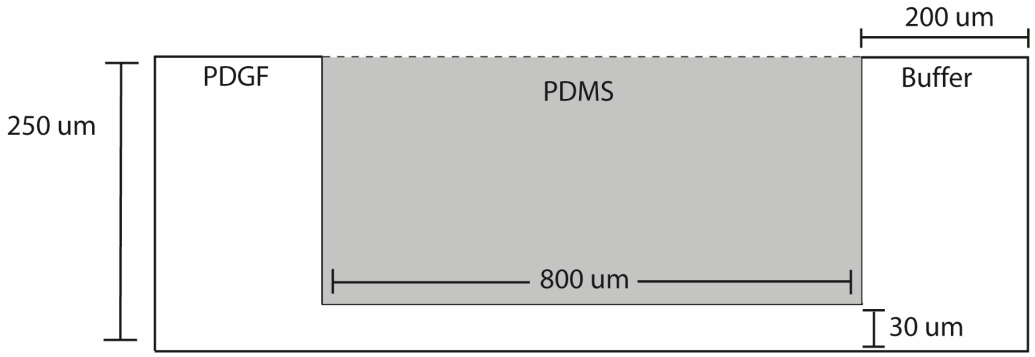

Figure 3.3 Side view of ladder microfluidics device. A side view of the ladder device shows the relative difference in heights between the side and center channels, which allows for reduced flow across the cells while simultaneously generating a gradient of chemoattractant across the channel by diffusion.

To prevent flow across the center channels, the device was fabricated so that the height of the side channels (~250 µm) was much greater than the heights of the center channels (~30 µm) (Figure 3.3). As a result, the bulk of the flow resides in the side channels, while a gradient of chemoattractant develops across the center channels by diffusion. The

premise of designing the center channels with various lengths is that linear gradients of different steepness are achieved. Thus, environments with gradients of varying steepness can be viewed in a single experiment. One technical drawback is that the cells must enter the device via the same inlet ports as the experimental solutions; however, we were able to devise a methodology that would maximize cell densities in the center channels without affecting the types of gradients generated (discussed later in this section). All inlet, outlet, and channel dimensions are specified in APPENDIX B.

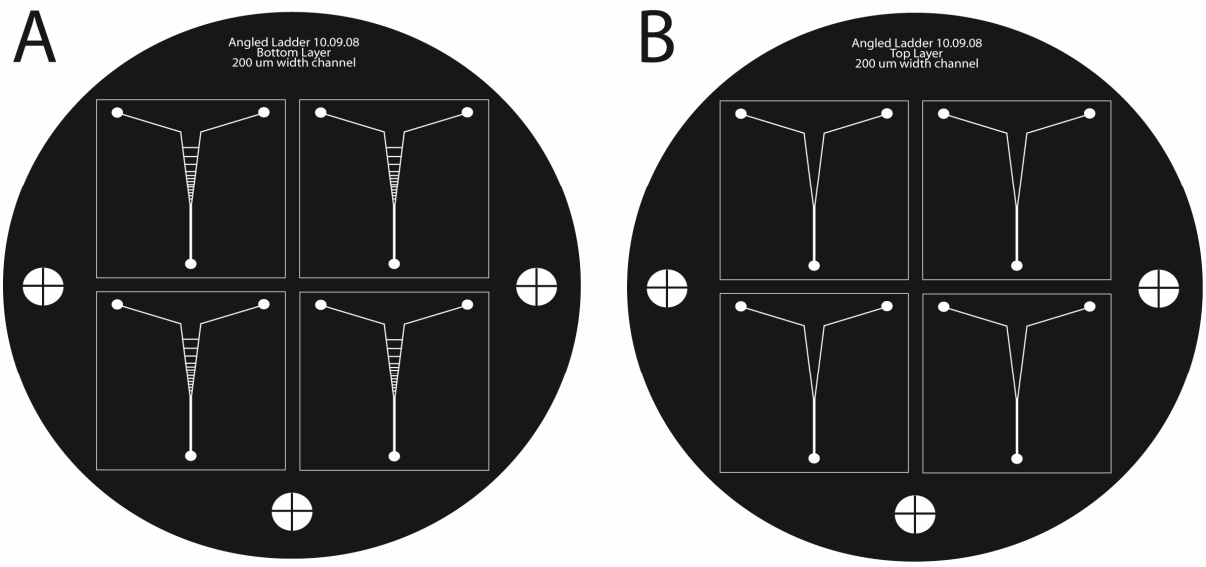

Figure 3.4 Transparency masks for the ladder device design. The transparency masks used to create a positive relief of SU-8 on the silicon wafers by exposing the white sections to UV light. (**A**) The mask used to create the 30 µm channels across the entire device. (**B**) The mask used to create the 250 µm side channels of a greater height according to the desired design schematics. The crosshairs on the sides and bottom are the markers needed to properly align the second mask to the first mask.

Adobe Illustrator CS was used to construct and export the final design into a file format appropriate for printing (AI). Because the ladder device requires channels of different heights, the entire soft lithography process was carried out in two steps (Figure 3.4). The first mask contains the complete device design along with three alignment markers at the left, right and bottom. The second mask is similar to the first, except it does not include the bridging center channels. Thus, the side channels are built up to a greater height than that of the center channels in the soft lithography mold. The designs were printed in transparency

form at 3556 DPI by Filmgraphics (Raleigh, NC). These transparencies serve as masks for transferring the design to the silicon master.

3.2.2 Microdevice fabrication

Soft Lithography Processing

The method of using soft lithography is well established in the literature as a successful and relatively cheap way to make microfluidics devices (McDonald et al., 2000). Typically, this approach uses SU-8, a high-contrast, epoxy-based, negative photoresist designed specifically for the fabrication of micro-size features. This photo-sensitive polymer was spun-coated onto a 3-inch, p-type, silicon wafer (Silicon Quest International), which was then exposed to a UV light source through the mask to crosslink and solidify the polymer in the transparent regions of the mask, thereby generating a positive relief on the wafer. To ensure a certain frequency of making enough devices with adequately precise dimensions, this protocol was carried out for four silicon wafers per batch. As each master was produced, it was incubated on a hot plate at 65^{o}C until all four wafers in the batch were ready, at which point the temperature was ramped to the desired baking temperature. The soft lithography procedure is summarized in Figure 3.5.

First, the silicon wafer was centered on the spinning chuck of a Laurell WS-400B-6NPP-LITE Spin Coater. While spinning at 3500 rpm, the wafer was washed twice with acetone and then twice with isopropyl alcohol, until the solvents completely evaporate. The wafer was then placed on a hot plate and baked for five minutes at 125 ^{o}C. The hot plates used for the fabrication process are all Dataplate PMC 720 series digital hot plates with an 'auto cool' function, such that the heating element was turned off once the allotted baking time is completed, and the wafers were allowed to cool down to room temperature. Hence, the wafer was repositioned on the Spin Coater, and roughly 3 mL of SU-8 2025 (MicroChem Corp) was added to the center of the wafer, slowly adding it to the center of the wafer while rotating the wafer manually to expand the center layer to form a circle (Figure 3.5A). This step is essential to establish a uniform coat of SU-8 across the surface of the wafer. To obtain a uniform, 30-µm-thick layer, the following spin protocol was used: (1) 500 rpm,

ramp up for 100 rpm/s, total time of 5 s, (2) 2500 rpm, ramp up for 300 rpm/s, total time of 30 s and (3) 0 rpm, ramp down for 300 rpm/s, total of 40 s. Following spin coating, excess SU-8 was removed from the edges of the wafer with acetone to prevent the wafer from sticking to the hot plate.

The wafer was then placed on the hot plate and baked for 20 minutes at 95^{o}C. Next, the wafer was exposed to UV light to cross-link the SU-8 according to the microfluidic design (Figure 3.5B).

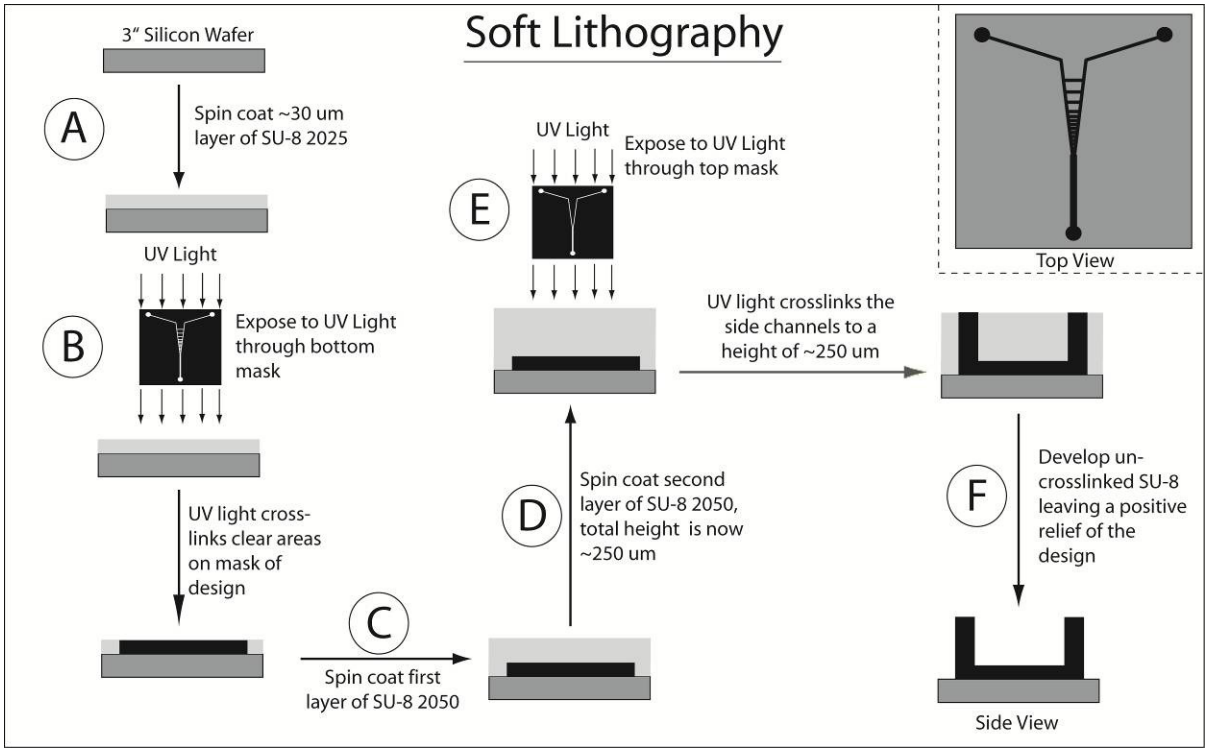

Figure 3.5 Soft lithography to make a silicon master. Soft lithography steps required to make a silicon master microfluidics device mold with channels of different heights. (**A**) SU-8 2025 is spin coated onto a 3" inch silicon wafer and then (**B**) exposed to UV light through a transparency mask with the microfluidics device. The white areas of the mask are the only ones where the UV light will pass through and crosslink the SU-8. (C-D) Two additional layers of SU-8 2050 are spin coated on top of the base layer to generate a thickness of 250 µm required for the side channels. (**E**) UV light is then exposed to the wafer through the top mask, only crosslinking the SU-8 on the side channels at this height. (**F**) The entire wafer is then immersed in SU-8 developer and all uncrosslinked SU-8 is removed leaving the final product, a silicon wafer with a positive relief of the ladder design with side channels at a height of ~250 µm and center channels at a height of ~30 µm.

An 'exposure sandwich' was constructed consisting of the SU-8-coated silicon wafer, the transparency mask bearing the device design, and a filter glass square to enhance UV cross-linking of the polymer; this assembly was exposed to UV light for 60 seconds. The transparency was then removed, and the wafer was baked for 5-10 minutes at 95^{o}C, until the microfluidics design was visible. After cooling the wafer, alignment markers were painted on using a white paint pen. The white marks are unaffected by the spin coating process and allow for proper alignment of the second transparency mask to the already cross-linked design.

Additional spin coating is required to make the side channels, following a similar protocol. A lower viscosity formulation of SU-8 was used to obtain a layer with total thickness of 250 µm; we choose to apply two layers of SU-8 2050 (MicroChem Corp) rather the even lower-viscosity SU-8 2100. This required additional preparation and fabrication steps but resulted in fewer mistakes and eliminated technical difficulties such as clumping and non-uniform coating. A first layer of 2050 (the second layer overall) was added to the center of the wafer as previously described and then spin coated using the following algorithm: (1) 500 rpm, ramp up for 100 rpm/s, total time of 5 s, (2) 1200 rpm, ramp up for 250 rpm/s, total time of 30 s and (3) 0 rpm, ramp down for 300 rpm/s, total of 40 s (Figure 3.5C). After cleaning off the edges with acetone, the wafer was baked at 65^{o}C for 5 minutes, 95^{o}C for 3 hours, and then cooled to room temperature. The second layer of 2050 was then applied to the wafer (the third overall layer) and coated using the same procedure (Figure 3.5D). The edges were cleaned with acetone, and the wafer was baked for 5 minutes at 65^{o}C, 4 hours at 95^{o}C, and then cooled to room temperature.

The wafer was then taped to a 4-inch, pre-cleaned wafer and aligned with the top transparency mask using a bench-top microscope. This is the most critical step in the fabrication process, and extra care must be taken to align the already crosslinked design with the transparency mask to ensure that the side channels remain uniform across the multiple layers of SU-8. Once the mask was aligned, the 'exposure sandwich' was constructed as previously described, and the wafer was exposed to UV light for a total of 165 seconds (Figure 3.5E). To prevent the heat generated by the UV lamp from affecting the silicon

wafer, the exposure was carried out for durations of 60 and 105 seconds, with a 90-second break in between. A piece of card stock was placed over the exposure sandwich during the break to prevent any mask shifting that could occur from moving the device manually. After UV crosslinking, the wafer was baked for 6 hours at 95^{o}C, after which the wafer was placed in a glass dish containing ~1-2 inches of SU-8 developer (MicroChem Corp) inside a fume hood. The wafer was incubated in the developing solution for ~50 minutes while manually agitating the dish every 5 minutes (Figure 3.5F). Next, the wafer was rinsed with isopropyl alcohol to remove residual SU-8 or SU-8 developer and inspected under a microscope. Finally, the wafer was baked for 40 minutes at 150^{o}C, cooled and then stored in a Petri dish until use. The end result is a silicon master with positive, micron-sized design features of varying heights that can be used to generate microfluidic device replicas.

PDMS Replica Molding and Device Construction

The silicon-based elastomer polydimethylsiloxane (PDMS) (Sylgard 184 Dow Corning) is the most widely used material in the fabrication of microfluidics devices (Dertinger et al., 2001; Duffy, Schueller, Brittain, & Whitesides, 1999; Sia & Whitesides, 2003). It is optically clear (refractive index of 1.43), cheap, and easy to manipulate and, until recently, thought to be biologically inert (Regehr et al., 2009). For these reasons, it has become the standard material for construction of microfluidics devices.

PDMS is a binary mixture that solidifies gradually as a result of combining an elastomer base and a curing agent. To make our replicas (Figure 3.6), the two components were mixed together manually in a 10:1 ratio by weight (1.0 g of base for every 0.1 g of curing agent) for 5 minutes before being placed in a vacuum desiccator for 60 minutes at room temperature to remove bubbles formed during the mixing process. The degassed PDMS was then slowly poured over the silicon SU-8 master (either the serpentine or the ladder design) and cured at 80^{o}C for 24 hours (Figure 3.6A), and then allowed to cool to room temperature prior to removal from the master mold (Figure 3.6). The heating process enhances the rate of PDMS cross-linking, generating a polymeric network with an elastic modulus of ~ 2-7 MPa. Additional heating was carried out to increase the extent of

polymerization and reduce the amount of un-crosslinked oligomers. Once cooled, the replicas were separated from the silicon master and cut from the PDMS monolayer. Holes were punched into the PDMS replicas with a 16-gauge needle at the inlet and outlet ports so that fluid could be introduced to the channels via Tygon tubing. Care was taken to reduce the chance of introducing debris into the channels.

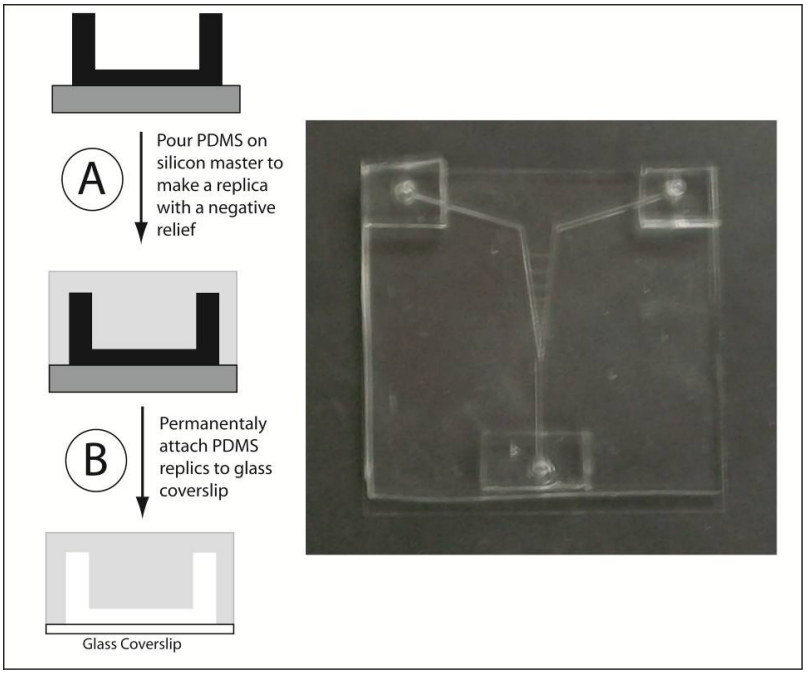

Figure 3.6 Generation of a PDMS replica microfluidics device (**A**) PDMS is poured in a 10:1 ratio on top of the silicon master and baked for 24 hours at 80^{o}C to solidify. The replica is separated from the master, excised from the excess PDMS and holes are punched in the inlet/outlet ports. (**B**) The device is then permanently bound to a glass coverslip via plasma oxidative treatment.

To prevent fluid leakages, the PDMS replicas were permanently bonded to the glass coverslip. Both the PDMS replica (channel side up) and the glass coverslip were treated by plasma oxidation for 30 seconds, using a PDC-32G Plasma Cleaner (Harrick Plasma), functionalizing the surfaces with hydroxyl groups (Chaudhury & Whitesides, 1991; McDonald et al., 2000). Once the two surfaces contact one another, they form irreversible Si-O-Si linkages, effectively sealing the channels and creating the fourth wall of the microfluidics device (Figure 3.6B). PDMS blocks on top of the inlet and outlet ports were

added once it was determined that the Tygon tubing connected to the device required a greater thickness of PDMS to maintain a proper seal. The blocks were prepared similar to the PDMS replicas, as detailed above, except the heating time at 80^{o}C was only 60 minutes. Once the PDMS replica was permanently bound to the glass coverslip, the PDMS replica was treated in the plasma cleaner again along with three PDMS blocks for 30 seconds. The blocks were then placed, manually, at each of the inlet and outlet ports, taking care to properly align the two sets of holes.

Extraction of Uncrosslinked Oligomers with Organic Solvents

Once it was suspected that uncrosslinked oligomers were negatively affecting cell migration and cell behavior, the removal of these contaminants became of utmost importance. The hydrophobicity of PDMS, a quality which makes it an advantageous material for microfluidics devices, also causes it to have a high solubility in nonpolar organic solvents (Lee, Park, & Whitesides, 2003), which results in swelling of the polymer and the suspected removal of any contaminates. To extract oligomers from our PDMS replicas, we carried out a serial extraction method adapted from work performed by Millet and colleagues (Millet, Stewart, Sweedler, Nuzzo, & Gillette, 2007) that has shown some success in removing uncrosslinked oligomers. The following steps were carried out after the generation of the PDMS replica from the silicon master but before the permanent plasma bonding of the replica to the glass coverslip.

The PDMS replicas and PDMS blocks were placed in a Pyrex glass dish and immersed in 100 mL of toluene, with continuous agitation, for 36 hours at room temperature in a fume hood. The toluene was discarded and replaced with a fresh 100 mL for an additional 12 hours. The toluene was removed, and the replicas and blocks were next immersed in 200 proof ethanol for 2 hours, 22 hours, and then 7 hours, replacing the ethanol with a fresh 100 mL each time, for a total incubation time of 31 hours. The devices were then placed in 100 mL of deionized water for 24 hours once again under constant agitation. Once the extraction steps were completed, the PDMS replicas and blocks were baked for 48

hours at 90°C in a vacuum oven to completely remove the solvents. The replicas and blocks were then subjected to plasma cleaning as previously described.

3.2.3 Cell culture and reagents

Stable expression of the 3' phosphoinositide-specific biosensor construct EGFP-AktPH (Haugh, Codazzi, Teruel, & Meyer, 2000) in NIH 3T3 mouse fibroblasts (American Type Culture Collection) was achieved by retroviral infection after cloning into the NotI/BamH1 sites of the pBm-IRES-puro vector (a gift from Dr. Steven Wiley, Pacific Northwest National Laboratory). The ecotropic ΦNX packaging cell line was transiently transfected, and virus-containing supernatants were used for serial infection of NIH 3T3 cells as previously described (Kaur, Park, Lewis, & Haugh, 2006). Cells were maintained in regular growth medium (Dulbecco's modified Eagle's medium supplemented with 10% v/v fetal bovine serum and 1% v/v penicillin/streptomycin/glutamate) in a 37°C incubator with 5% carbon dioxide. All tissue culture reagents were purchased from Invitrogen (Carlsbad, CA) and cells were used between passages 10-40. Human plasma fibronectin was obtained from BD Biosciences (San Jose, CA). Human recombinant PDGF-BB was from Peprotech (Rocky Hill, NJ). Imaging buffer (20 mM HEPES pH 7.4, 125 mM NaCl, 5 mM KCl, 1.5 mM $MgCl_2$, 1.5 mM $CaCl_2$, 10 mM glucose, and 2 mg/mL fatty acid-free bovine serum albumin) was prepared in the laboratory and supplemented with 1% v/v fetal bovine serum.

3.2.4 Chemotaxis experiments

Preparations of PDMS microfluidic devices for experiments were carried out as follows. First, a 3-inch segment of Tygon tubing (Cole Parmer) was inserted into each inlet/outlet port. A 0.5-inch piece of a blunted, 27-gauge metal needle was inserted into the tubing to act as a connector between the tubing in the device and the tubing connected to the syringes. Next, two 10-cc syringes are filled with pre-warmed, degassed deionized water and connected to the device with ~12 inches of Tygon tubing each. The dH_2O was flushed manually through the device to remove air trapped in the center channels. Depending on the experimental conditions, the device was either allowed to incubate with water in the channels

at 37^0C for 15 minutes (without extraction), or the entire device was immersed in deionized water and allowed to incubate for 24 hours at 37^oC (with extraction). For the 'with extraction' experiments, the devices were prepared the day before the experiments, whereas the 'without extraction' experiments used devices that were prepared on the same day. Regardless of method, the protocol from this point forward was the same. Once the water flush was completed, the 10-cc water syringes were removed, and two 5-cc syringes filled with a solution of 10 µg/mL human fibronectin were connected. The fibronectin solution was added manually to (1) remove the deionized water and (2) thoroughly coat the inside channels with fibronectin. The fibronectin solution was incubated in the channels for 1 hour at 37^oC to ensure uniform adsorption on the glass surface.

The day before each experiment, EGFP-AktPH-expressing NIH 3T3 cells were seeded on 10-cm tissue culture plates to yield a sufficiently high cell density (>90% confluency). On the day of the experiment, cells were detached via a brief trypsin-EDTA treatment and suspended in imaging buffer. Following centrifugation at 100 rcf for 3 minutes, the cells were resuspended in ~5 mL of imaging buffer and distributed into two 3-cc syringes. The cells were slowly added to the device via the two inlet ports. The reason for the initial high cell density is that only a small percentage of cells are distributed into the center, experimental channels. Once an appropriate cell density was achieved in the center channels (~4-10 cells/channel), the still-connected device was placed in the 37^oC incubator for 60 minutes to allow cell adhesion and spreading on the fibronectin-coated glass. Meanwhile, two 10-cc syringes were prepared, one containing imaging buffer with 1 nM human recombinant PDGF-BB and 1-5 µM rhodamine-dextran (Sigma) as a visual marker, the other containing imaging buffer only. Both solutions were well mixed and pre-heated to 37^oC.

The device was then removed from the incubator and connected to the two experimental syringes using matching, 24-inch lengths of Tygon tubing; the tubing was primed with the experimental solutions before attaching them to the blunted metal connectors. With the tubing connected, the device was loaded onto the microscope stage, which is enclosed by a plexiglass chamber maintained at 37^oC (Figure 3.7). The majority of

the tubing was also housed in the plexiglass chamber to pre-heat the solutions before they enter the PDMS device. The two syringes were each secured to a Pico Plus Syringe pump (Harvard Apparatus), which controls the flow rate of the injected solution (0-10 µL/min). The time course begins as soon as flow is initiated from the pumps. As discussed previously, the set-up protocol was somewhat different for the serpentine device but roughly followed the same protocol of dH_2O flush, fibronectin treatment, addition of cells, and initiation of flow.

3.2.5 Microscopy

TIRF microscopy was used to selectively excite fluorophores within ~100 nm of the cell contact area, effectively illuminating the plasma membrane of fibroblasts and ~5-10% of the cytoplasm directly above it (Schneider & Haugh, 2004). The details and theory behind TIRF microscopy are included in APPENDIX A. Our prism-based TIRF microscope (Figure 3.7) has been described previously (Schneider & Haugh, 2005; Weiger et al., 2009). Briefly, the glass coverslip is optically coupled to the prism with 518F immersion oil (Zeiss). A laser beam is then aimed through the prism at an angle greater than the critical angle, imparting an evanescent wave that selectively excites the intracellular biosensor (EGFP) and volume marker (rhodamine-dextran) close to the glass-water interface. EGFP is excited using a 60 mW 488 nm line from a tunable wavelength argon ion laser head (Melles Griot, Irvine, CA), whereas rhodamine-dextran is imaged using a 100 mW diode-pumped 561 nm laser (Crystalaser, Reno, NV). The emission filters are 515/30 nm for EGFP and 630/60 nm for rhodamine-dextran (Chroma, Brattleboro, VT). A 10X water immersion objective (Zeiss Achroplan, 0.5 NA) and 0.63X camera mount were used. Digital images, with 2x2 binning, were acquired at 20-second intervals using a Hamamatsu ORCA ER cooled CCD (Hamamatsu, Bridgewater, NJ) with a fixed exposure time X gain of 1000-1600 ms for EGFP and 1600 ms for rhodamine-dextran. Image acquisition is controlled using Metamorph imaging software (Universal Imaging, West Chester, PA).

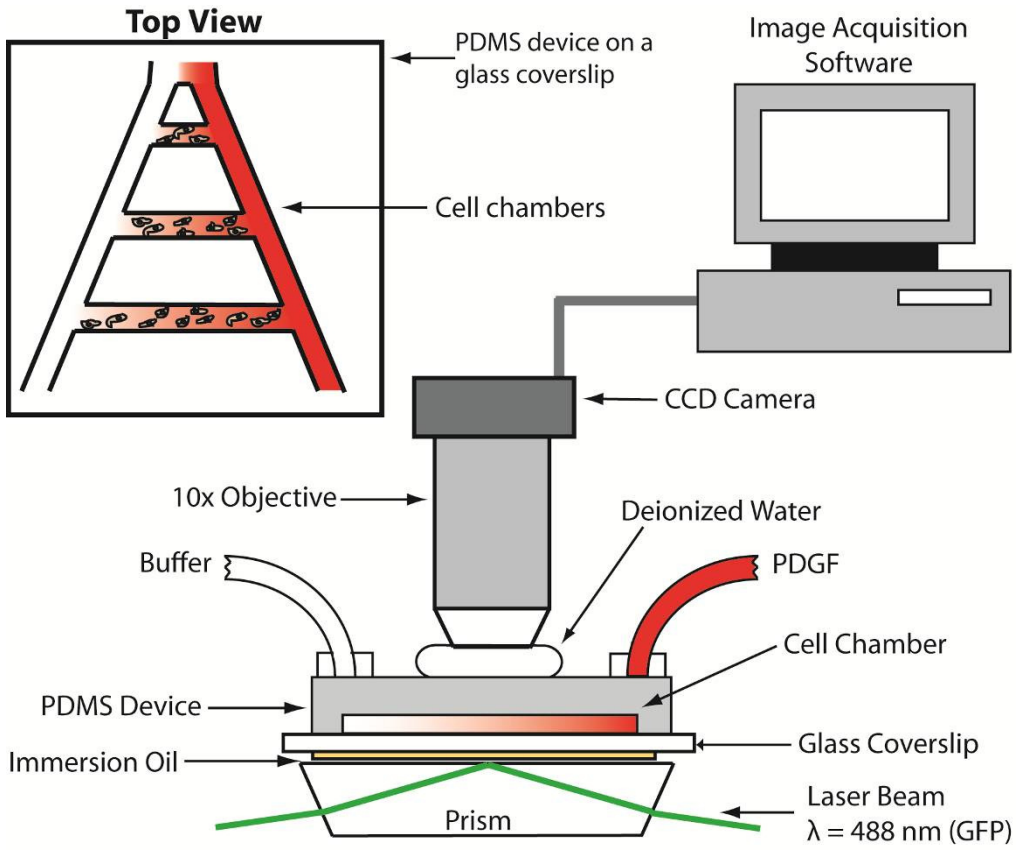

Figure 3.7 PDMS microfluidics device integrated with TIRF microscopy. The microfluidics devices is prepared as previously detailed and placed in the microscope stage. The glass coverslip of the device is then optically coupled to the prism with immersion oil and ready for TIRF microscopy. A droplet of deionized water is placed on top of the microfluidics devices to accommodate the 10X water immersion objective of the microscope connected to a CCD camera connected to our imaging software. The entire setup is encased in a plexiglass chamber to maintain an experimental temperature of 37°C.

3.2.6 Image and data analysis

Evaluation of the gradient produced in both the serpentine and ladder devices was performed by analyzing line-scan fluorescence profiles taken across the migration region. To calculate the relative gradient around a particular cell required additional calculations. A 50-100 µm line scan (depending on the starting/finishing position of the cell) was acquired above a migrating cell during the initial 2-hour migration period. An average slope, $\Delta F/\Delta x$, was calculated (assuming a linear gradient profile) for time (image) i (Equation 3.1). The mid-point fluorescence is the estimated value of the fluorescence evaluated at the mid-point position of the cell, $x_{mid,i}$, with the background fluorescence value, $F_{BG,i}$, subtracted (Equation

3.2). The relative gradient, *RG*, may then be calculated, taking into account the length of the cell, L_{cell} (Equation 3.3). For example, a value of $RG = 0.1$ indicates a 10% difference in concentration across the length of the cell.

$$F_i = (\Delta F / \Delta x)_i * x_i + B_i . \tag{3.1}$$

$$F_{mid,i} = \left[(\Delta F / \Delta x)_i * x_{mid,i}\right] + B_i - F_{BG,i} . \tag{3.2}$$

$$RG_i = \frac{L_{cell}}{F_{mid,i}} \left(\frac{\Delta F}{\Delta x} \right)_i . \tag{3.3}$$

Only cells present in the center channels of the ladder device were analyzed. Additionally, the cells could not come into contact with other cells during the course of the experiment, and the cells had to exhibit average fluorescence intensities significantly above background values (>500) but below the saturation level of the camera (<4000). Two quantities were assessed as a function of time for each cell meeting the above criteria: (1) the normalized cell fluorescence (*CF*; Equation 3.4), and (2) the normalized contact area (*CA*; Equation 3.5).

$$CF = \frac{F_{cell} - F_{end}}{F_{end} - F_{back}} . \tag{3.4}$$

$$CA = \frac{A_{cell}}{A_o} . \tag{3.5}$$

Here, F_{cell}, F_{end}, and F_{back} are the fluorescence intensity values of the cell (averaged over the cell area, determined using a suitable threshold), of the cell at the end of the experiment (averaged over the last 4 minutes), and of the background. Thus, since the fluorescence intensity generally decays as the cell viability suffers during the experiment, the value of CF decays to zero, and its initial value indicates the extent of the decay. *CA* is the ratio of the contact area above threshold, A_{cell}, relative to its initial value, A_0. Thus, *CA* has a value of one initially and approaches zero as the cell detaches.

3.3 RESULTS

3.3.1 Generation of stable, tunable PDGF gradients in the serpentine microfluidics device

Since the success of the serpentine PDMS device was already established, we began our study by fabricating this device as previously described and using it to generate PDMS replicas capable of generating controllable chemoattractant gradients. To evaluate the types of gradients that could generated by this device as well as their sustainability, we used test solutions containing rhodamine-dextran (Rho-Dex) as a fluorescent volume marker. We validated that the gradients generated in the center channels are directly related to the relative flow rates of the inlet streams (Figure 3.8). When equal flow rates of 0.5 μL/min were administered from the buffer and Rho-Dex syringes, a step gradient is generated in the main channel (Fig 3.8A), indicative of laminar flow; the step pattern is smoothed by diffusion to produce a linear gradient with decreasing steepness at more distant points in the main channel (Weiger, 2008). Increasing either the Rho-Dex inlet flow rate (Fig. 3.8B) or the buffer inlet flow rate (Fig. 3.8C) to 10 μL/min while maintaining the other inlet flow at a rate of 1 μL/min produced either very steep or very shallow gradients, respectively. A change of inlet buffer/Rho-Dex syringe flow rates causes an observable change in the micro channels on the order of seconds to minutes, allowing for fairly rapid switching of the gradient.

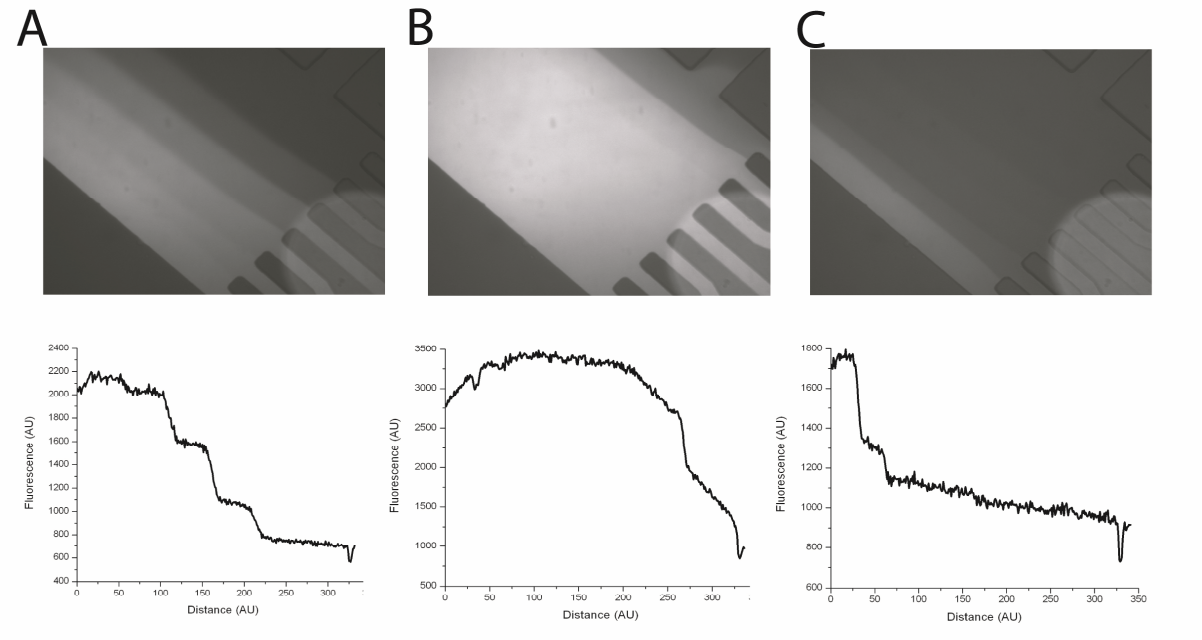

Figure 3.8 Tunable gradient generation in the serpentine device. Tunable gradients at the convergence point of the seven outlet channels from the serpentine device into the main channel. Fluorescence rhodamine-dextran is illuminated by the yellow laser and quantified with TIRF microscopy. (**A**) Step gradient generated by equal flow rates of the buffer and rhodamine-dextran solutions of 0.5 µL/min. (**B**) Steep gradient caused by 10 µL/min rhodamine-dextran and 1 µL/min buffer flow. (**C**) Shallow gradient the result of 1 µL/min rhodamine-dextran and 10 µL/min buffer flow rates.

Calculations were performed based on the channel dimensions and flow rates to determine the values of the Reynolds number, *Re*, for the flows. They were found to be between 0.1 and 7 in the mixing channels and between 0.01 and 0.5 in the main channel, all well below the transition between laminar and turbulent flow.

3.3.2 Technical problems encountered with the serpentine design

Although the serpentine design offers suitable gradient control, it suffers from certain issues that precluded its use for studying chemotaxis over long time periods. In our experiments, NIH 3T3 fibroblasts expressing GFP-AktPH, a fluorescent reporter of PI3K signaling, were seeded in the main channel of the device (Figure 3.1) after an initial flush with buffer to remove air bubbles present in the channels. The cells were allowed to adhere for 30-45 minutes to the fibronectin-coated surface at a greatly reduced flow rate (0-0.1

μL/min) before initiating flow of the experimental solutions at an increased flow rate (between 0.1-5 μL/min) for a migration time course ranging from 2-4 hours.

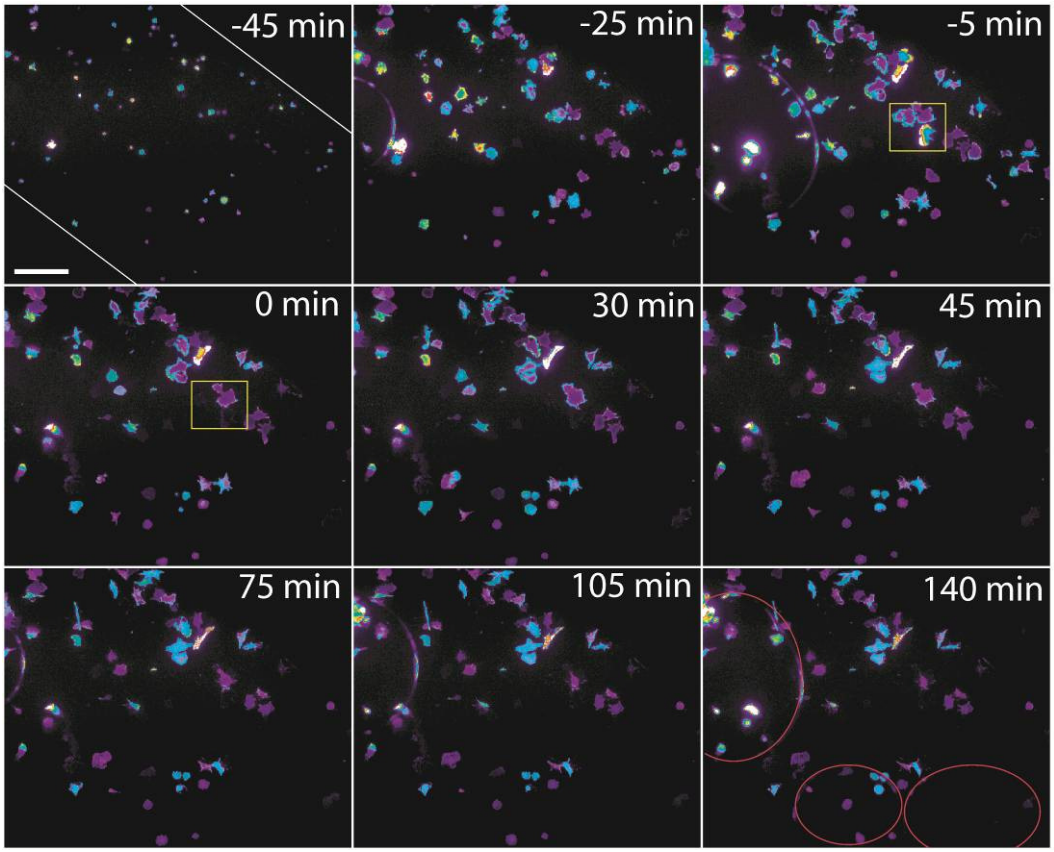

Figure 3.9 Appearance of bubbles in the main channel negatively affects cell migration. Time lapse images were taken during the migration experiment where 0 min indicates the initiation of 0.1 μL/min flow. Prior to the 0 min time point a flow of 0 μL/min was maintained while the cells adhered and spread to the fibronectin-coated glass coverslip. The yellow box in the -5 min and 0 min frames show the removal of cells due to flow necessary to removal the bubble from the channel. Red circles at the 140 min frame highlight 3 bubbles present at the termination of the experiment. Scale bar is 200 μm.

The first issue with the serpentine design was the appearance of air bubbles in the center channel. A typical time course is depicted in Figure 3.9, showing the appearance of multiple bubbles. Initially, no bubbles were found in the main channel, but as time progressed during the cell adhesion time course (flow rate of 0 μL/min), a bubble appeared and grew in size. Just before the migration experiment was initiated, flow of buffer was increased to 20 μL/min to remove the bubble from the field as well as a few bubbles that had

formed upstream; this resulted in a few cells being sheared off of the surface (Figure 3.9, yellow box) in this experiment. Once flow was restored to 0.1 µL/min, we did observe an increase in probe fluorescence accompanied by a change in cell morphology to adopt a more polarized phenotype. Nevertheless, before any substantial migration could be observed more bubbles began to appear from both downstream and upstream of the field (75-140 minutes), resulting in impaired flow in the channels, aberrant TIRF fluorescence, and ultimately cell death.

The second issue is the decline in cell viability with time under flow. Once flow was initiated in the serpentine device, if no bubbles were encountered, the experiment nonetheless ended with systematic cell detachment. As shown in Figure 3.10B, the cells typically adhered and spread nicely during the first 30 minutes, and they typically responded to the PDGF gradient 15-30 minutes after flow is initiated; however, after 30-60 minutes the cells exhibit progressive decreases in fluorescence and contact area. Based on control experiments in which flow was not initiated, the indication is that direct flow, and not some component in the solutions (e.g. Rho-Dex), is the main cause of the decline in viability.

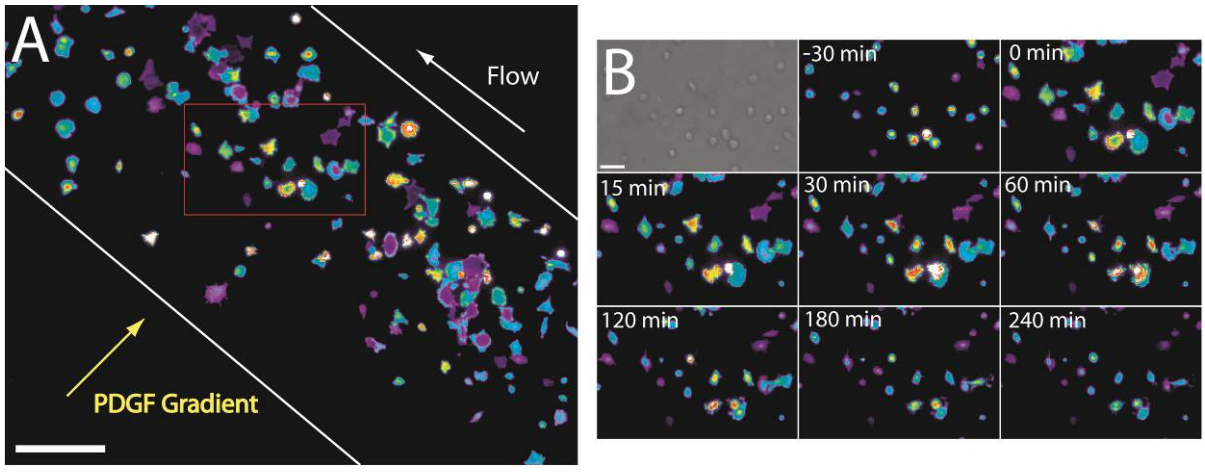

Figure 3.10 Rapid decay of cell viability in the serpentine device. (**A**) PI3K dynamics and cell directionality were monitored in cells plated in the main channel of the serpentine device exposed to a gradient of PDGF. The white lines indicate the boundary of the main channel while the direction of flow and the direction of the PDGF gradient are indicated. Scale bar is 200 µm. (**B**) Time lapse images were taken during the migration time course where 0 min indicates the initiation of 1 µL/min flow. Prior to the 0 min time point a flow of 0.1 µL/min was maintained while the cells adhered and spread to the fibronectin-coated glass coverslip. All images are representative of the red square region in (**A**). Scale bar is 150 µm.

3.3.3 Time-dependent generation of a PDGF gradient in the ladder device

Once it was decided that the serpentine device was not going to be suitable to study fibroblast chemotaxis, we implemented a device that would allow for a gradient of chemoattractant to develop without the migrating cells being exposed to significant flow or bubbles. Our design was based on a ladder device described by Saadi and colleagues (Saadi et al., 2007), with minor modifications. This device has a substantial difference in channel height between the side and center channels, such that most of the direct flow (0.5-10 µL/min) will bypass the cells located in the center channels. Thus, gradients develop across the center channels predominantly by diffusion. In our device, the sides channels are tapered, with center channels of varying length to produce linear gradients of varying steepness (Figure 3.2).

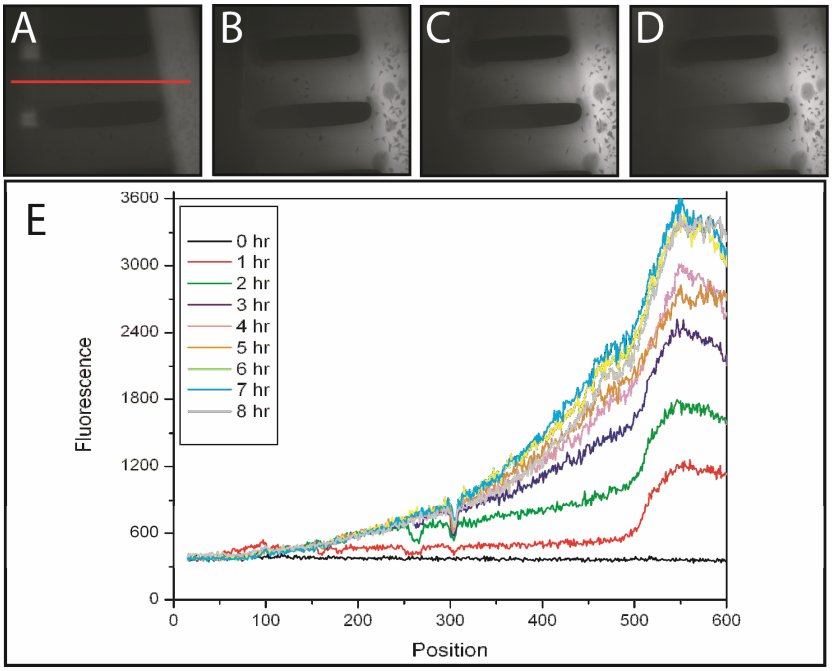

Figure 3.11 Development of a gradient across the center channels of the ladder design. An 8 hour time course was conducted to evaluate the generation of the chemoattractant gradient. Images were taken at 1, 3, 6, and 8 hours during the experiment (**A-D**) to show the development of a gradient of Rho-Dex as a result of a flow rate of 10 µL/min and a concentration of 1 µM. (**E**) Line scans were performed using Metamorph Imaging Software to determine the fluorescence of the tracer in the center channels over time. The red line is the line scan performed across the center channel.

To evaluate the formation and stability of gradients that could be generated in this device, we evaluated the gradient during fibroblast migration experiments. The inlet ports were connected to syringes with either imaging buffer or imaging buffer supplemented with 1 μM of the fluorescent volume marker Rho-Dex and 1 nM PDGF.

During 8-hour time courses, we observed that the Rho-Dex/PDGF gradient was slow to develop, on the order of hours, in contrast with the serpentine design. As seen in a representative experiment (Figure 3.11), the gradient required ~ 3-4 hours to develop. Although these results confirm that a gradient of chemoattractant was produced, the slow response of the gradient is less than ideal. The slow time scale can be attributed partially, but not solely, to that of diffusion across the channel; the channel width was ~ 10^3 μm, and the diffusivities of both Rho-Dex and PDGF are ~ 100 $\mu m^2/s$, corresponding to a time scale of ~ 1 hour for equilibration; however, as seen in Figure 3.11, the fluorescence intensity also steadily increases in the side channel, which is surprising given the fast flow rate of 10 μL/min (residence time ~ 15.9 sec). One possibility that cannot be ruled out is accumulation of nonspecific Rho-Dex adsorption to the glass surface.

3.3.4 Fibroblast polarization and chemotaxis in response to PDGF gradients

PI3K dynamics and cell motility were studied using EGFP-AktPH-expressing fibroblasts in the ladder device (Figure 3.12). Preliminary studies were carried out on cells during two-hour time courses in the ladder design. After an initial serum starvation/cell adhesion period, a flow rate of 5-10 μL/min was initiated in the device with buffer in the left channel and buffer supplemented with 1 μM Rho-Dex and 1 nM PDGF in the right channel. The result is, once again, a gradient orthogonal to the direction of flow across the center channels of the device. All of the cells analyzed were evaluated based on their (1) response to PDGF (increase in cellular fluorescence after flow begins), (2) net displacement (migration away from the initial position), and (3) polarized phenotype (presence of fluorescent hot spots and adjustment in cell morphology aligned with the direction of the gradient) and then assigned to three distinct groups: not polarized, polarized but not aligned

with the gradient, and polarized in the direction of the gradient. A total of 40 cells were analyzed from 30 independent experiments, summarized in Table 3.1.

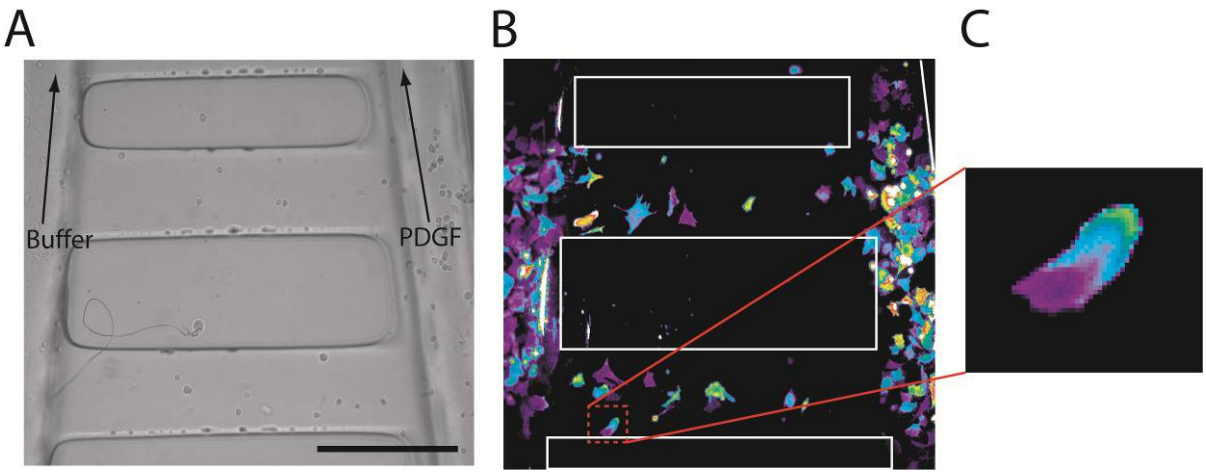

Figure 3.12 Cell migration in the ladder microfluidics device. The ladder microfluidics device is visualized in both brightfield (**A**) to find the channels and TIRF (**B**) to observe cell migration. (**C**) A single cell is then isolated from one of the channels, enlarged and analyzed for polarity and directionality.

Table 3.1 Summary of cellular response to a PDGF gradient in the ladder microfluidics device. A total of 40 cells were analyzed from 30 independent experiments and sorted into three groups. No response indicates cells that did not exhibit a polarized phenotype and did not have any net displacement. Non-aligned migration consist of cells that did exhibit a polarized phenotype but migrated in a direction other than up the PDGF gradient while aligned migration consists of cells with a polarized phenotype that did migrate up the gradient.

	Not polarized	Polarized but not aligned with the gradient	Polarized in the direction of the gradient
Total number of cells	24	4	12
Percent of population	60%	10%	30%

The polarized phenotype of a migrating fibroblast has been well established and is defined by an elongated morphology parallel to the direction of the gradient accompanied by PI3K hot spots at the front of the cell (Schneider, Parrish, & Haugh, 2005). This polarized

phenotype, when observed in the ladder device, developed during the first hour of PDGF stimulation and usually preceded the directed migration of the cell up the gradient of PDGF (Figure 3.13A-B). Presumably, the timing of the response to PDGF coincided with the arrival of PDGF in the center channel (Figure 3.11).

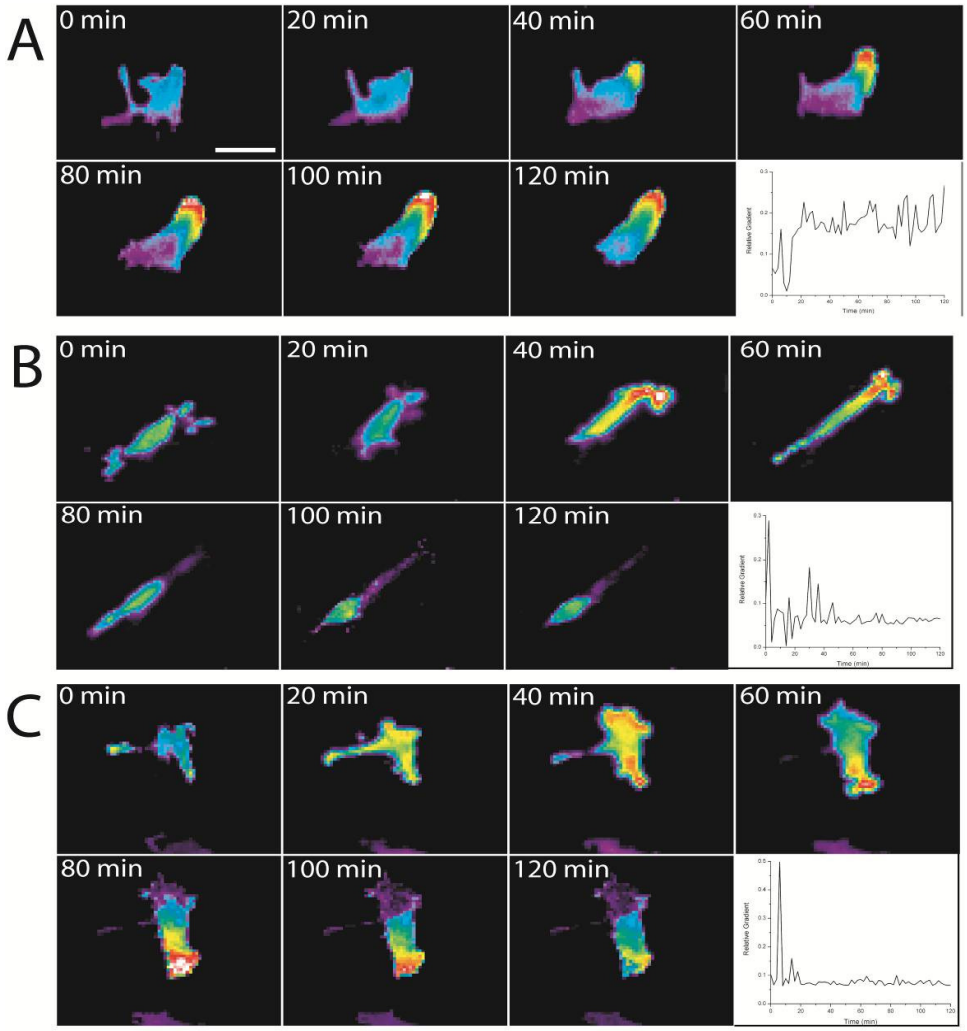

Figure 3.13 Cell morphology polarized towards a gradient of PDGF followed by directed migration. Time lapse images of a two hours time course were collected at the specified times to demonstrate the correlation between cell polarization and PI3K hot spots with direction of migration. (**A-B**) Cells representative of the aligned migration type with a pronounced front and rear and a PI3K hot spot at the front. (**C**) Representative cell from the non-aligned type with directed migration perpendicular to the direction of the PDGF gradient. Plots in the lower right of each montage are relative gradient development over time during the 2 hour time course. Scale bar is 40 µm.

Every instance of the polarized phenotype was accompanied by persistent migration, either up the gradient (Figure 3.15A-B) or in another direction (Figure 3.15C). This migration phenotype, with a defined front and rear accompanied by polarized PI3K signaling, was expected based on observations previously reported for a variety of chemotactic cells. Analysis of the relative gradients seen by the cells suggest that the correctly polarized phenotype might be more likely for cells in a gradient with > 10% steepness, consistent with previous indications (Schneider & Haugh, 2005) and the analysis presented in Chapter 2.

3.3.5 Fibroblast viability in the ladder device

As stated previously, a two-hour time course is not sufficient to properly correlate PI3K signaling and cell directionality. Hence we sought to extend the migration time courses to 6-8 hours (and in some cases the initial two hour time course was extended to either 6 or 8 hours).

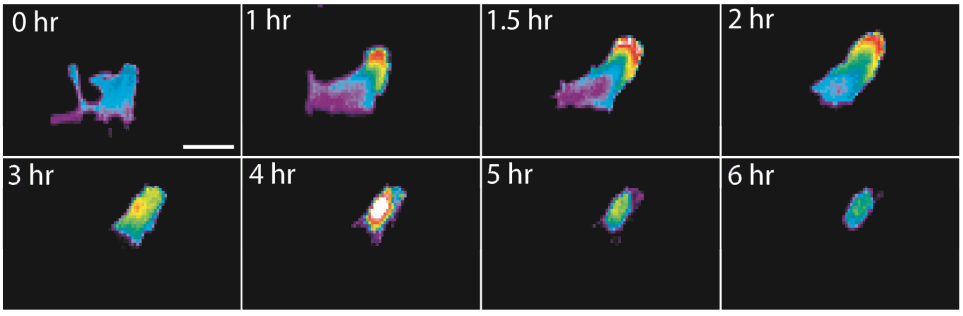

Figure 3.14 Longer incubation times in the device result in loss of polarity and death. Time-lapse images were captured at the specified time points. Note the loss of polarization between the second and third hour of migration, accompanied by a loss of contact area and irregular fluorescence. Scale bar is 40 µm.

As demonstrated above, the device is capable of maintaining a PDGF gradient for this length of time without running out of solution or losing gradient stability. It is also noteworthy that we routinely carry out random migration experiments of that duration, with the same cells, but not in PDMS devices (Weiger, Ahmed, Welf, & Haugh, 2010; Weiger et al., 2009); however, the viability of the cells declined rapidly after ~ 2 hours of stimulation in the ladder device. Thereafter, the cells consistently exhibited a decrease in contact area and irregular fluorescence patterns (Figure 3.14). Even cells that showed a robust response to the gradient

during the first two hours would halt their migration, lose the polarized phenotype, and detach from the surface. Quantification of the normalized cell fluorescence and contact area size of > 100 cells shows the consistency of this behavior and its kinetics (Figure 3.15). Whereas the cells typically show increases in fluorescence and spreading area in their initial responses to PDGF as expected, both responses steadily decline thereafter.

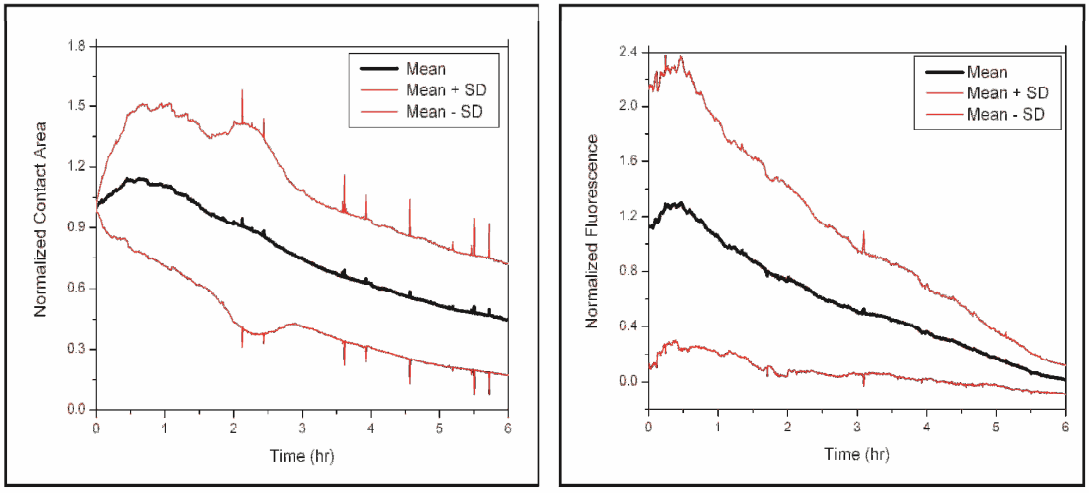

Figure 3.15 Long incubation times in the ladder device results in compromised cell viability. Normalized contact area and normalized fluorescence were calculated (based on Equations 3.4 and 3.5) for all cells analyzed during migration time courses in the ladder device. A total of 124 cells were analyzed with the average values shown in black while the average +/- one standard deviation is depicted in red.

Indications from the literature have implicated the negative effect of fluid shear on cells in PDMS devices similar to our serpentine design (Walker et al., 2005) as well as the potentially toxic effects of un-crosslinked PDMS and other soluble species leaching from the polymer (Millet et al., 2007; Regehr et al., 2009). Since the migrating cells are not exposed to significant flows in the ladder device, we focused on the latter possibility; to extract and thereby minimize the amounts of soluble species in our PDMS devices without deforming their shape, we incubated the polymer in a series of solvents from high to low solubility (toluene, ethanol, and water) (Lee et al., 2003), after which the devices were dried.

Observations of cells in devices that were prepared with and without extraction did not show any difference in cell polarization, cell movement, or PI3K signaling (Figure 3.16).

A quantitative analysis of the normalized contact area and normalized fluorescence over the 6-hour time course also did not reveal any benefit of solvent extraction (Figure 3.17). Based on these findings, it appears unlikely that leaching of species derived from the PDMS material is the cause of the observed decline in cell viability.

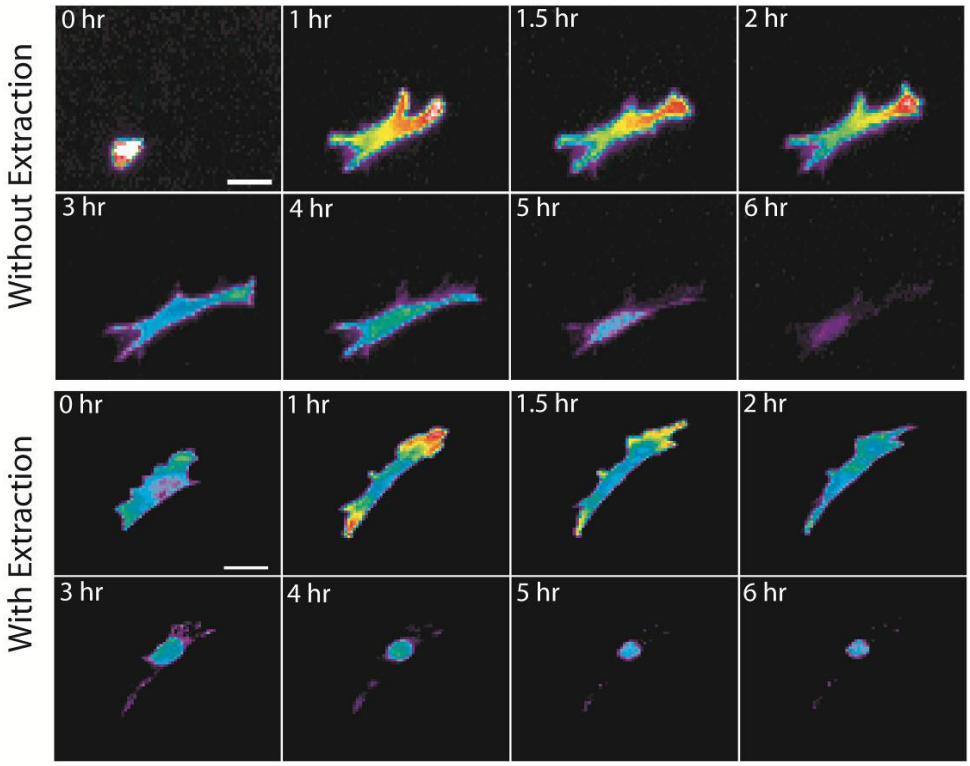

Figure 3.16 Cell migration behavior is unaffected by organic extraction of un-crosslinked oligomers. Both montages of representative cells are from 6 hour migration experiments in the ladder device in response to a gradient of PDGF (source concentration of 1 μM). Top cell is from an untreated device while the bottom montage has a cell from a device that was treated with toluene, 200 proof ethanol and deionized water in an attempt to remove un-crosslinked oligomers from the bulk PDMS. Scale bars represent 30 μm.

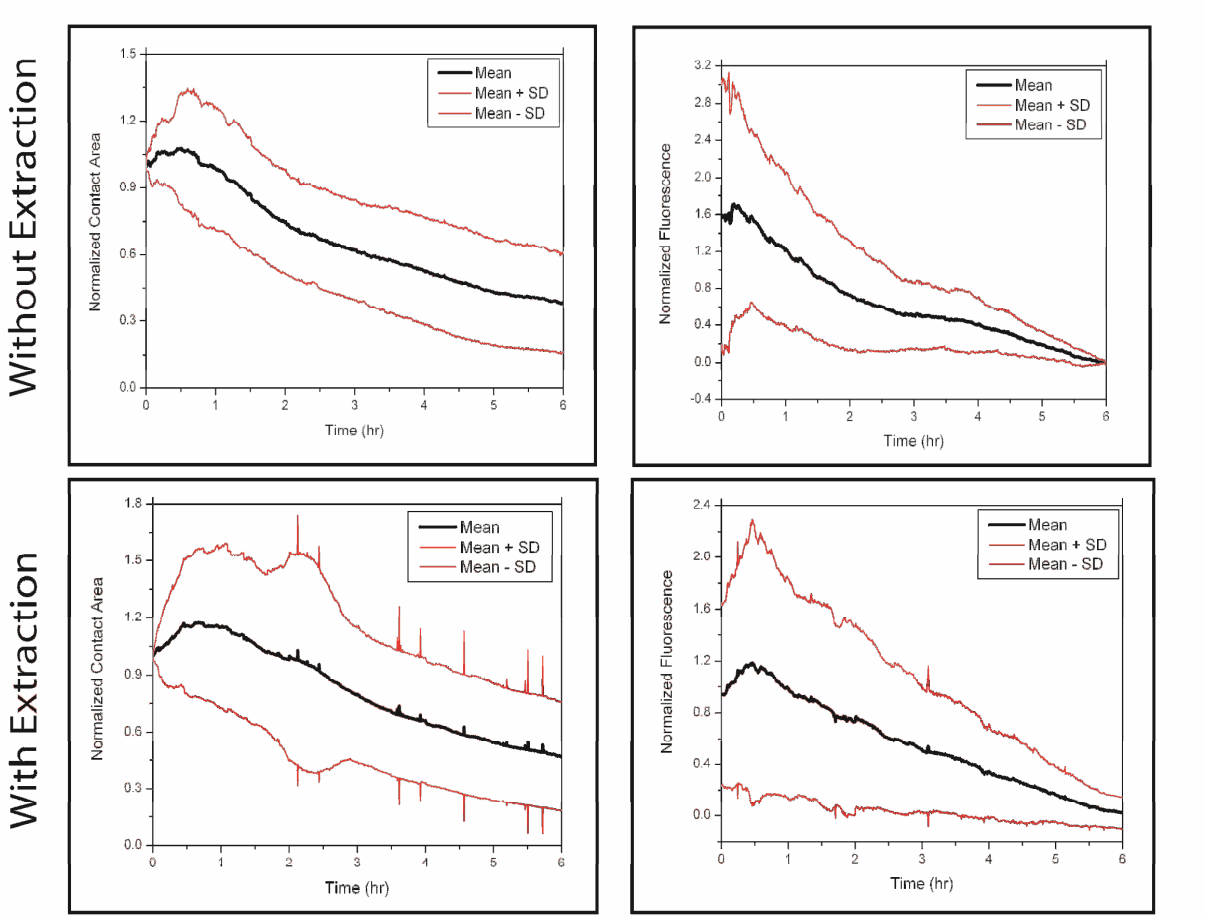

Figure 3.17 Treatment of PDMS replicas with organic solvents to remove un-crosslinked oligomers has no affect on cell behavior. Normalized contact area and normalized fluorescence were calculated (based on Equations 3.4 and 3.5) for all cells analyzed during migration time courses in the ladder device to compare the effectiveness of organic solvent extraction. A total of 36 cells were analyzed without extraction while 88 cells were analyzed with extraction. The average values shown in black while the average +/- one standard deviation is depicted in red.

3.4 DISCUSSION

Microfluidic, gradient generator devices hold great promise for quantitative analysis of cellular and microbial responses. In this study, we tested the suitability of two such devices for analysis of fibroblast polarization and chemotaxis. The first is based on an established, serpentine (split and mix) design, wherein a series of laminar flow streams flow over the cells, and the chemoattractant gradient develops across the channel by diffusion, whereas in the second, ladder design, there are two flowing streams with a relatively stagnant chamber between them, across which the chemoattractant gradient is formed. As discussed

in Chapter 1, the serpentine design and related devices control the gradient by flow; thus, insofar as the flow is controlled, there is the potential for rapid and precise control over the chemoattractant concentration field in the migration chamber. Practically however, the large surface area to volume ratio inside the device make it prone to the nucleation and growth of gas bubbles, despite measures such as degassing the solutions. The bubbles can be controlled to some extent by increasing the flow, but at the expense of control over the gradient. Cell viability was also compromised in the serpentine design, irrespective of the presence of bubbles, which we could attribute to the exposure of our cells to flow. Although the effect of shear on adherent cell lines in microfluidics devices has not been studied in detail, there are indications that some cells can tolerate moderate flows (Walker et al., 2005); however, these studies have only examined this issue for cell types such as neutrophils and T cells, cells found both in circulation and, during infection, in other tissues. It is possible that fibroblasts and certain other cell types that are not normally exposed to such flows rely on a chemical microenvironment that they and their neighbors establish, a microenvironment that would be disturbed by external flows.

The ladder design avoids direct exposure of the cells to bubbles or significant flow rates; however, it shares a technical drawback with other approaches such as the Zigmond and Dunn chambers (Chapter 1): the time scale required to establish the gradient (> 1 hour) is too long, relying on diffusion across lengths of ~ 1 mm. Although the gradient was changing significantly with time, the relative gradient (% difference across cell dimensions) was found to be stable enough to induce polarization of PI3K signaling in a fraction of the cells exposed to steep PDGF gradients, and migration of those cells in the direction of polarization.

Despite the lack of direct flow in the ladder device, it did not allow for chemotaxis experiments of longer duration as hoped, since cell viability was again compromised. Extracting potentially toxic compounds from the PDMS replicas did not resolve the issue. Although we cannot rule out the possibility that the extraction protocol was insufficient to remove all contaminants, the lack of any significant change in cell detachment kinetics suggests otherwise. A plausible explanation is that the flow in the side channels, while not subjecting the cells in the center channels to significant flow, is nonetheless a mechanism for

net transport through the device. Thus, according to the 'microenvironment disruption' hypothesis, factors secreted by the cells are lost by diffusion into the rapidly flowing side channels. We did perform control experiments observing chemotaxis in the ladder device (both with and without extraction) in the absence of flow and observed similar levels of cell death (results not shown); however we do not believe this death was the result of PDMS-based toxicity. At experimental temperatures of 37^{o}C, the small amount of buffer present in the chamber (~2.65 μL) slowly evaporates from the exit tubing. Without any fresh buffer being replaced via flow, the volume in the chamber drops over time, affecting both the pH and microenvironment, resulting in cell death. We have observed a similar behavior in randomly migrating cells (Weiger et al., 2010) when the buffer evaporates over time. Other possibilities, which we cannot control for, include acidification of the buffer by the cells, insufficient gas exchange, and gradients in osmolarity.

The use of microfluidics devices to study chemotaxis is an exciting and emerging field. Our studies shed light on some of the inherent difficulties associated with this approach, particularly for experiments of longer duration. Nevertheless, the directionality of PI3K signaling and cell migration were found to be well-correlated during the first two hours of stimulation. We have also shown, for the first time, the feasibility of integrating microfluidic devices with TIRF microscopy to study intracellular signaling dynamics in real time. Technical limitations notwithstanding, we believe that such devices, with additional engineering, will prove to be valuable tools in the study of chemotaxis and other important subfields of cell biology.

3.5 REFERENCES

Agrawal, N., Toner, M., & Irimia, D. (2008). Neutrophil migration assay from a drop of blood. *LAB ON A CHIP, 8*(12), 2054-2061.

Andrew, N., & Insall, R. (2007). Chemotaxis in shallow gradients is mediated independently of ptdins 3-kinase by biased choices between random protrusions. *NATURE CELL BIOLOGY, 9*(2), 193-U191.

Barkefors, I., Thorslund, S., Nikolajeff, F., & Kreuger, J. (2009). A fluidic device to study directional angiogenesis in complex tissue and organ culture models. *LAB ON A CHIP, 9*(4), 529-535.

Chaudhury, M., & Whitesides, G. (1991). Direct measurement of interfacial interactions between semispherical lenses and flat sheets of poly(dimethylsiloxane) and their chemical derivatives. *Langmuir, 7*(5), 1013-1025.

Dertinger, S., Chiu, D., Jeon, N., & Whitesides, G. (2001). Generation of gradients having complex shapes using microfluidic networks. *ANALYTICAL CHEMISTRY, 73*(6), 1240-1246.

Doran, M., Mills, R., Parker, A., Landman, K., & Cooper-White, J. (2009). A cell migration device that maintains a defined surface with no cellular damage during wound edge generation. *LAB ON A CHIP, 9*(16), 2364-2369.

Duffy, D., Schueller, O., Brittain, S., & Whitesides, G. (1999). Rapid prototyping of microfluidic switches in poly(dimethyl siloxane) and their actuation by electro-osmotic flow. *JOURNAL OF MICROMECHANICS AND MICROENGINEERING, 9*(3), 211-217.

Haugh, J., Codazzi, F., Teruel, M., & Meyer, T. (2000). Spatial sensing in fibroblasts mediated by 3 ' phosphoinositides. *JOURNAL OF CELL BIOLOGY, 151*(6), 1269-1279.

Hoeller, O., & Kay, R. (2007). Chemotaxis in the absence of pip3 gradients. *CURRENT BIOLOGY, 17*(9), 813-817.

Jeon, N., Baskaran, H., Dertinger, S., Whitesides, G., Van de Water, L., & Toner, M. (2002). Neutrophil chemotaxis in linear and complex gradients of interleukin-8 formed in a microfabricated device. *NATURE BIOTECHNOLOGY, 20*(8), 826-830.

Jeon, N., Dertinger, S., Chiu, D., Choi, I., Stroock, A., & Whitesides, G. (2000). Generation of solution and surface gradients using microfluidic systems. *LANGMUIR, 16*(22), 8311-8316.

Kaur, H., Park, C., Lewis, J., & Haugh, J. (2006). Quantitative model of ras-phosphoinositide 3-kinase signalling cross-talk based on co-operative molecular assembly. *BIOCHEMICAL JOURNAL, 393*, 235-243.

Keenan, T., & Folch, A. (2008). Biomolecular gradients in cell culture systems. *LAB ON A CHIP, 8*(1), 34-57.

Keenan, T., Frevert, C., Wu, A., Wong, V., & Folch, A. (2010). A new method for studying gradient-induced neutrophil desensitization based on an open microfluidic chamber. *LAB ON A CHIP, 10*(1), 116-122.

Kolsch, V., Charest, P., & Firtel, R. (2008). The regulation of cell motility and chemotaxis by phospholipid signaling. *JOURNAL OF CELL SCIENCE, 121*(5), 551-559.

Lauffenburger, D., & Horwitz, A. (1996). Cell migration: A physically integrated molecular process. *CELL, 84*(3), 359-369.

Lee, J., Park, C., & Whitesides, G. (2003). Solvent compatibility of poly(dimethylsiloxane)-based microfluidic devices. *ANALYTICAL CHEMISTRY, 75*(23), 6544-6554.

Lin, F., Nguyen, C., Wang, S., Saadi, W., Gross, S., & Jeon, N. (2004). Effective neutrophil chemotaxis is strongly influenced by mean il-8 concentration. *BIOCHEMICAL AND BIOPHYSICAL RESEARCH COMMUNICATIONS, 319*(2), 576-581.

Lin, F., Nguyen, C., Wang, S., Saadi, W., Gross, S., & Jeon, N. (2005). Neutrophil migration in opposing chemoattractant gradients using microfluidic chemotaxis devices. *ANNALS OF BIOMEDICAL ENGINEERING, 33*(4), 475-482.

McDonald, J., Duffy, D., Anderson, J., Chiu, D., Wu, H., Schueller, O., et al. (2000). Fabrication of microfluidic systems in poly(dimethylsiloxane). *ELECTROPHORESIS, 21*(1), 27-40.

Millet, L., Stewart, M., Sweedler, J., Nuzzo, R., & Gillette, M. (2007). Microfluidic devices for culturing primary mammalian neurons at low densities. *LAB ON A CHIP, 7*(8), 987-994.

Petrie, R., Doyle, A., & Yamada, K. (2009). Random versus directionally persistent cell migration. *NATURE REVIEWS MOLECULAR CELL BIOLOGY, 10*(8), 538-549.

Regehr, K., Domenech, M., Koepsel, J., Carver, K., Ellison-Zelski, S., Murphy, W., et al. (2009). Biological implications of polydimethylsiloxane-based microfluidic cell culture. *LAB ON A CHIP, 9*(15), 2132-2139.

Saadi, W., Rhee, S., Lin, F., Vahidi, B., Chung, B., & Jeon, N. (2007). Generation of stable concentration gradients in 2d and 3d environments using a microfluidic ladder chamber. *BIOMEDICAL MICRODEVICES, 9*(5), 627-635.

Schneider, I., & Haugh, J. (2004). Spatial analysis of 3 ' phosphoinositide signaling in living fibroblasts: Ii. Parameter estimates for individual cells from experiments. *BIOPHYSICAL JOURNAL, 86*(1), 599-608.

Schneider, I., & Haugh, J. (2005). Quantitative elucidation of a distinct spatial gradient-sensing mechanism in fibroblasts. *JOURNAL OF CELL BIOLOGY, 171*(5), 883-892.

Schneider, I., & Haugh, J. (2006). Mechanisms of gradient sensing and chemotaxis - conserved pathways, diverse regulation. *CELL CYCLE, 5*(11), 1130-1134.

Schneider, I., Parrish, E., & Haugh, J. (2005). Spatial analysis of 3 ' phosphoinositide signaling in living fibroblasts, iii: Influence of cell morphology and morphological polarity. *BIOPHYSICAL JOURNAL, 89*(2), 1420-1430.

Sia, S., & Whitesides, G. (2003). Microfluidic devices fabricated in poly(dimethylsiloxane) for biological studies. *ELECTROPHORESIS, 24*(21), 3563-3576.

Soon, L., Mouneimne, G., Segall, J., Wyckoff, J., & Condeelis, J. (2005). Description and characterization of a chamber for viewing and quantifying cancer cell chemotaxis. *CELL MOTILITY AND THE CYTOSKELETON, 62*(1), 27-34.

Veltman, D., Keizer-Gunnik, I., & Van Haastert, P. (2008). Four key signaling pathways mediating chemotaxis in dictyostelium discoideum. *JOURNAL OF CELL BIOLOGY, 180*(4), 747-753.

Veltman, D., & van Haastert, P. (2008). The role of cgmp and the rear of the cell in dictyostelium chemotaxis and cell streaming. *JOURNAL OF CELL SCIENCE, 121*(1), 120-127.

Walker, G., Sai, J., Richmond, A., Stremler, M., Chung, C., & Wikswo, J. (2005). Effects of flow and diffusion on chemotaxis studies in a microfabricated gradient generator. *LAB ON A CHIP, 5*(6), 611-618.

Wang, S., Saadi, W., Lin, F., Nguyen, C., & Jeon, N. (2004). Differential effects of egf gradient profiles on mda-mb-231 breast cancer cell chemotaxis. *EXPERIMENTAL CELL RESEARCH, 300*(1), 180-189.

Weibel, D., Garstecki, P., & Whitesides, G. (2005). Combining microscience and neurobiology. *CURRENT OPINION IN NEUROBIOLOGY, 15*(5), 560-567.

Weibel, D., & Whitesides, G. (2006). Applications of microfluidics in chemical biology. *CURRENT OPINION IN CHEMICAL BIOLOGY, 10*(6), 584-591.

Weiger, M. (2008). *Integration of soluble and adhesive signals during fibroblast migration.* North Carolina State University, Raleigh, NC.

Weiger, M., Ahmed, S., Welf, E., & Haugh, J. (2010). Directional persistence of cell migration coincides with stability of asymmetric intracellular signaling. *BIOPHYSICAL JOURNAL, 98*(1), 67-75.

Weiger, M., Wang, C., Krajcovic, M., Melvin, A., Rhoden, J., & Haugh, J. (2009). Spontaneous phosphoinositide 3-kinase signaling dynamics drive spreading and random migration of fibroblasts. *JOURNAL OF CELL SCIENCE, 122*(3), 313-323.

Wessels, D., Lusche, D., Kuhl, S., Heid, P., & Soll, D. (2007). Pten plays a role in the suppression of lateral pseudopod formation during dictyostelium motility and chemotaxis. *JOURNAL OF CELL SCIENCE, 120*(15), 2517-2531.

Zheng, J., Felder, M., Connor, J., & Poo, M. (1994). Turning of nerve growth cones induced by neurotransmitters. *Nature, 368*(6467), 140-144.

APPENDICIES

APPENDIX A: Total Internal Reflection Fluorescence Microscopy (TIRF)

Total internal reflection fluorescence (TIRF) microscopy, also termed evanescent wave microscopy, is a well characterized microscopy technique that provides a means to selectively excite fluorophores in an aqueous or cellular environment very near a solid surface without exciting fluorescence from regions farther from that surface (Axelrod, 2001). TIRF microscopy has been demonstrated as a valuable technique in the measurement of cell-substrate separation distances, as assays to determine the strength of adhesions, and as a means to monitor key events in cellular trafficking that occur at the cell surface in live cells (Axelrod, 2001; Burmeister, Olivier, Reichert, & Truskey, 1998). The phenomena of total internal reflection (TIR), according to Snell's law, occurs if a light traveling in a dense medium (high refractive index, n_1) strikes a less dense medium (of lower refractive index, n_2) beyond a certain 'critical angle', θ_c, according to equation A.1 (Toomre & Manstein, 2001).

$$\theta_c = \sin^{-1}\left(\frac{n_2}{n_1}\right) \tag{A.1}$$

The smaller the ratio of n_1/n_2 results in an easier achievement of total internal reflection (TIR), for example, the interface between air and diamond has an n_2/n_1 ratio of (1.0/2.4), yielding a critical angle of 24.6^{o}. In practice, an evanescent wavelength is generated by a beam of light from a laser directed into a prism that is optically coupled to a glass coverslip. The coupling of prism and cover-slip is accomplished using immersion oil with the same refractive index as glass. When the light approaches the prism at an incident angle, θ, greater than the critical angle, θ_c, some of the energy slightly penetrates the aqueous medium containing the cells as an 'evanescent wave' resulting in TIR. The evanescent wave propagates parallel to the surface with an intensity, I, that decays exponentially with perpendicular distance, z, from the prism according to equations A.2 and A.3 (Axelrod, 1981):

$$I = I_o \exp\left(-\frac{z}{d}\right) \tag{A.2}$$

$$d = \frac{\lambda}{4\pi n_2}\left(\frac{\sin^2\theta}{\sin^2\theta_c} - 1\right)^{-1/2} \qquad \text{(A.3)}$$

With λ being the wavelength of the incoming beam in a vacuum and I_o equaling the intensity of the wave at $z = 0$, the glass-buffer interface. In our experimental set-up, n_1 and n_2 are the refractive indices of glass (~1.52) and buffer/cell cytosol (~1.33) respectively.

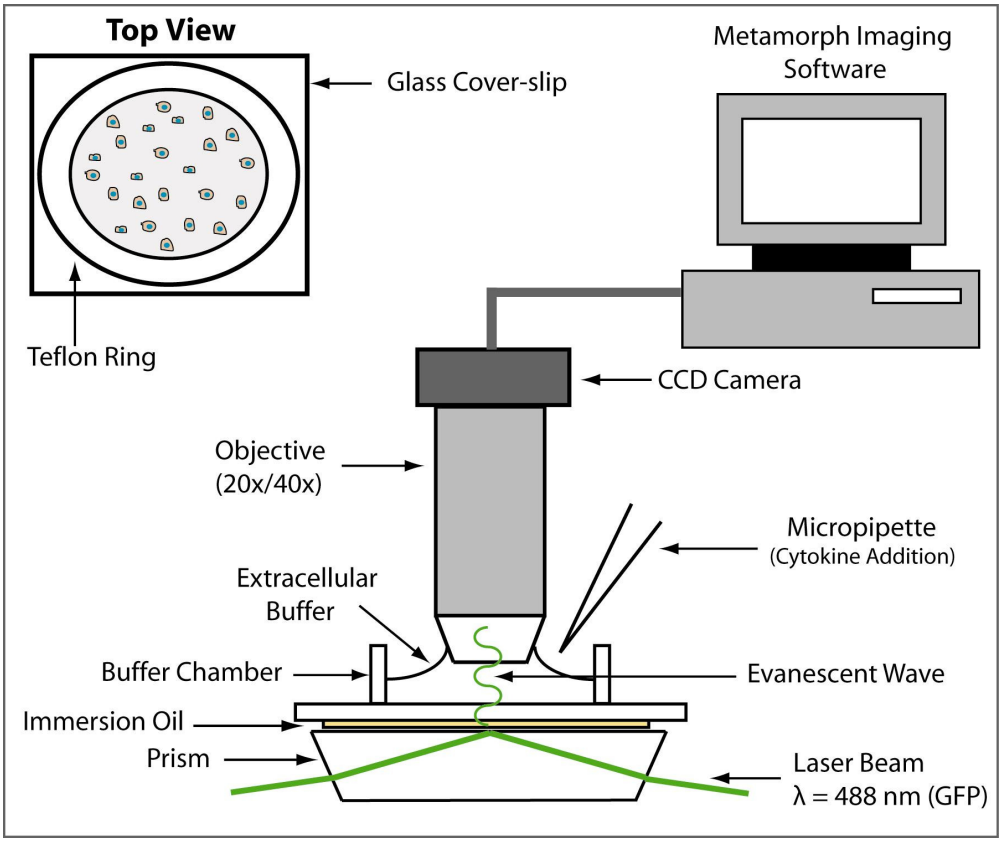

Figure A.1 Experimental setup for TIRF microscopy – A glass coverslip with NIH3T3 cells expressing the stable PI3K probe EGFP-AktPH is optically coupled with a prism with immersion oil. A laser beam from an Argon laser is then passed through the prism at an angle greater than the critical angle, resulting in an evanescent wave propagating perpendicular to the coverslip which effectively illuminates the plasma membrane of the cell.

TIRF allows for the live cell imaging, as well as the ability to make quantitative measurement, of intracellular signaling events that occur at the plasma membrane due to the excitation field selectively exciting fluorescent probes in a small volume at the contact region

of the cell (Toomre & Manstein, 2001). Essentially, TIRF is capable of exciting fluorophores within ~100 nm of the cell contact area, effectively illuminating the plasma membrane of cells and ~5-10% of the cytoplasm directly above it.

Our TIRF setup (Figure A.1) consists of a Zeiss upright microscope equipped with three water immersion objectives (10x, 20x and 40x). A prism directly beneath the stage is optically coupled to the glass cover-slip with 518F immersion oil (Zeiss). Our excitation sources include a 60 mW 488 nm line from a tunable wavelength argon ion laser head (Melles Griot, Irvine, CA) for EGFP (488 nm) and YFP (514 nm) and a 100 mW diode-pumped 561 nm laser (Crystalaser, Reno, NV) for mCherry, RFP and rhodamine-dextran. Shutter controllers regulate the exposure times of the excitation beams. The microscope is fitted with an emission filter wheel and controller as well as emission filters compatible with GFP, YFP, CFP and Texas Red excitation and emission wavelengths. The relevant filter sets are 515/30 nm for EGFP and 630/60 nm for rhodamine-dextran or mCherry (Chroma, Brattleboro, VT). Digital images, with 2x2 binning, are with a Hamamatsu ORCA ER cooled CCD (Hamamatsu, Bridgewater, NJ) and analyzed with Metamorph Imaging software. Samples are prepared by securing a Teflon ring, coated with vacuum grease, to a 25 mm square cover-slip coated with 10 µg/mL fibronectin and cultured with NIH3T3 fibroblasts; however, our setup is able to visualize any adherent cell line expressing a biosensor. A volume of ~1 mL of imaging buffer can be contained in this 'imaging chamber'. The coverslip is then mounted on a custom made, x-y directional motorized stage to allow for visualization of different fields across the coverslip. The stage, objectives and prism are then enclosed within a plexiglass container to maintain an ambient temperature of 37^{o}C during experimentation.

REFERENCES

Axelrod, D. (1981). Cell-substrate contacts illuminated by total internal-reflection fluorescence. *Journal Of Cell Biology, 89*(1), 141-145.

Axelrod, D. (2001). Total internal reflection fluorescence microscopy in cell biology. *Traffic, 2*(11), 764-774.

Burmeister, J. S., Olivier, L. A., Reichert, W. M., & Truskey, G. A. (1998). Application of total internal reflection fluorescence microscopy to study cell adhesion to biomaterials. *Biomaterials, 19*(4-5), 307-325.

Toomre, D., & Manstein, D. J. (2001). Lighting up the cell surface with evanescent wave microscopy. *Trends In Cell Biology, 11*(7), 298-303.

APPENDIX B: Ladder Microfluidic Design Dimensions

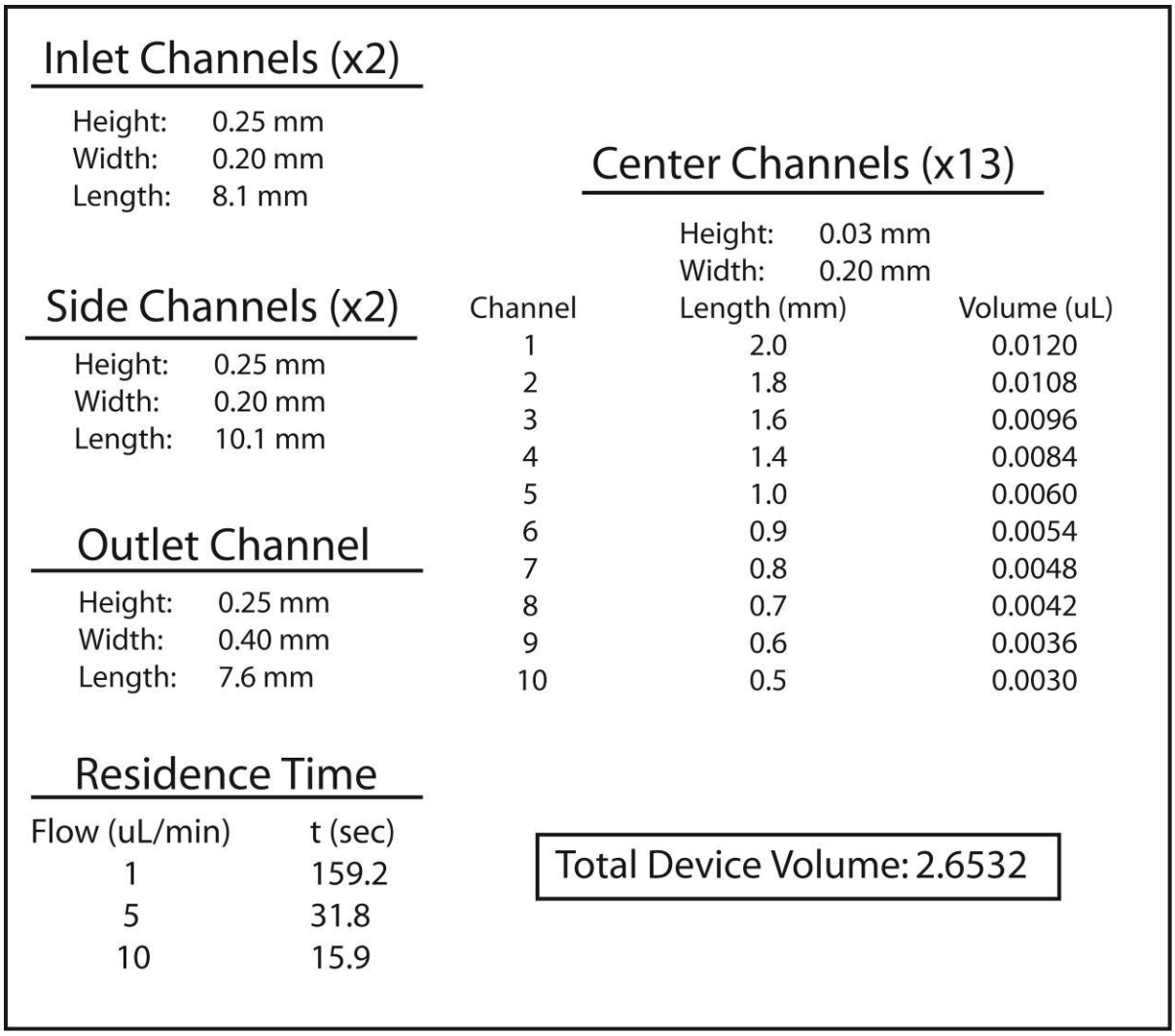

Figure B.1 Summary of dimensions, volumes and residences time inside the channels of the ladder microfluidics design

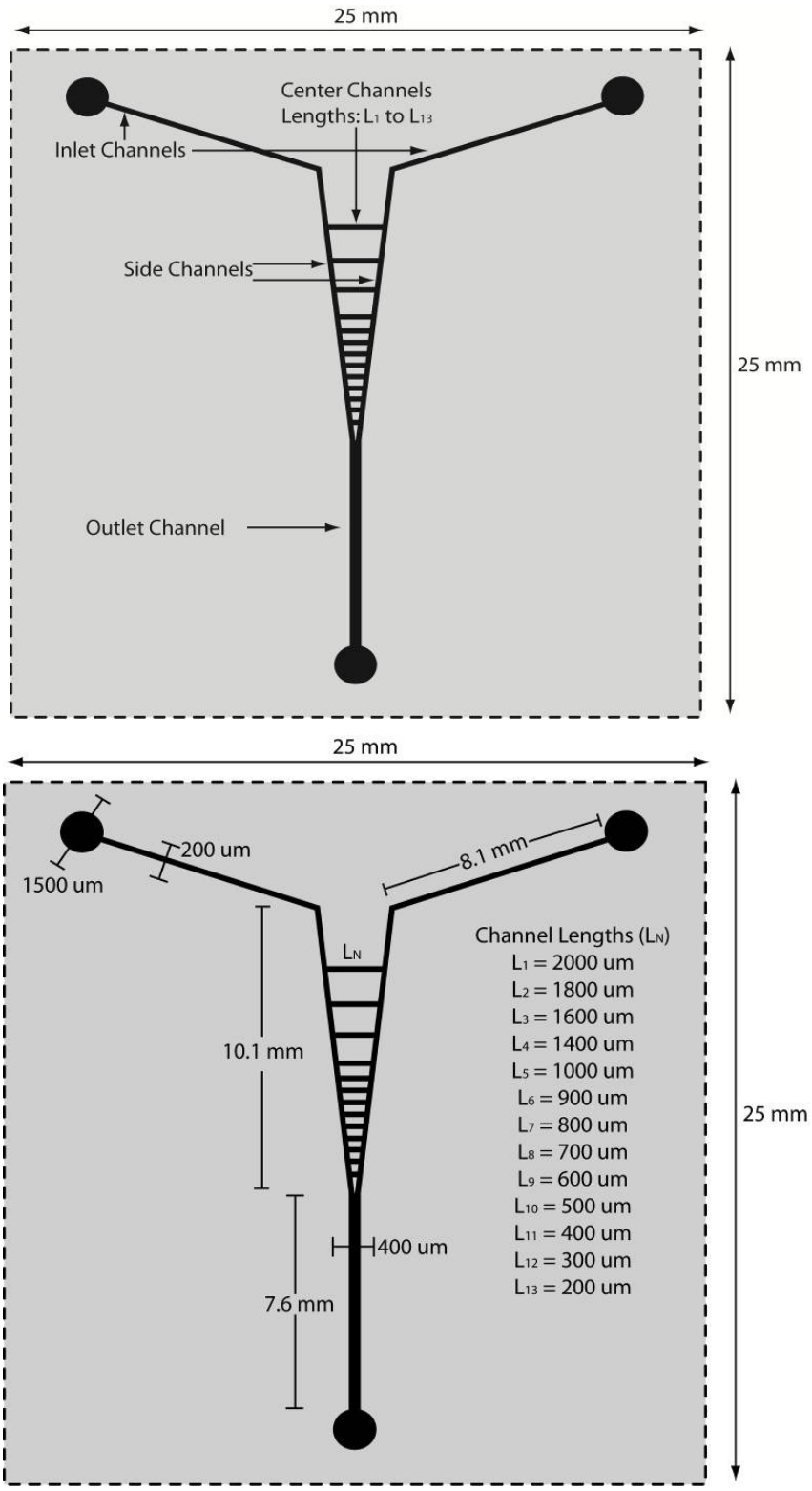

Figure B.2: Ladder design schematic with dimensions and labels